MODELLING AND OPTIMISATION OF THERMOPHYSICAL PROPERTIES AND CONVECTIVE HEAT TRANSFER OF NANOFLUIDS BY USING ARTIFICIAL INTELLIGENCE METHODS

by

MEHDI MEHRABI

Submitted in partial fulfilment of the requirements for the degree

Doctor of Philosophy in Mechanical Engineering

in the

Faculty of Engineering, Built Environment and Information Technology

University of Pretoria

2015

ABSTRACT

Title : Modelling and optimisation of thermophysical properties and convective heat transfer of nanofluids by using artificial intelligence methods

Author : Mehdi Mehrabi
Supervisors : Dr. Mohsen Sharifpur and Prof. Josua P. Meyer
Department : Mechanical and Aeronautical Engineering
University : University of Pretoria
Degree : Doctor of Philosophy (Mechanical Engineering)

Nanofluids are modern heat transfer fluids which can significantly increase the thermal performance of a thermal system. It enhances the thermal conductivity of working fluids due to adding solid nanoparticles to the base fluid. In order to use nanofluids widely in industrial applications knowing the thermophysical properties of these new heat transfer fluids are essential. In this research, the GA-PNN and FCM-ANFIS methods are employed to present models for thermophysical properties of nanofluids. Furthermore, modified NSGA-II technique has been used to optimise the convective heat transfer of nanofluids in a turbulent flow regime.

In recent years considerable correlations have been suggested by different researchers for thermophysical properties of nanofluids based on the experimental and theoretical works, which a large number of those correlations are failed to predict the thermophysical properties of nanofluids for a wide range of particle size, temperature and nanoparticle volume concentrations. In this thesis, experimental data available in literature have been used to propose models for thermophysical properties of nanofluids to overcome this problem by using artificial intelligence-based techniques. Two models based on FCM-ANFIS and GA-PNN techniques have been proposed for the thermal conductivity and viscosity of nanofluids. To show the

UNIVERSITEIT VAN PRETORIA
UNIVERSITY OF PRETORIA
YUNIBESITHI YA PRETORIA

accuracy of the proposed models, the predicted result has been compared with experimental data as well as well-cited correlations in literature. Furthermore, the convective heat transfer of nanofluids was studied and different models based on artificial intelligence techniques have been proposed to model the Nusselt number and pressure drop of nanofluids in a turbulent regime. Finally, a multi-objective optimisation technique was used to optimise the convective heat transfer characteristics and pressure drop of nanofluids to find the best design point base on the Pareto front of the results. The predictions of the models for all cases agreed with the experimental data much better than the available correlations.

Keywords: *Nanofluids, thermophysical properties of nanofluids, Brownian motion, nanolayering, artificial intelligence, multi-objective optimisation, GA-PNN (genetic algorithm-polynomial neural network) method, FCM-ANFIS (fuzzy C-means clustering- adaptive neuro-fuzzy inference system) technique, convection heat transfer, NSGA-II (modified non-dominated sorting genetic algorithm) multi-objective optimisation*

ACKNOWLEDGEMENTS

I wish to express my gratitude to my supervisor, Dr. Mohsen Sharifpur, for his technical guidance and support throughout the research work.

My deepest thanks go to my co-supervisor and head of the department, Prof Josua P. Meyer, for his technical and financial support, which allowed the successful completion of this study.

I also wish to thank all my postgraduate colleagues and friends in the department, as well as our departmental secretary, Ms Tersia Evans.

TABLE OF CONTENTS

ABSTRACT.....**ii**

ACKNOWLEDGEMENTS.....**iv**

TABLE OF CONTENTS.....**v**

LIST OF FIGURES.....**viii**

LIST OF TABLES.....**xi**

NOMENCLATURES.....**xii**

PUBLICATIONS IN JOURNALS AND CONFERENCE PROCEEDINGS.....**xvii**

CHAPTER 1: INTRODUCTION.....**1**

1.1. BACKGROUND.....1

1.2. AIM OF THE PRESENT RESEARCH.....2

1.3. OBJECTIVE OF THE PRESENT RESEARCH.....3

1.4. SCOPE OF THE STUDY.....3

1.5. ORGANISATION OF THE THESIS.....4

CHAPTER 2: THERMAL CONDUCTIVITY OF NANOFLUIDS.....**6**

2.1. INTRODUCTION.....6

2.2. POSSIBLE MECHANISMS OF THERMAL CONDUCTION ENHANCEMENT IN NANOFLUIDS.....7

2.2.1. Brownian motion of nanoparticles.....7

2.2.2. Nanolayering of the liquid at the liquid/particle interface.....10

2.2.3. Electric charge on the surface of nanoparticles.....13

2.2.4. Thermophoretic effect.....14

2.2.5. Preparation and surfactants.....15

2.3. THEORETICAL MODELS FOR THERMAL CONDUCTIVITY OF NANOFLUIDS.....16

2.3.1. Theoretical models based on Brownian motion.....16

2.3.2. Theoretical models based on nanolayering.....30

2.3.3. Theoretical models based on clustering.....37

2.3.4. Hybrid models.....40

2.4. EXPERIMENTAL DATA OF THERMAL CONDUCTIVITY OF NANOFLUIDS IN LITERATURE.....50

2.5. SUMMARY 51

CHAPTER 3: THERMAL CONDUCTIVITY OF NANOFLUIDS BASED ON ARTIFICIAL INTELLIGENCE TECHNIQUES 53

3.1. INTRODUCTION 53

3.2. ADAPTIVE NEURO-FUZZY INFERENCE SYSTEM (ANFIS) 54

3.2.1. Neuro-fuzzy networks 55

3.2.2. Architecture of ANFIS 56

3.2.3. Fuzzy C-means Clustering Based Neuro-Fuzzy Inference System (FCM-ANFIS) Modelling Technique 58

3.3. POLYNOMIAL NEURAL NETWORKS 59

3.3.1. Polynomial networks training algorithms 60

3.3.2. Training the polynomial networks by GMDH algorithm 60

3.3.3. GMDH polynomial neural networks 62

3.3.4. Application of genetic algorithm in optimisation of GMDH-type polynomial neural networks design 64

3.4. APPLICATION OF THE NEURO-FUZZY INFERENCE SYSTEM (ANFIS) AND THE GENETIC ALGORITHM-POLYNOMIAL NEURAL NETWORK (GA-PNN) METHODS FOR MODELLING THE THERMAL CONDUCTIVITY OF AL_2O_3-WATER NANOFLUID 66

3.5. RESULTS AND DISCUSSION 67

3.6. CONCLUSION AND RECOMMENDATIONS 72

CHAPTER 4: VISCOSITY OF NANOFLUIDS BASED ON AN ARTIFICIAL INTELLIGENCE MODEL 73

4.1. INTRODUCTION 73

4.2. APPLICATION OF THE FUZZY C-MEANS CLUSTERING NEURO-FUZZY INFERENCE SYSTEM (FCM-ANFIS) FOR MODELLING THE VISCOSITY OF NANOFLUIDS 74

4.3. EXPERIMENTAL DATA USED FOR THE TRAINING AND TESTING PROCEDURE 76

4.4. PREDICTION MODELS 79

4.5. RESULT AND DISCUSSION 80

4.6. CONCLUSION AND RECOMMENDATIONS 85

CHAPTER 5: MULTI-OBJECTIVE OPTIMISATION OF THE CONVECTIVE HEAT TRANSFER CHARACTERISTICS AND PRESSURE DROP OF NANOFLUIDS 87

5.1. INTRODUCTION 87

5.2. GENETIC ALGORITHM-POLYNOMIAL NEURAL NETWORK HYBRID SYSTEM 87

5.3. CONVECTIVE HEAT TRANSFER OF TIO_2-WATER NANOFLUID 88

5.4. PRESSURE DROP OF TIO_2-WATER NANOFLUIDS 89

5.5. PREDICTIVE ABILITY OF THE PROPOSED MODELS 90

5.5.1. Nusselt Number Prediction 90

5.5.2. Pressure Drop Prediction 91

5.6. MULTI-OBJECTIVE OPTIMISATION BY USING NSGA-II 93

5.8 CONCLUSION AND RECOMMENDATIONS 103

CHAPTER 6: CONCLUSIONS AND RECOMMENDATIONS 105

6.1. SUMMARY 105

6.2. CONCLUSIONS 106

6.3. RECOMMENDATIONS 107

REFERENCES 109

LIST OF FIGURES

Figure 2.1: Schematics of Brownian motion process 8
Figure 2.2: Schematics picture of the nanolayering concept 11
Figure 3.1: Architecture of ANFIS 56
Figure 3.2: A GMDH typical processor unit 61
Figure 3.3: The second generation output y as a function of the input parameters x_i, x_j, x_k, and x_l 61
Figure 3.4: A complete GMDH model, showing the relationship between the input variables and the output 62
Figure 3.5: Combination of genetic algorithm and GMDH type polynomial neural network approaches in a hybrid system 65
Figure 3.6: Structure of GA-PNN-type neural network for thermal conductivity ratio (k_{eff}/k_{bf}) modelling 68
Figure 3.7: Comparison between the experimental data of Lee *et al* [15] and the proposed models for dp= 38.4 nm and T= 21 ^{o}C and Hamilton-Crosser [94] and Xuan *et al* [34] correlations 70
Figure 3.8: Comparison between the experimental data of Li and Peterson [10] and the proposed models for dp= 36 nm and T= 30.5 ^{o}C and Hamilton-Crosser [94] and Xuan *et al* [34] correlations 70
Figure 3.9: Comparison between the experimental data of Kim *et al* [18] and the proposed models for dp= 38 nm and T= 25 ^{o}C and Hamilton-Crosser [94] and Xuan *et al* [34] correlations 71
Figure 4.1: Comparison between the experimental data of Kwek *et al* [146] with Model I and correlations from literature for an Al_2O_3-water nanofluid, with an average particle size of 25 nm at a volume concentration of 2% 81
Figure 4.2: Comparison between the experimental data of Anoop *et al* [144] with Model I and correlations from literature for an Al_2O_3-water nanofluid, with an average particle size of 95 nm at a volume concentration of 2% 82
Figure 4.3: Comparison between the experimental data of Pastoriza-Gallego *et al* [86] with Model I and correlations from literature for an Al_2O_3-water nanofluid, with an average particle size of 43 nm at a volume concentration of 1.4% 82

Figure 4.4: Comparison between the experimental data of Tavman *et al* [141] with Model I and correlations from literature for an Al_2O_3-water nanofluid, with an average particle size of 30 nm at a volume concentration of 0.5%.....83
Figure 4.5: Comparison between the experimental data of Pastoriza-Gallego *et al* [86] with Model II and correlations from literature for a CuO-water nanofluid, with an average particle size of 11±3 nm at a volume concentration of 0.5% 84
Figure 4.6: Comparison between the experimental data of Fedele *et al* [147] with Model III and correlations from literature for a TiO_2-water nanofluid, with an average particle size of 76 nm at a volume concentration of 5.54%.....84
Figure 4.7: Comparison between the experimental data of Tavman *et al* [141] with Model IV and correlations from literature for a SiO_2-water nanofluid, with an average particle size of 12 nm at a volume concentration of 1.85%.....85
Figure 5.1: Structure of the GA-PNN hybrid system for the Nusselt number of TiO_2-water nanofluids modelling.....91
Figure 5.2: Structure of the GA-PNN hybrid system for pressure drop of TiO_2-water nanofluids modelling 92
Figure 5.3: Comparison of the experimental data of Sajadi and Kazemi [159] with the GA-PNN proposed model for the Nusselt number and existing correlations (TiO_2-water nanofluid, with an average particle size of 30 nm at a volume concentration of 0.1%).....96
Figure 5.4: Comparison of the experimental data of Duangthongsuk and Wongwises [158] with the GA-PNN proposed model for the Nusselt number and existing correlations (TiO_2-water nanofluid, with an average particle size of 21 nm at a volume concentration of 1%).....96
Figure 5.5: Comparison of the experimental data of Abbasian Arani and Amani [162] with the GA-PNN proposed model for the Nusselt number and existing correlations (TiO_2-water nanofluid, with an average particle size of 50 nm at a volume concentration of 1%).....97
Figure 5.6: Comparison of the experimental data of Abbasian Arani and Amani [162] with the GA-PNN proposed model for the Nusselt number and existing correlations (TiO_2-water nanofluid, with an average particle size of 10 nm at a volume concentration of 1.5%).....98

Figure 5.7: Comparison of the experimental data of Abbasian Arani and Amani [162] with the GA-PNN proposed model for the Nusselt number and existing correlations (TiO_2-water nanofluid, with an average particle size of 20 nm at a volume concentration of 2%).....99
Figure 5.8: Comparison of the experimental data [158, 159 and 162] with the GA-PNN proposed model for pressure drop (a-TiO_2-water nanofluid, with an average particle size of 30 nm at a volume concentration of 0.15% [159] b-TiO_2-water nanofluid, with an average particle size of 21 nm at a volume concentration of 1.5% [158] c-TiO_2-water nanofluid, with an average particle size of 30 nm at a volume concentration of 1% [162] d-TiO_2-water nanofluid, with an average particle size of 50 nm at a volume concentration of 1.5% [162]) 100
Figure 5.9: Multi-objective Pareto front of the Nusselt number and pressure drop ..101

LIST OF TABLES

Table 2-1: Summary of the studies on the theoretical models for thermal conductivity of nanofluids – conventional models 45
Table 2-2: Summary of the studies on the theoretical models for thermal conductivity of nanofluids – dynamic models 47
Table 4-1: The most cited correlations of nanofluids viscosity 78
Table 4-2: Statistical criteria used for the analysis of the results 80
Table 5-1: The value of design variables (input variables) and objective functions of the start and end section points 102

NOMENCLATURES

A_{cell}	cross-sectional area of the cubical volume of cell, m^2
A_{co}	constant
A_{eco}	empirical constant
B	constant for the Kapitza resistance per unit area
b	dipole factor
B_{co}	constant
Bi	Biot number
c_{bf}	specific heat of liquid phase (base fluid), J/kg·K
C_{co}	constant
c_{cp}	specific heat capacity of complex particle, J/kg·K
c_f	heat capacity per unit volume of the fluid, $J/m^3.K$
C_{ft}	fitting parameter
c_p	specific heat capacity of nanoparticle, J/kg·K
C_{pco}	proportional constant
c_v	specific heat, J/K
d	diffusion coefficient
$d(j,v)$	depolarisation factor
d_{bf}	molecular diameter of base fluid, m
D_{esf}	empirical shape factor
D_f	fractal dimension
d_f	fractal dimension
d_l	fractal dimension of backbones
d_{min}	minimum diameter of nanoparticles, m
d_{max}	maximum diameter of nanoparticles, m
$\overline{d_p}$	average diameter of nanoparticles, m
d_p	nanoparticle diameter, m
D_0	nanoparticle diffusion coefficient, m^2/s
d_0	diameter of the outermost layer, m
e	elementary charge (electric charge carried by a proton), C
E_{esf}	empirical shape factor
G_T	total interparticle potential
h	heat transfer coefficient, $W/m^2.K$

H_{co}	constant
i	number of time steps used in the simulation
J	net energy flux, J/ m^2
$\bar{k}$	equivalent thermal conductivity,W/m.K
K_B	Boltzmann's constant, J/K
k_{bf}	thermal conductivity of base fluid ,W/m.K
$k_{Brownian}$	thermal conductivity due to particle Brownian motion,W/m.K
k_{CNT}	thermal conductivity of carbon nanotubes,W/m.K
k_{CNTe}	effective thermal conductivity of carbon nanotubes,W/m.K
k_{cp}	thermal conductivity of complex particle,W/m.K
k_{diff}	thermal conductivity due to diffusive heat conduction,W/m.K
k_{EDL}	thermal conductivity due to the electrical double layer ,W/m.K
k_{eff}	effective thermal conductivity ,W/m.K
k_{eff-nf}	effective thermal conductivity of nanofluid ,W/m.K
k_{excess}	thermal conductivity enhancement due to Brownian motion,W/m.K
k_m	matrix conductivity, W/m.K
$k_{Maxwell}$	thermal conductivity based on Maxwell conductivity model,W/m.K
k_{nf}	thermal conductivity of nanofluid ,W/m.K
k_{nl}	nanolayer (interfacial layer) thermal conductivity,W/m.K
k_p	thermal conductivity of nanoparticle ,W/m.K
k_{pe}	equivalent thermal conductivity based on effective theory medium,W/m.K
$k_{p_{eff}}$	effective thermal conductivity of the nanoparticle ,W/m.K
k_{pj}	equivalent thermal conductivities along the axes of the complex ellipsoid in which $j(= a, b \text{ and } c)$ is along the semiaxis directions of the ellipsoid,W/m.K
k_{pn}	effective thermal conductivity of nanoparticles,W/m.K
k_{se}	thermal conductivity of the solid ellipsoid,W/m.K
k_{sl}	thermal conductivity of the solid ellipsoid's surrounding layer,W/m.K
l_B	Bjerrum length, m
l_{bf}	liquid mean free path, m
L_{cell}	length scale of liquid volume, m
L_{CNT}	length of carbon nanotubes, m
l_p	mean free path of nanoparticle, m
l_t	thickness of the liquid layer, m
m	power law exponent

M_{eco}	empirical constant
m_{mw}	molecular weight of the liquid on the solid interface, kg
m_p	mass of the nanoparticle, kg
N	particle concentration, m^{-3}
n	number density of nanoparticles
N_A	Avogadro's constant, mol^{-1}
n_{c-n}	number of carbon nanotubes in a chain
N_{p-c}	number of parallel carbon nanotubes chain
n_v	number of complicated particles per volume
Nu	Nusselt number
O_{co}	constant
p_{co}	constant
$\mathbf{P}_L$	dipole moment of spheres for longitudinal field, C.m
p_{sde}	system dependent exponent
$\mathbf{P}_T$	dipole moment of spheres for transverse field, C.m
$\mathbf{P}_0$	dipole moment of sphere, C.m
Pr	Prandtl number
q	electric charge, C
$\langle Q(0)Q(j\,\Delta t)\rangle$	time-autocorrelation function of $Q(t)$
Q_{esf}	empirical shape factor
R	radius of the outer interface, m
r	spherical coordinate radius, m
R_b	thermal boundary resistance, m^2.K/W
r_{bf}	radius of the base fluid molecule, m
R_C	contact resistance, m^2.K/W
r_c	cluster radios, m
$R_{Fi,P}$	thermal resistance in the parallel liquid path, m^2.K/W
R_{net}	net thermal resistance of the entire nanofluid, m^2.K/W
r_p	radios of nanoparticle, m
R_{tr}	thermal resistance per unit area of the particle/fluid interface, m^2.K/W
Re	Reynolds number
T	temperature, ºC or K
t	time, s
t_{br}	characteristic time of Brownian motion, s
T_{fr}	freezing point of the base liquid, ºC or K

T_{nl}	temperature inside the nanolayer, ºC or K
V	volume of the domain, m^3
V_r	volumetric ratio
$\overline{u_p}$	average particle velocity, m/s
u_p	Brownian velocity of the nanoparticle, m/s
X, Y	parameters determined from the continuity of thermal conductivity at the interface

Greek symbols

α	thermal diffusivity, m^2/s
β	parameter that represents the hydrodynamic interaction between particles and affected fluid
β_a	semi-empirical parameter
β_p	semi-empirical parameter
Γ	Coulomb constant, $N.m^2/C^2$
γ	ratio of the particle radius to the equivalent matrix thickness
Δt	time step
δ_{nl}	nanolayer (interfacial layer) thickness, m
δ_T	thermal boundary layer thickness, m
ε	permittivity of the liquid, F/m
ε_{bf}	dielectric constant of medium
${\kappa_D}^{-1}$	Debye length, m^{-1}
μ	dynamic viscosity, Pa.s
μ_{bf}	dynamic viscosity of the base fluid, Pa.s
μ_{nf}	dynamic viscosity of nanofluid, Pa.s
ν	kinematic viscosity, m^2/s
ν_p	kinematic viscosity of nanoparticle, m^2/s
ρ_{bf}	density of liquid phase (base fluid), kg/m^3
ρ_{cp}	density of complex particle, kg/m^3
ρ_i	number density of ionic charge in the bulk liquid, kg/m^3
ρ_{nf}	density of nanofluid, kg/m^3
ρ_p	density of nanoparticle, kg/m^3
ς	Kapitza resistance, $K^4.m^2/W$
τ	particle relaxation time, s
Φ	volume of the particle, m^3

ϕ	volume fraction
ϕ_e	equivalent volume concentration of complex ellipsoids
ϕ_{eff}	effective volume fraction
ϕ_{nl}	nanolayer (interfacial layer) volumetric fraction
ϕ_o	original volume fraction of nanoparticles
ϕ_p	volume fraction of nanoparticle
ϕ_{pl}	volume fraction of nanoparticle plus the nanolayer
ϕ_t	total volume fraction
Ψ	sphericity
ψ	empirical parameter
Ω	Kapitza length and the particle radius ratio
ω	empirical constant

Abbreviations

ASPN	algorithm for synthesis of polynomial networks
FCM − ANFIS	fuzzy C-means clustering- adaptive neuro-fuzzy inference system
GA − PNN	genetic algorithm- polynomial neural network
GMDH	group method of data handling
NSGA	non-dominated sorting genetic algorithm
NSGA − II	modified non-dominated Sorting genetic algorithm
PNTR	polynomial network training routine

PUBLICATIONS IN JOURNALS AND CONFERENCE PROCEEDINGS

The following articles and conference papers were produced during this research.

Journal articles

H.S. Aybar, M. Sharifpur, M.R. Azizian, **M. Mehrabi**, J.P. Meyer, A review of thermal conductivity models of nanofluids, *Heat Transfer Engineering*, accepted on 25 April 2014, accepted and scheduled for Vol. 36, No. 16, 2015.

M. Mehrabi, M. Sharifpur, J.P. Meyer, Modelling and multi-objective optimisation of the convective heat transfer characteristics and pressure drop of low concentration TiO_2-water nanofluids in the turbulent flow regime, *International Journal of Heat and Mass Transfer*, Vol. 67, No. 1, pp. 646-653, 2013.

M. Mehrabi, M. Sharifpur, J.P. Meyer, Viscosity of nanofluids based on an artificial intelligence model, *International Communications in Heat and Mass Transfer*, Vol. 43, No.1, pp. 16-21 , 2013.

M. Mehrabi, M. Sharifpur, J.P. Meyer, Application of the FCM-based Neuro-fuzzy Inference System and genetic algorithm-polynomial neural network approaches for modelling of the thermal conductivity of Alumina-water nanofluids, *International Communications in Heat and Mass Transfer*, Vol. 39, No. 7, pp. 971-977, 2012.

Conference papers

M. Mehrabi, M. Sharifpur, J.P. Meyer, Convective heat transfer characteristics of low concentration CuO-water nanofluids in the turbulent flow regime based on an artificial intelligence models, *Proceedings of the 15th International Heat Transfer Conference, Kyoto*, paper IHTC15-8461, 11- 15 August 2014.

M. Mehrabi, M. Sharifpur, J.P. Meyer, Adaptive Neuro-Fuzzy Modeling of the Thermal Conductivity of Alumina-Water Nanofluids, *Proceedings of the ASME 2012 3rd Micro/Nanoscale Heat & Mass Transfer International Conference*, Atlanta, paper MNHMT2012-75023, pp. 155- 161, 3 -6 March 2012.

1

CHAPTER 1: INTRODUCTION

1.1. BACKGROUND

One of the most important issues in order to make system, "energy-efficient" is to minimise the size of the system. On the other hand, due to rapid technological developments, a considerable amount of industrial equipment operates at a high temperature and/or speed for more power output. Therefore, cooling for sustaining desirable performance and durability of such devices in a minimum size could be one of the technological issues encountered by high-tech industries. One of the ways to sort out this matter is to find a heat transfer fluid with the potential of more heat capacity. Conventional heat transfer fluids generally have poor thermal conductivities in comparison with solids. Therefore, scattering solid particles into liquids could be a solution which is not a new idea, since it can be traced back to Maxwell's theoretical work in 1873. Consequently, fluids that contain mm- or μm-sized particles were used to increase the effective thermal conductivity of the fluid. However, the mm- or μm-sized particles were large to traverse the channel smoothly. Other main problems were the rapid settling of the mm- or μm-sized particles in the base fluid and the consequent erosion of the particles. Currently, modern technology makes it possible to produce smaller particles on a nano scale which is called nanoparticles which can be dispersed easily without rapid settling in a base fluid. Therefore, a novel generation of coolants called nanofluids was invented to meet the required cooling rate from heat transfer equipment.

This new and advanced heat transfer fluid can be described as the suspension of nanometre-sized (1-100nm) metallic, non-metallic, polymeric particles, oxides and nanotubes in a conventional heat transfer fluid (called base fluid) such as water, mineral oil, ethylene glycol, etc. These fluids have the capability to be used in many industrial processes such as power generation, chemical processes, heating and cooling processes, grinding processes, fuel cells and micro-electronics. For example,

their application in the automotive industry can minimise the size of radiators, which in turn reduce the overall weight of the vehicle.

Nanofluids show better stability and rheological properties, higher thermal conductivity, and no increase in pressure drop when compared with suspended particles of millimetre-or-micrometre dimensions. However, nanofluids do not take its real place in the designed new heat transfer equipment through lack of hybrid accurate models for prediction of the effective thermal conductivity and effective viscosity which they needed for heat transfer calculations.

Thermophysical properties of nanofluids are very important in thermal applications where heat transfer and fluid flow occur. For example, changes in nanofluid viscosity in industrial applications influence the pumping power required as well as the convective heat transfer coefficients. Therefore, accurate information on the thermophysical properties of nanofluids is essential. Although the heat capacity and density of nanofluids can be predicted accurately it is challenging to determine the thermal conductivity and viscosity of nanofluids with acceptable accuracy due to hydrodynamic interactions and particle-particle interactions of nanoparticles in dispersions. Modelling and optimising the thermophysical properties of nanofluids are therefore vital for heat transfer applications.

1.2. AIM OF THE PRESENT RESEARCH

The aim of this research is to propose accurate models for thermophysical properties of nanofluids by using GA-PNN[1], FCM-ANFIS[2] and input-output experimental data. The necessity of research on thermophysical properties of nanofluids to find accurate models is thus essential. Consequently, two methods of artificial intelligence methods have been implemented to model thermal conductivity and viscosity of nanofluids.
A multi-objective optimisation technique (NSGA-II)[3] has also been proposed and developed to optimise the convective heat transfer of nanofluids which have given

[1] Genetic Algorithm- Polynomial Neural Network
[2] Fuzzy C-means Clustering- Adaptive Neuro-Fuzzy Inference System
[3] modified Non-dominated Sorting Genetic Algorithm

better design points based on heat transfer characteristics and pressure drop of nanofluids.

1.3. OBJECTIVE OF THE PRESENT RESEARCH

The objective of this study is to model the thermal conductivity and viscosity of nanofluids by using artificial intelligent techniques as well as optimisation of convection heat transfer of nanofluids in such a way to achieve the maximum heat transfer performance and minimum pressure drop.

1.4. SCOPE OF THE STUDY

In this thesis, two artificial intelligence approaches are employed to model the effective thermal conductivity and viscosity of nanofluids based on the input-output experimental data set. Detailed information about modelling the thermal conductivity are provided in chapter 3, two models are proposed based on GA-PNN and FCM-ANFIS techniques for thermal conductivity of Al_2O_3-water nanofluids for a wide range of particle sizes (11–150 nm), temperatures (20–71 ^oC) and volume concentrations (0.3–14.6 %).

Four prediction models were suggested for viscosity of Al_2O_3, CuO, TiO_2 and SiO_2 water-based nanofluids based on the effect of volume concentration, temperature and nanoparticles size as the input (design) parameters. The viscosities were also compared with several of the most cited correlations in literature.

Furthermore, the Nusselt number and the pressure drop of TiO_2-water nanofluid in a turbulent flow regime were simulated by using the GA-PNN hybrid system approach and experimental data sets. Subsequently, the objective functions were used to obtain polynomial models for the effects of volume concentration, average particle diameter, Reynolds and Prandtl numbers on both the Nusselt number and the pressure drop. Finally, the obtained polynomial models were used in a Pareto-based multi-objective optimisation approach for finding the best possible combinations of the Nusselt number and pressure drop, known as the Pareto front.

1.5. ORGANISATION OF THE THESIS

This thesis consists of six chapters and each chapter is divided into sections and subsections. These provide a detailed description of the subject matter and make for easy reading and referencing. The chapters of the thesis are itemised below:

- Chapter one introduces brief information about our research work and presents the motivation and background of the study.

- Chapter two presents a review on possible mechanisms of thermal conduction enhancement in nanofluids as well as a brief review on theoretical models for thermal conductivity of nanofluids.

- Chapter three deals with the subject of artificial intelligence techniques and focuses on the operation of the GA-PNN and FCM-ANFIS methods for modelling the thermal conductivity of nanofluids by using input-output experimental data sets obtained from literature review. Two models have therefore been proposed for effective thermal conductivity of Al_2O_3-water nanofluids with respect to temperature, nanoparticle size and concentration and compared with experimental data sets.

- Chapter four provides a background on viscosity of nanofluids and theoretical models for viscosity of nanofluids and presents two models based on artificial intelligence modelling techniques for viscosity of nanofluids and the same as chapter three, the result compared to the experimental data as well as three statistic criteria.

- Chapter five develops a multi-objective optimisation technique to optimise the convective heat transfer characteristics and pressure drop TiO_2-water nanofluids to achieve the best results to maximise the Nusselt number and minimise the pressure drop. In this chapter, the Nusselt number and pressure drop of TiO_2-water nanofluids were modelled first by using GA-PNN method and

subsequently the NSGA-II multi-objective optimisation method has been implemented for multi-objective optimisation.

- Chapter six provides a general summary of the findings of the study. It also presents the conclusions and contributions, as well as recommendations for future work.

2

CHAPTER 2: THERMAL CONDUCTIVITY OF NANOFLUIDS[4]

2.1. INTRODUCTION

Nanofluids are a new type of heat transfer fluids used in engineering applications, and they are simply a base fluid with nanoparticles suspended. Nanofluids show a significant enhancement in thermal conductivity and this enhancement is related to different parameters [1, 2].

The most important parameters which potentially influence the heat transfer enhancement of nanofluids are the Brownian motion of nanoparticles, nanoparticle size/distribution and formation of aggregates, nanolayering of the liquid at the fluid/particle interface, electric charge on the surface of nanoparticles, the thermophoretic effect and the nanofluids preparation methods as well as added surfactants [3] which are described in this chapter.

Furthermore, this chapter has provided a review on different correlations proposed by researchers to calculate the thermal conductivity enhancement of base fluids in the presence of nanoparticles. Most of those theoretical models are focused on the influence of the Brownian motion of nanoparticles, nanolayering and clustering. In section 2.3.4, some hybrid models for modelling the thermal conductivity of nanofluids are also mentioned. Those hybrid models have taken into account the Brownian motion as well as the effect of nanolayering of the liquid at the fluid/particle interface.

[4] This chapter has been published in part: H.S. Aybar, M. Sharifpur, M.R. Azizian, M. Mehrabi and J.P. Meyer, "A Review of Thermal Conductivity Models for Nanofluids", *Heat Transfer Engineering*, accepted on 25 April 2014 and scheduled for Vol. 36 (16), 2015.

2.2. POSSIBLE MECHANISMS OF THERMAL CONDUCTION ENHANCEMENT IN NANOFLUIDS

In the following subsections, potential mechanisms which may describe the enhancement of the thermal conductivity of nanofluids have been summarised and described in detail [4-6].

2.2.1. Brownian motion of nanoparticles

A wide variety of fine-scale particles displays an irregular motion on a random path when suspended in a base fluid, which is known as the Brownian motion. The Brownian motion was first observed by Robert Brown in 1828 [6] and was first described analytically by Einstein in 1905 as a part of his doctoral thesis to determine the size of molecules [7]. It has been shown in his work that adding solid particles into the base fluid generates an additional pressure called the osmotic pressure which can be expressed by an expression similar to the ideal gas law when the solute is dilute as

$$p = n\,\kappa_B T \tag{2.1}$$

where n is the particle concentration per unit volume, T is the temperature and κ_B is the Boltzmann constant.

When small particles move into a base fluid, a drag force exerts against the motion which can be expressed by the well-established Stokes law in fluid mechanics as

$$\mathbf{F}_D = 3\pi\mu d_p \mathbf{u} \tag{2.2}$$

where μ is the dynamic viscosity, d_p is the particle diameter and $\mathbf{u}$ is the particle velocity.

At steady-state, the pressure-driven force due to particle movement and the resistance on the particle due to the drag force as well as considering a control volume in x-direction (Figure 2.1) give a balance equation as

$$A_c[p(x) - p(x+dx)] - 3\pi\mu d_p u_x . dN = 0 \tag{2.3}$$

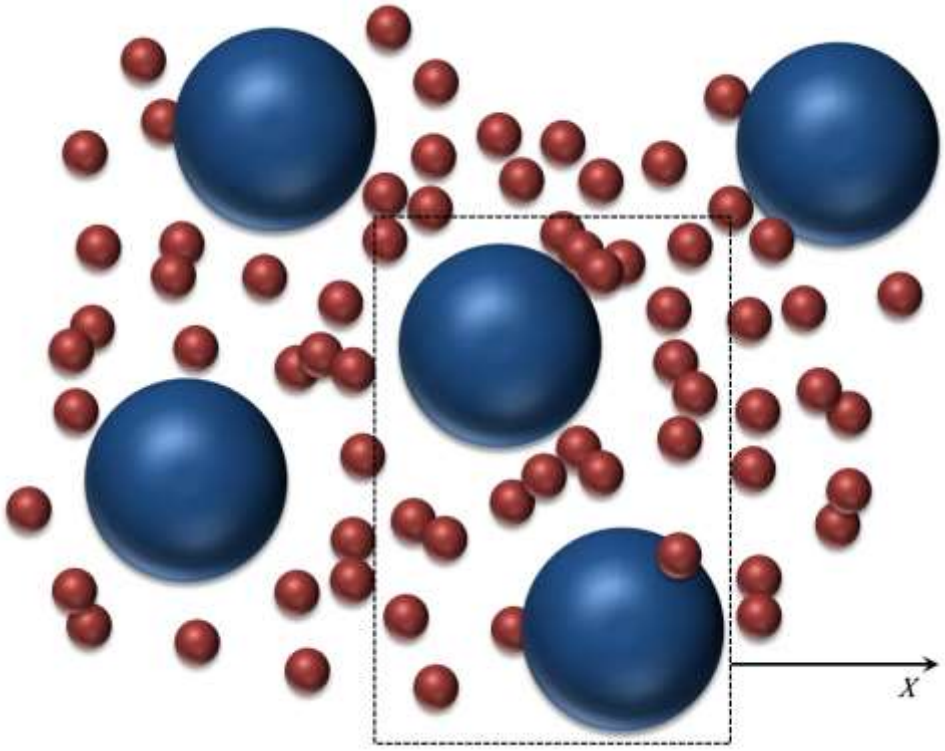

Figure 2.1: Schematics of Brownian motion process

where dN is the number of particles in the volume $dV = A_c dx$. By substituting Eq. (2.1) into Eq. (2.3) leads to

$$n.u_x = -\frac{1}{3\pi\mu d_p}\frac{dp}{dx} = -\frac{\kappa_B T}{3\pi\mu d_p}\frac{dn}{dx} \tag{2.4}$$

By considering Fick's laws of diffusion ($J_x = -d\ dn/dx$) the diffusivity determine by the following equation [8],

$$d = \frac{\kappa_B T}{3\pi\mu d_p} \tag{2.5}$$

In a conventional approach, the effect of the particle Brownian motion is neglected due to the large particle size. The contribution of Brownian motion of nanoparticles in order to enhance the thermal conduction could be effected in two different ways: first due to the movement of the nanoparticles which can transfer the heat and the second

way is the micro convection of the fluid around individual nanoparticles. Nanoparticle size, concentration, distribution and formation of aggregates

Chon *et al* [9] measured the thermal conductivity of nanofluids containing three different sizes of alumina nanoparticles with diameters of 11, 47 and 150 nm. It has been indicated that the thermal conductivity of nanofluids increased as particle size decreased. Li and Peterson [10] observed up to 4% positive thermal conductivity enhancement for Al_2O_3-water nanofluids containing 36 nm Al_2O_3 particles compared with nanofluids containing 47 nm Al_2O_3 particles at 2% volume concentration. Patel *et al* [11] measured the thermal conductivity of nanofluids containing different sizes of Al_2O_3, CuO, and Cu in water, ethylene glycol and in transformer oil. They observed positive thermal conductivity enhancements for Al_2O_3-water with smaller nanoparticles. For Al_2O_3-water nanofluid at 2% volume concentration at 50^{o}C, the thermal conductivity enhancement for the 11 nm sample (15.5%) was approximately double the enhancement for the 150 nm (7%) sample and about 1.5 times the enhancement for the 45 nm (10.5%) sample.

Most of the nanofluids thermal conductivity data in the literature exhibited a linear relationship with the particle volume concentration. However, some exceptions have showed a non-linear relationship especially at low volume concentrations [12]. In these studies, the slope of the thermal conductivity versus volume concentration can be divided into two linear regimes. At low concentrations, the slope was greater than at high concentrations. Most thermal conductivity data in the literature for Al_2O_3-water nanofluids showed that with increasing nanoparticle volume concentration, the thermal conductivity also increased [9- 18], however, the intensity of the increase decreased for the larger volume concentrations.

Timofeeva *et al* [19] investigated the effect of different particle shapes of nanoparticles on thermophysical properties of Al_2O_3-EG/water nanofluids. Based on the experiments which were carried out at different shape and volume fractions of

nanoparticles and by keeping all the other parameters constant, a model was proposed to predict the thermal conductivity of Al_2O_3- EG/water nanofluids.

The result showed that the overall thermal conductivity started to decrease below the sphericity of 0.6 for non-spherical alumina nanoparticles.

A particle aggregation phenomenon in nanofluids is a two-step process. In the first step which is called the transport step, the nanoparticles approach and collide with each other and in the attachment step colliding particles stick to each other and form a chain structure.
Nanoparticle aggregation can enhance the thermal conductivity of nanofluids due to a chain structure which allows more heat transport along the heat flux direction [20].

On the other hand, nanofluids must stabilise by electric repulsion or steric hindrance to prevent particles from sticking together and create large clusters which will result in settling down the particles.

2.2.2. Nanolayering of the liquid at the liquid/particle interface

Due to primary inter-atomic bonding at the solid particle interface, some of the base fluid molecules attach themselves on the nanoparticle and form a layer which has been shown schematically in Figure 2.2.
This layer is called a nanolayer and has the properties of the solid phase of the base fluid. This molecular thin film at the solid/liquid interface plays a crucial role in the thermal conductivity of nanofluids enhancement [21].

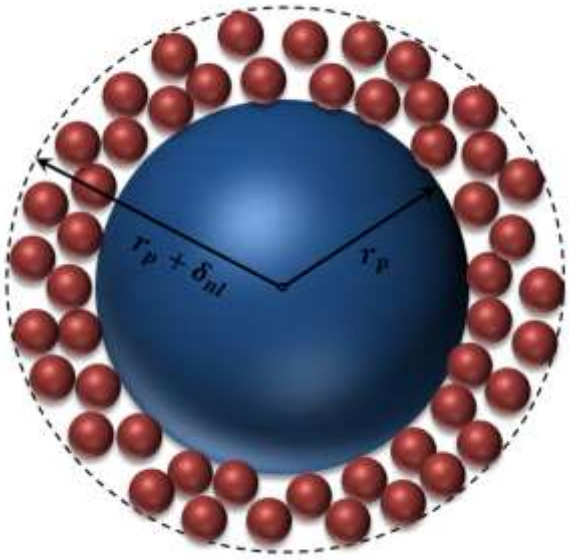

Figure 2.2: Schematics picture of the nanolayering concept

Choi *et al* [22] measured the thermal conductivity of oil-based carbon nanotubes dilution. Since the existing theoretical models were unable to predict the thermal conductivity of nanofluids as well as the strange nonlinear relationship between nanotube loading and thermal conductivity enhancement, the nanolayering as a possible mechanism for enhancing the thermal conductivity of nanofluids was first proposed.

Xue *et al* [23] have shown that the layering of the liquid atoms at the liquid-solid interface as a proposed mechanism for the observed enhancement in the thermal transport of nanofluids is not viable by using molecular dynamics simulation for the specific model system involving a simple (mono-atomic) liquid. However, it has been mentioned that more complex liquids, such as water or liquids of molecular chains, might behave differently.

The width of this crystalline layer which is typically 1-5 atomic layers ($\sim 1nm$) is the prime variable to explain the nanolayering mechanism. Tillman and Hill [24] proposed a revised procedure to determine the nanolayer thickness and the thermal conductivity profile inside a nanolayer. They explained that there was no known

procedure to properly calculate the nanolayer thickness and all previous investigators just chose the nanolayer thickness to match their results with the experimental data. They assumed that the thermal conductivity profile within the nanolayer is given as

$$k_{nl}(r) = X(1 - Yr)^m \tag{2.6}$$

where X and Y are parameters determined from the continuity of thermal conductivity at the interface, m is a power law exponent and r is a spherical coordinate radius. To calculate the temperature profile inside the nanolayer, they assumed the steady-state heat conduction in spherical coordinates with axial symmetry and realised that the temperature profile inside the nanolayer can be obtained by using the separation of variable method as

$$T_{nl}(r, \theta) = A(r)cos\theta = [Ey_1(r) + Fy_2(r)]\, cos\theta \tag{2.7}$$

where E and F are parameters that should be determined through the relevant boundary conditions for temperature, and $y_1(r)$ and $y_2(r)$ are the non-linear independent solutions of the second-order differential equation of

$$\frac{d^2A}{dr^2} + \left(\frac{2}{r} + \frac{1}{k}\frac{dk}{dr}\right)\frac{dA}{dr} - \frac{2}{r^2}A = 0 \tag{2.8}$$

They also calculated the critical nanolayer thickness by solving the following equation,

$$\frac{\frac{d}{dr}\left[\frac{y_1(r_p)}{r_p}\right]}{\frac{d}{dr}\left[\frac{y_2(r_p)}{r_p}\right]} = \frac{\frac{d}{dr}[R^2 y_1(R)]}{\frac{d}{dr}[R^2 y_2(R)]} \tag{2.9}$$

The calculated nanolayer thicknesses for alumina-in-EG and CuO-in-water nanofluids are approximately 19% and 22% of the corresponding nanoparticle radius respectively, which are consistent with data used in other studies. They also compared the results of their model with alumina-in-EG, CuO-in-EG, Cu-in-oil, CuO-in-water experiments and their results show good agreement with these experimental data. However, in their model, three functions for thermal conductivity of nanolayers were tested, but just one of them produced stable results. This means that their model needs

more validation for determining an accurate function of the nanolayer thermal conductivity.

2.2.3. Electric charge on the surface of nanoparticles

Wamkam *et al* [25] experimentally studied the influence of surface charge on the stability of ZrO_2-water and TiO_2-water nanofluids and observed a significant enhancement on thermal conductivity of nanofluids near the iso-electric point. The iso-electric point is the pH value that particle surface carries no net electrical charge and is sometimes abbreviated to IEP in literature.

Furthermore, it has been observed that at the IEP, the repulsive forces among the nanoparticles are zero and nanoparticles stuck together and became rigid. Based on DLVO (Derjaguin, Landau, Verwey and Overbeek) theory, nanoparticles tend to aggregate to each other and form a cluster when the pH of the dilution is equal or close to the IEP value. Consequently, the bigger clusters trap more water molecules and therefore volume fraction of nanoparticles will increase due to well-packed water molecules inside the clusters. Furthermore, the shape of the clusters with trapped water is like chains which result in higher thermal transport due to a longer link and finally enhance the thermal conductivity of nanofluids.

Lee *et al* [26] studied the influence of pH on the ξ potential, surface charge and stability of CuO-Water and SiO_2-water nanofluids. In their experimental investigations, it has been observed that as the pH moves away from point of zero charge (PZC), the surface charge increases due to more frequent attacks on the surface hydroxyl groups. Furthermore, it has been shown that the pH of the colloidal liquid strongly affects the thermal conductivity of the nanofluids. They observed that the colloidal particles get more stable when the pH of the solution moves far from the IEP of particles and eventually alter the thermal conductivity.

2.2.4. Thermophoretic effect

Mobile particles suspended in a liquid are subject to a force under the effect of a temperature gradient, directed in the opposite direction of the temperature gradient. This force, which is equivalent to Soret effect, is called thermophoretic force and is the result of differences in momentum and energy transferred to the particles by bombardment of higher energy molecules on the higher temperature side [5].

The particles experiencing thermophoretic force are also subject to a drag force. Assuming steady-state in the Stokes regime, the balance of the thermophoretic and drag forces results in a particle migration velocity which is called thermophoretic velocity $\mathbf{V}_T$ and can be found as [27]:

$$\mathbf{V}_T = -\beta \frac{\mu}{\rho} . \frac{\nabla T}{T} \tag{2.10}$$

The thermophoretic velocity depends on the physical properties of the base fluid at the fluid temperature in the vicinity of the particle. An expression for the proportionality factor β which usually is called thermophoretic diffusion coefficient is given by McNab and Meisen [28] as follows:

$$\beta = 0.26 \frac{k_{bf}}{k_{bf} + 2k_p} \tag{2.11}$$

It has been mentioned in Buongiorno [29] that thermophoretic effect may become important as a slip mechanism when there are no turbulent eddies. Theoretical analysis by Koo and Kleinstreuer [30] and experimental work by Wang *et al* [5] showed that the impact of thermophoretic on thermal conductivity enhancement is not significant and can be neglected in comparison with Brownian motion effect.

2.2.5. Preparation and surfactants

Nasiri *et al* [31] studied the effect of dispersion method on thermal conductivity of different CNT nanofluids in which functionalisation, SDS/ultrasonic probe and SDS/ultrasonic bath were chosen as preparation methods. It has been concluded that the preparation method has a significant effect on thermal conductivity of CNT nanofluids. Furthermore, they observed that the functionalised CNT structures have the best dispersion and least tendency for agglomeration due to having the smallest mean diameter of particles which had increased from functionalisation method to SDS/ultrasonic bath method. It has also been shown that thermal conductivity of all CNT nanofluids decrease over time, but the rate varies based on the dispersion methods. The functionalised nanofluids had soon begun to level off but the other two types of nanofluids had been continuing their downward trend.

Hwang *et al* [32] measured the thermal conductivity of nanofluids by using a transient hot-wire system. Furthermore, the stability of nanofluids with sedimentation time has been estimated with UV-vis spectrum analysis. The effect of addition of a surfactant has been studied by adding SDS (sodium dodecyl sulphate) to the nanofluid and it has been indicated that it can improve the stability of nanoparticles in aqueous suspensions.

Furthermore, it has been concluded that morphology, the chemical structure of the nanoparticle and base fluid and the addition of a surfactant can strongly affect the stability of nanofluids and consequently the thermo physical properties of nanofluids such as the thermal conductivity.

Ghadimi *et al* [33] studied the effect of preparation methods as well as adding surfactant on stability and thermal conductivity of nanofluids. The single and two-step preparation methods have been studied and it has been shown that nanofluid preparation methods affect the stability of nanofluids since the two-step method needs

a higher nanoparticle concentration to achieve the same heat transfer enhancement by the single-step method. Consequently, a higher concentration caused more sedimentation, although in the most experimental works to date the two-step method is applied for nanofluid preparation since the single-step method is not yet industrialised. Another factor is the higher cost of this method in comparison with the two-step method.

Adding a surfactant as one of the general methods to avoid sedimentation has been studied and it has been shown that addition of surfactant can improve the stability of nanofluids. However, care should be taken to choose the right surfactant as well as applying enough surfactant since choosing the wrong surfactant or applying inadequate surfactant will not encourage the stability of nanofluids.

2.3. THEORETICAL MODELS FOR THERMAL CONDUCTIVITY OF NANOFLUIDS

The different heat transfer mechanisms which potentially influence the heat transfer enhancement of nanofluids are mentioned in section 2.2. Until now most of the studies have been focused on the Brownian motion of the nanoparticles, molecular-level layering of the liquid at the liquid/particle interface (nanolayer), nanoparticle clustering, and a combination of these factors together with other conditional parameters such as temperature, nanoparticles size and volume fraction. In the following subsections the theoretical models for modelling the thermal conductivity of nanofluids based on three important parameters; the Brownian motion, nanolayering and clustering have been described and in subsection 2.3.4 some hybrid models which are taking into account two parameters simultaneously have been presented.

2.3.1. Theoretical models based on Brownian motion

Das *et al* [13] explained that the main mechanism for thermal conductivity enhancement in nanofluids can be the stochastic motion of the nanoparticles. They indicated that the Brownian motion was not important in the conducting behaviour at

low temperatures. They also showed the possibility of a threshold temperature corresponding to each particle size in which the effective thermal conductivity of nanofluids commences to enhance through stochastic motion of the particles. They finally indicated that the stochastic motion of the particles will be greater for smaller particles.

Xuan *et al* [34] offered a model that takes into account the effect of Brownian motion and the aggregation structure of nanoparticle clusters. Their simulation is unique from the point of view of including the fluid temperature and the structure of nanoparticle clusters in the thermal conductivity [1]. The resulting model expressed as:

$$\frac{k_{eff}}{k_{bf}} = \frac{k_p + 2k_{bf} - 2\phi(k_{bf} - k_p)}{k_p + 2k_{bf} + \phi(k_{bf} - k_p)} + \frac{\rho_p \phi\, c_p}{2k_{bf}} \sqrt{\frac{K_B T}{3\pi\mu r_c}} \tag{2.12}$$

In spite of the fact that their model is among pioneer models to include the Brownian motion effect, it cannot predict the linear increase of conductivity with temperature, as obtained by Das *et al* [13].

Koo and Kleinstreuer [30, 35] indicated that the Brownian motion produces micro-mixing and is, therefore, dominant in enhancing the thermal conductivity of nanofluids. They offered a new model for thermal conductivity of nanofluids by adding the effect of Brownian motion to the conventional conductivity model and taking into account factors such as temperature, particle size, volume concentration, and the properties. They combined the thermal conductivity of a static dilute suspension and conductivity due to Brownian motion as follows:

$$k_{eff} = k_{static} + k_{Brownian} \tag{2.13}$$

Wasp's model [36] was used for the static part of the model. A dynamic model of thermal conductivity due to Brownian motion of a large portion of surrounding liquid travelling with randomly moving nanoparticles was used for the second part. Finally, the model offered as

UNIVERSITEIT VAN PRETORIA
UNIVERSITY OF PRETORIA
YUNIBESITHI YA PRETORIA

$$k_{eff} = \left[\frac{k_p + 2k_{bf} - 2\phi(k_{bf} - k_p)}{k_p + 2k_{bf} + \phi(k_{bf} - k_p)}\right] k_{bf} + \left[5 \times 10^4 \beta \phi_p \rho_{bf} c_{bf} \sqrt{\frac{K_B T}{\rho_p d_p}} f(T, \phi_p, etc.)\right] \quad (2.14)$$

where β represents the hydrodynamic interaction between particles and affected fluid and f considers the augmented temperature dependence due to particle interactions. It is difficult to obtain β as well as the function f theoretically and they should be determined from experimental data for different nanofluids. For Al_2O_3-water nanofluids ($1\% < \phi_p$), $\beta = 0.0017(100\phi_p)^{-0.0841}$ $f(T, \phi) = (-6.04\phi_p + 0.4705)T + (1722.3\phi_p - 134.63)$ and is valid for $1\% < \phi_p < 4\%$ and $300\ K < T < 325\ K$.

Prasher *et al* [37] compared the effect of translational Brownian motion and convection induced by Brownian motion. They investigated the existence of an interparticle mechanism. By making an order-of-magnitude analysis, they concluded that the local convection due to the Brownian motion of the nanoparticles is the only mechanism that could explain the anomalous enhancement of thermal conductivity of nanofluids. They also indicated that the thermal conductivity for large particle sizes should be explained based on the conventional effective medium theory such as the Maxwell-Garnett model. Therefore, they modified the Maxwell-Garnett model by including the Brownian-motion-induced convection from multiple nanoparticles. Their semi-empirical model was written as

$$k_{eff} = (1 + A_{eco}\ \mathrm{Re}^{M_{eco}}\ \mathrm{Pr}^{0.333}\ \phi)\left[\frac{k_p + 2k_{bf} + 2(k_p - k_{bf})\phi}{k_p + 2k_{bf} - (k_p - k_{bf})\phi}\right] k_{bf} \quad (2.15)$$

where the Reynolds number is defined as $\mathrm{Re} = \frac{1}{\nu}\sqrt{\frac{18K_B T}{\pi \rho_p d_p}}$. Their suggested model has two empirical constants (A_{eco} and M_{eco}) which have to be determined by experiments. They indicated that the Brownian motion model would be semi-empirical in nature due to the complexities involved with the interaction of multiple

nanoparticles. They also suggested that a numerical simulation is needed to understand the exact origin of the empirical constants.

Chon *et al* [9] have developed empirical correlations for the effective thermal conductivity of nanofluids. Based on the Buckingham-Pi theorem with a linear regression for the experimental results, the following empirical correlation proposed for the effective thermal conductivity

$$\frac{k_{eff}}{k_{bf}} = 1 + 64.7\,\phi^{0.7460}\left(\frac{d_{bf}}{d_p}\right)^{0.3690}\left(\frac{k_p}{k_{bf}}\right)^{0.7476}\mathrm{Re}^{1.2321}\mathrm{Pr}^{0.9955} \tag{2.16}$$

where d_{bf} denotes the molecular diameter of base fluid. The Prandtl number and the Reynolds number are respectively defined as

$$\mathrm{Pr} = \frac{\mu}{\rho_{bf}\alpha} \tag{2.17}$$

$$\mathrm{Re} = \frac{\rho_{bf}\,u_p d_p}{\mu} = \frac{\rho_{bf} K_B T}{3\pi\mu^2 l_{bf}}$$

The temperature dependence of the base fluid viscosity μ was expressed as $= A_{co}.10^{B_{co}/(T-C_{co})}$, where A_{co}, B_{co}, and C_{co} are constants and equal to 2.414×10^{-5}, 247.8, and 140, for water. u_p is the Brownian velocity of nanoparticles based on the Einstein diffusion theory

$$u_p = \frac{K_B T}{3\pi\mu d_p l_{bf}} = \frac{K_B}{3\pi d_p l_{bf}}.\frac{T}{A_{co}.10^{B_{co}/(T-C_{co})}} \tag{2.18}$$

Bhattacharya *et al* [38] developed a semi-empirical Brownian model showing the localised convection caused by Brownian motion is the main reason for enhancement in the effective thermal conductivity of nanofluids. Their model is a combination of the Maxwell conduction model and the convection caused by the Brownian movement of the nanoparticles. The convective-conductive model which they offered accounts for the effects of particle size, base fluid properties, thermal interfacial resistance between the particles and liquid, and temperature. The model is called

multisphere Brownian model (MSBM) which is a modified version of the Prasher *et al* model [37]

$$k_{eff} = (1 + A_{eco}\,\mathrm{Re}^{M_{eco}}\,\mathrm{Pr}^{0.333}\,\phi)\left(\frac{[k_p(1+2Bi)+2k_m]+2\phi[k_p(1-Bi)-k_m]}{[k_p(1+2Bi)+2k_m]-\phi[k_p(1-Bi)-k_m]}\right)k_{bf} \qquad (2.19)$$

where k_m is the matrix conductivity and $Bi = \frac{2R_b k_m}{d_p}$ is Biot number and R_b is thermal boundary resistance. They also showed that contrary to the Keblinski *et al* [3 4] model, the energy transport due to Brownian diffusion is smaller than the energy transport of conduction in liquid. However, they did not consider the energy transport due to convection caused by the Brownian movement of the particles. They simply analysed that the Brownian motion time scale is greater than the convection time scale. This means that the effects of convection are almost propagated instantaneously relative to the Brownian diffusion of the particles. They also indicated that bigger particles show better convection effects in the base fluids, regardless of the thermal conductivity of the nanoparticles. To validate the model, they compared their results with the experimental data of alumina-in-EG, Cu-in-EG, CuO-in-EG, alumina-in-oil and Cu-in-oil. However, in their model there are two constants which should be defined according to each experiment. Furthermore, they provided some research directions in order to remove the imperial constants.

Xu *et al* [39] were the first group to develop a fractal convection model which takes into account the fractal size distribution of nanoparticle convection caused by Brownian motion. Their model takes into account the particle concentration, average size, fractal dimension and temperature. Engagingly, their model shows that the contribution of Brownian motion-induced convection reaches a maximum value at a critical concentration of 12.6 vol% which is in an acceptable agreement with experimental data for oxide nanofluids [1]. The model is as

$$\frac{k_{eff}}{k_{bf}} = \frac{k_p + 2k_{bf} - 2\phi(k_{bf} - k_p)}{k_p + 2k_{bf} + \phi(k_{bf} - k_p)} \tag{2.20}$$

$$+ H_{co}\frac{Nu\, d_{bf}}{\mathrm{Pr}} . \frac{(2 - D_f)D_f}{(1 - D_f)^2} \frac{\left[\left(\frac{d_{max}}{d_{min}}\right)^{1-D_f} - 1\right]^2}{\left[\left(\frac{d_{max}}{d_{min}}\right)^{2-D_f} - 1\right]} \frac{1}{\overline{d_p}}$$

where Nu is the Nusselt number, D_f is the fractal dimension and can be found from $D_f = d - [\ln \phi / \ln(d_{min}/d_{max})]$. d = 2 in two dimensions and d_{min} and d_{max} are respectively the minimum and maximum diameters of nanoparticles.

Vladkov and Barrat [40] simulated the thermal properties of nanofluids by using the molecular dynamics simulations. Based on their simulation results, they conclude that the Brownian motion of the particle does not affect the cooling process. Furthermore, the Maxwell-Garnett model can predict the effective thermal conductivity of nanofluids. They also concluded that the essential parameter which influences the effective thermal conductivity is the ratio of the Kapitza length to the particle radius. Therefore, heat transfer enhancements observed in nanofluids comes from aggregation effects, such as particle clustering and percolation or cooperative heat transfer modes. Their final expression for the effective thermal conductivity is as

$$\frac{k_{eff}}{k_{bf}} = \frac{\left(\frac{k_p}{k_{bf}}(1 + 2\Omega) + 2\right) + 2\phi\left(\frac{k_p}{k_{bf}}(1 - \Omega) - 1\right)}{\left(\frac{k_p}{k_{bf}}(1 + 2\Omega) + 2\right) - \phi\left(\frac{k_p}{k_{bf}}(1 - \Omega) - 1\right)} \tag{2.21}$$

where $\Omega = \varsigma k_{bf}/r_p$ is the ratio between the Kapitza length (equivalent thermal thickness of the interface) and the particle radius.

Li and Peterson [41] analysed the mixing effect of the base fluid directly adjacent to the nanoparticles due to the Brownian motion of nanoparticles by using CFX 5.5.1 software in order to simulate the corresponding temperature, pressure and velocity fields. They investigated the effects of single, adjacent and multiple nanoparticles. Their results imply that Brownian motion-induced micro convection and the mixing

significantly enhances the macroscopic heat transfer in the nanofluids. Moreover, Brownian motion is one of the important factors for anomalous enhancement of the effective thermal conductivity of nanofluids.

Sarkar and Selvam [42] developed the nanofluids system that consists of a base fluid of argon and copper particles with various nanoparticle concentrations. They used an equilibrium molecular dynamics simulation to model this nanofluid system. Therefore, by applying the Green-Kubo relation they calculated the thermal conductivity of the base fluid and nanofluids. They found out that the effective thermal conductivity of copper-argon nanofluids was much bigger than predicted by the Hamilton-Crosser model at both of low volume concentration (up to 0.4%) and high volume concentration (up to 8%). They also found that the liquid atoms motion in nanofluids increases considerably in comparison with the pure base fluid (1.41 times for 1% nanofluid). The nanoparticle motion was also 28 times slower than that of the liquid phase for 1% nanofluids. This implies that the Brownian motion of the nanoparticles is too slow to transport the heat. On the other hand, localised fluid movement around nanoparticles is induced by much faster liquid atoms. They concluded that these phenomena are the main mechanisms for enhanced thermal conductivity of nanofluids. However, their simulation considered only single nanoparticles and excluded the effects of aggregation.

Yu-Hua *et al* [43] analysed the mechanism of the thermal conductivity of a nanofluid including the Brownian motion effect, particle agglomeration and viscosity as well as the influence of the temperature. Their model combined the Maxwell model and the Brownian motion effect based on Xuan *et al* [34] findings. They considered while the particles are on a nanoscale, the surface area of the particles is larger and this could influence the performance of the particles. Therefore, they calculated the thermal conductivity of the nanoparticles as

UNIVERSITEIT VAN PRETORIA
UNIVERSITY OF PRETORIA
YUNIBESITHI YA PRETORIA

$$\frac{k_{eff}}{k_{bf}} = \frac{k_{p_{eff}} + 2k_{bf} - 2\phi_{eff}(k_{bf} - k_{p_{eff}})}{k_{p_{eff}} + 2k_{bf} + \phi_{eff}(k_{bf} - k_{p_{eff}})} + \frac{\rho_p \phi_{eff}\, c_p}{2k_{bf}} \sqrt{\frac{K_B T}{3\pi\mu r_c}} \tag{2.22}$$

where $\phi_{eff} = (1 + l_t/r_p)^3\, \phi$ and l_t is the thickness of the liquid layer which can be expressed as

$$l_t = \frac{1}{\sqrt{3}} \left(\frac{4m_{mw}}{\rho_{bf} N_A} \right)^{\frac{1}{3}} \tag{2.23}$$

where m_{mw} is the molecular weight of the liquid on the solid interface and N_A is Avogadro's constant. They also showed that the changes of viscosity and particle agglomeration with temperature are important issues. By increasing the temperature, the reduction of the particle surface energy would decrease the agglomeration of nanoparticles, and the reduction of viscosity would improve the Brownian motion. To validate their model, they compared the model with the experimental results of Cu-water, which were in good agreement. The results indicated that the maximum error decreased from 7% to 3% when the temperature effects of agglomeration nanoparticles were taken into account.

Shukla and Dhir [44] developed a microscopic model for predicting the thermal conductivity of nanofluids based on the Brownian motion of nanoparticles in the liquid. They divided the net heat flux due to Brownian motion into a kinetic and an interaction part. Their model is based on ensemble averaging technique assuming the existence of small departures from equilibrium and the presence of pair-wise additive interaction potential between various nanoparticles as

$$k_{eff} \tag{2.24}$$
$$= \left\{\frac{k_p + 2k_{bf} + 2\phi(k_p - k_{bf})}{k_p + 2k_{bf} - \phi(k_p - k_{bf})}\right\} k_{bf} + \phi \frac{\rho_p c_p K_B T}{\gamma} + \left\{\frac{nK_B^2 T}{\gamma}\right\}$$
$$\times \left\{\frac{(1-\phi)Z}{8(1+(\rho_i/nZ))}\right\}\left\{\frac{3.29(r_p\kappa_D)^2 + 3.61(r_p\kappa_D) + 1.89}{a\kappa_D(1+r_p\kappa_D)^2}\right\}$$
$$+ \left\{\frac{\rho_p c_p K_B T}{\gamma}\right\}\left\{\frac{(1-\phi)Z}{16(1+(\rho_i/nZ))}\right\} \times \left\{\frac{9.87(r_p\kappa_D)^2 + 21.64(r_p\kappa_D) + 17.05}{r_p\kappa_D(1+r_p\kappa_D)^2}\right\}$$
$$+ \left\{\frac{\rho_p c_p K_B T}{\gamma}\right\}\left\{\frac{(1-\phi)^2 Z^2}{48(1+(\rho_i/nZ))^2}\right\}$$
$$\times \left\{\frac{1.92(r_p\kappa_D)^4 + 1.80(r_p\kappa_D)^3 + 1.05(r_p\kappa_D)^2 + 0.29(r_p\kappa_D)}{(1+r_p\kappa_D)^4}\right\}$$

Where ρ_i is the number density of ionic charge in the bulk liquid, nZ accounts for the contribution of charged nanoparticles through the number of counterions and $r_p\kappa_D$ stands for the non-dimensional inverse Debye length. κ_D is defined as

$$\kappa_D = \left(\frac{4\pi l_B(\rho_i + nZ)}{1-\phi}\right)^{\frac{1}{2}} \tag{2.25}$$

where the Bjerrum length l_B is $l_B = e^2/(4\pi\varepsilon K_B T)$.

In the model, the kinetic contribution to the effective thermal conductivity was neglected. The specific form of the repulsive DLVO potential which accounts for the electrostatic repulsion between charged spherical nanoparticles was also selected to design the interparticle interaction between various nanoparticles. They analysed the interparticle potential effect on thermal conductivity through calculations involving DLVO interaction between the electric double layers on spherical nanoparticles. These calculations show the importance of long-range repulsive potentials for the enhancement of thermal conductivity of nanofluids.

Yang [45] developed a thermal conductivity model based on the kinetic theory of particles in the fluids under relaxation time approximations. The model takes into account convective heat transfer due to the Brownian motion of nanoparticles. It is

also expressed as a combination of diffusive heat conduction and the particle Brownian motion as

$$k_{eff} = k_{diff} + k_{Brownian} \tag{2.26}$$

where k_{diff} is

$$k_{diff} = \left(1 + 3\Phi \frac{\frac{r_p}{R_b k_{bf}} - 1}{\frac{r_p}{R_b k_{bf}} + 2} \right) k_{bf} \tag{2.27}$$

$$\Phi = (4/3)\pi r_p^3 \tag{2.28}$$

where Φ is the volume of the particle r_p is the particle radius and R_b is the thermal resistance per unit area of the particle/fluid interface. The second term of Eq. (2.26) is corresponded to the convection due to the Brownian motion of the nanoparticles. It is analytically derived from integration of the fluid velocity over the hydrodynamic boundary layer around the Brownian particle and expressed as

$$k_{Brownian} = 157.5\Phi c_f u_p^2 \tau \tag{2.29}$$

where c_f is the heat capacity per unit volume of the fluid, τ is the particle relaxation time, and u_p is the Brownian velocity of the particle of which two former ones are expressed as

$$\tau = \frac{m_p}{6\pi \mu_{bf} r_p} \tag{2.30}$$

$$u_p = \sqrt{\frac{3K_B T}{m_p}} \tag{2.31}$$

where K_B is the Boltzmann constant and m_p is the mass of the particle.

Furthermore, he founded that the relaxation time of particle Brownian motion could be significantly affected by the long-time tail in Brownian motion.

Nie *et al* [46] represented a new valuable mathematical model based on the Green-Kubo linear theory. They used the exact expression for the heat flux vector of the base fluid with the nanoparticles to estimate the contribution of nanoparticle Brownian motion to the thermal conductivity of the nanofluid. They derived an equation for the

contribution of the enhancement of thermal conductivity due to the Brownian motion of a nanoparticle as

$$k_{excess} = \frac{85}{96\pi^2}\frac{\phi K_B^2 T}{r_p^4 \mu} \tag{2.32}$$

Their result represented that the thermal conductivity improvement is proportional to T/μ , where T is the temperature (K) and μ is viscosity (Pa.s). They also found that the Brownian motion contribution to the enhancement of thermal conductivity of nanoparticles is on the order of $10^{-15}\, W/mK$ at temperature of 320 K. Therefore, the contribution of the Brownian motion is negligible in comparison with the value of thermal conductivity of base fluid (water).

Vasu *et al* [47] have developed two correlations for the effective thermal conductivity of Al_2O_3-water and Cu-water nanofluids by using experimental data taken from literature. Their models consider the effects of temperature, volume fraction and nanoparticle size as

$$\frac{k_{nf}}{k_{bf}} = \left(\frac{1}{\nu_p}\sqrt{\frac{18K_B T}{\pi \rho_p d_p}}\right)\phi^{0.05}\left(\frac{k_p}{k_{bf}}\right)^{0.2324} \tag{2.33}$$

$$\frac{k_{nf}}{k_{bf}} = 0.74\left(\frac{1}{\nu_p}\sqrt{\frac{18K_B T}{\pi \rho_p d_p}}\right)\phi^{0.05}\left(\frac{k_p}{k_{bf}}\right)^{0.2324} \tag{2.34}$$

Equations (2.33) and (2.34) are applicable for Al_2O_3-water and Cu-water nanofluids respectively. Although their proposed correlations were able to predict the effective thermal conductivity of nanofluids effectively, the correlations are only valid for the nanofluids whose data were used to formulate the correlation in the range of the data.

Jain *et al* [48] used the Brownian dynamic simulation technique coupled with the Green-Kubo model to calculate the effective thermal conductivity of nanofluids by considering the effect of various parameters. They consist of particles concentration ranging from 0.5 to 3 vol%, particle size ranging from 15 to 150 nm, and temperature ranging from 290 to 320 K. The effect of base fluid hydrodynamic interactions was

UNIVERSITEIT VAN PRETORIA
UNIVERSITY OF PRETORIA
YUNIBESITHI YA PRETORIA

considered through a position-dependent interparticle friction tensor. It was also shown that the simulation based on *N*-coupled Langevin equations is able to involve the effects of different parameters such as particle size, particle concentration and temperature of the fluid on the effective thermal conductivity of nanofluids. A combined parallel model was used for the calculation of the effective thermal conductivity due to the assumption that thermal conduction caused by the motion of nanoparticles and the base fluid molecules occurs in parallel as Eq. (2.20), where k_p is the thermal conductivity owing to the Brownian motion of the nanoparticles and calculated by using the Green-Kubo relation as

$$k_p = \frac{1}{K_B T^2 V} \sum_{j=0}^{i} \left(\frac{1}{3(i-j)} \sum_{ii=0}^{i-j} Q(ii\Delta t).Q[(ii+j)\Delta t] \right) \Delta t \tag{2.35}$$

where T is the temperature, V is the volume of the domain, i is the number of time steps used in the simulation and Δt is the time step. They also concluded that their model can predict the effective thermal conductivity of nanofluids properly where the Brownian motion of the particles is the key mechanism for the enhancement in the thermal conductivity of nanofluids.

Jung and Yoo [49] developed a model to predict the thermal conductivity of nanofluids by using the kinetic theory in order to describe the contribution of the Brownian motion. They also considered the contribution of the interparticle interaction due to the existence of the electrical double layer (EDL). Their model is a modification of the Maxwell conventional conductivity model by adding Brownian motion and electrical double layer effects. Therefore, the model can account for various factors including temperature, particle size, volume fraction, the Brownian motion and interparticle interaction as follows

$$k_{eff} = k_{Maxwell} + k_{Brownian}\left(1 + \frac{k_{EDL}}{k_{Brownian}}\right) \tag{2.36}$$

where $k_{Brownian}$ is the thermal conductivity due to the Brownian motion and k_{EDL} is the thermal conductivity due to the electrical double layer which were expressed, respectively as

$$k_{Brownian} = \frac{N l_p c_v}{3} . \frac{K_B T}{3\pi \mu d_p l_{bf}} \tag{2.37}$$

$$k_{EDL} = \frac{N l_p c_v}{3} \sqrt{\frac{\Gamma q^2 l_p}{\varepsilon_{bf} m_p (r_p \phi^{-1/3})^2}} \tag{2.38}$$

where Γ is Coulomb constant ($9 \times 10^9\, Nm^2/C^2$) and $q\ is$ is electric charge (C). It was shown that the model is applied to Au-water nanofluids satisfactorily with respect to temperature, volume fraction and particle size. In the case of high concentration of Al_2O_3-water nanofluids, the effect of the interparticle interaction is more on enhancing the thermal conductivity due to EDL.

Murshed *et al* [50] developed a combined static and dynamic mechanism-based model to predict the effective thermal conductivity of nanofluids. Their model can count most of the possible parameters such as particle size, nanolayer, particle movements, interactions and surface chemistry of nanoparticles. Furthermore, it was shown that dynamic mechanisms such as particle Brownian motion, particle interactions and surface chemistry are significant when there are smaller-sized nanoparticles as well as low volume fractions. However, the major contributions to the enhancement are from static mechanisms. The model was considered to be the result of both static and dynamic mechanisms as follows:

$$\begin{aligned} k_{eff-nf} &= \left\{ k_{bf} \frac{\phi_p \omega (k_p - \omega k_{bf}) \left[2\left(1+\frac{\delta_{nl}}{2r_p}\right)^3 - \left(1+\frac{\delta_{nl}}{r_p}\right)^3 + 1 \right] + (k_p + 2\omega k_{bf}) \left(1+\frac{\delta_{nl}}{2r_p}\right)^3 \left[\phi_p \left(1+\frac{\delta_{nl}}{r_p}\right)^3 (\omega - 1) + 1 \right]}{\left(1+\frac{\delta_{nl}}{2r_p}\right)^3 (k_p + 2\omega k_{bf}) - (k_p - \omega k_{bf}) \phi_p \left[\left(1+\frac{\delta_{nl}}{2r_p}\right)^3 - \left(1+\frac{\delta_{nl}}{r_p}\right)^3 + 1 \right]} \right\} \\ &+ \left\{ \phi_p^2 \left(1+\frac{\delta_{nl}}{2r_p}\right)^6 k_{bf} \left[3\left(\frac{k_{cp}-k_{bf}}{k_{cp}+2k_{bf}}\right)^2 + \frac{3}{4}\left(\frac{k_{cp}-k_{bf}}{k_{cp}+2k_{bf}}\right)^2 + \frac{9}{16}\left(\frac{k_{cp}-k_{bf}}{k_{cp}+2k_{bf}}\right)^3 \left(\frac{k_{cp}+k_{bf}}{2k_{cp}+3k_{bf}}\right) + \frac{3}{2^6}\left(\frac{k_{cp}-k_{bf}}{k_{cp}+2k_{bf}}\right)^4 \right. \right. \\ &\left. \left. + \cdots \right] \right\} + \left\{ \frac{1}{2} \rho_{cp} c_{cp} d_p \left[\sqrt{\frac{3K_B T \left[1 - 1.5\left(1+\frac{\delta_{nl}}{r_p}\right)^3 \phi_p \right]}{2\pi \rho_{cp} \left(1+\frac{\delta_{nl}}{r_p}\right)^3 r_p^3}} + \frac{G_T}{6\pi\mu \left(1+\frac{\delta_{nl}}{r_p}\right) r_p d_p} \right] \right\} \end{aligned} \tag{2.39}$$

The significant features of the proposed model were summarised as follows:

- The model was developed by considering nanoparticles with a thin interfacial layer together with their static and dynamic mechanisms in the base fluid.

- The second term on the right hand side of Eq. (2.39) stands for the interactions between pairs of spherical nanoparticles in a stationary suspension.

- The third term on the right hand side of Eq. (2.39) represents the effect of particle Brownian motion, particle surface chemistry and inter-particle interactions for $\phi_p > 0.005$. This part is not applicable when $\phi_p < 0.005$, because at such a small volume fraction, the interparticle separation distance is too big to cause any interactions through the Brownian and potential forces of particles.

- In case of no interaction between pairs of nanoparticles and the interfacial layer, the static part of the model reduces to the Maxwell model and when $\phi_p = 0$ the entire model reduces to k_{bf}.

Emami-Meibodi *et al* [51, 52] offered a simple new model in order to count the Brownian motion. The particle size did not matter in their model; therefore, they mentioned that their model could work for any suspension including microparticles and nanoparticles. However, this is approved that at the same volume fraction and condition, the effective thermal conductivity of a nanofluid with smaller particles will be more [53].

Mehta *et al* [54] proposed a theoretical model to predict the thermal conductivity of nanofluids at low volume fraction of particles. The heat transfer contributions from liquid/solid conduction and micro-convection around particles were considered

separately using thermal resistance modelling. The diffusion velocities of particles due to Brownian motion were used for the modelling of micro-convection around the nanoparticles. In their proposed model, the particles were assumed to be spherical and mono-dispersed without agglomeration in the liquid. The model was validated against a variety of experimental data available in the literature for alumina, copper, copper oxide and titanium oxide-based nanofluids for different concentrations of nanoparticles.

Xiao *et al* [55] developed an analytical expression for effective thermal conductivity of nanofluids by considering the effect of heat convection between nanoparticles and liquids due to the Brownian motion of nanoparticles in fluids. The correlation of effective thermal conductivity of nanofluids was given by taking into account the fractal distribution of nanoparticles. The model was expressed as a function of the thermal conductivities of the base fluids and the nanoparticles, the average diameter of nanoparticles, the nanoparticle volume concentration, the fractal dimension of nanoparticles and physical properties of fluids.

Babaei *et al* [56] developed equilibrium molecular dynamics simulations in order to investigate the role of micro-convection on the thermal conductivity of well-dispersed nanofluids. Their results were shown that while individual convective terms in the heat current expression are significant, they essentially cancel each other. Consequently, micro-convection does not contribute noticeably to the thermal conductivity and the predicted thermal conductivity enhancements are consistent with the effective medium theory.

2.3.2. Theoretical models based on nanolayering

Nanofluid structure consists of solid nanoparticles, solid-like liquid layers (known as nanolayers) and a base fluid. An interfacial thermal resistance is present at interfaces of different components of mixtures, which is known as the Kapitza resistance. It has long been known that liquid molecules close to a solid surface form a layered solid-

like structure [57, 58], but little is known about the thermal properties of this nanolayer and the connection of this layer with the base fluid and the solid. According to Yu *et al* [58], the layered molecules are in an intermediate physical state between a solid and a base fluid. Therefore, the solid-like nanolayer of liquid molecules would be expected to lead to a higher thermal conductivity than that of the base fluid. This means that the solid-like nanolayer acts as a thermal bridge between a solid nanoparticle and a base fluid and is therefore the key to enhancing thermal conductivity [59].

Yu and Choi [59] modified the Maxwell equation to calculate the effective thermal conductivity of solid/liquid suspensions, including the effect of the nanolayer. They assumed that the nanolayer around each particle could be combined with the particle to form an equivalent particle and because of the particle volume concentration being so small; there is no overlap of those equivalent particles. According to Feng *et al* [60], this is not realistic, because the liquid molecules surrounding the particle surface form the interfacial layer and the concentration of these adsorbed molecules in the interfacial layer is lower than that of the solid particle. Therefore, the interfacial layer thermal conductivity should be lower than that of the solid particles but higher than that of the liquid. Consequently, they estimated an upper limit for the effect of the interfacial layer by replacing the thermal conductivity of the nanoparticle (k_p) with an equivalent one (k_{pe}), namely thermal nanoparticle thermal conductivity in the Maxwell model as:

$$k_{eff} = \frac{k_{pe} + 2k_{bf} + 2(k_{pe} - k_{bf})(1 + \frac{\delta_{nl}}{r_p})^3\phi}{k_{pe} + 2k_{bf} - (k_{pe} - k_{bf})(1 + \frac{\delta_{nl}}{r_p})^3\phi} k_f \tag{2.40}$$

with:

$$k_{pe} = \left[\frac{\left[2\left(1 - \frac{k_{nl}}{k_p}\right) + \left(1 + \frac{\delta_{nl}}{r_p}\right)^3 (1 + 2\frac{k_{nl}}{k_p})\right]\frac{k_{nl}}{k_p}}{-\left(1 - \frac{k_{nl}}{k_p}\right) + \left(1 + \frac{\delta_{nl}}{r_p}\right)^3 (1 + 2\frac{k_{nl}}{k_p})}\right] k_p \tag{2.41}$$

The model includes the nanolayer which can predict the presence of a nanolayer with a thickness of less than 10 nm.

A renovated Maxwell model, which was proposed by Yu and Choi [59] in 2003, was limited to suspensions with spherical particles. Yu and Choi [61], in 2004, extended the Hamilton-Crosser model suspensions of non-spherical particles to include the effect of the nanolayer as

$$k_{eff} = \left[1 + \frac{D_{esf}.\phi_e\left(\frac{1}{3}\sum_{j=a,b,c}\frac{k_{pj}-k_{bf}}{k_{pj}+(D_{esf}-1)k_{bf}}\right)}{1-\phi_e\left(\frac{1}{3}\sum_{j=a,b,c}\frac{k_{pj}-k_{bf}}{k_{pj}+(D_{esf}-1)k_{bf}}\right)}\right]k_{bf} \tag{2.42}$$

where D_{esf} is the empirical shape factor $D_{esf} = 3\Psi^{-\psi}$, ψ is an empirical parameter depending on the particle sphericity or eccentricity and the particle-to-liquid thermal conductivity ratio and Ψ is the sphericity.

$$k_{pj} = \left\{1 + \frac{k_{se}-k_{sl}}{k_p[V_r.d(j,0)-d(j,v)]-k_{sl}[V_r.d(j,0)-d(j,v)-V_r]}\right\}k_{sl} \tag{2.43}$$

k_{pj} is the equivalent thermal conductivities along the axes of the complex ellipsoid in which $j(=a,b\ and\ c)$ is along the semiaxis directions of the ellipsoid, k_{se} and k_{sl} are the thermal conductivities of the solid ellipsoid and its surrounding layer, V_r is the volumetric ratio and $d(j,v)$ is the depolarisation factor.

ϕ_e is the equivalent volume concentration of complex ellipsoids which is defined as

$$\phi_e = V_r\phi \tag{2.44}$$

where ϕ is a volume concentration of the solid ellipsoids without the surrounding layer. This model can predict the thermal conductivity of nanofluids consisting of carbon nanotubes-in-oil. However, it fails to predict the non-linear behaviour of the effective thermal conductivity of general oxide- and metal-based nanofluids. In the new model, they assumed that the thermal conductivity of the nanolayer around each particle is similar to that of the nanoparticle, which is unrealistic.

UNIVERSITEIT VAN PRETORIA
UNIVERSITY OF PRETORIA
YUNIBESITHI YA PRETORIA

Xue *et al* [62] used non-equilibrium molecular dynamic simulations in which a temperature gradient was imposed, and they determined the thermal resistance of liquid/solid interface. Their simulation indicates that the strength of the bonding between the liquid and the solid atoms plays a key role in determining the interfacial thermal resistance. They also found that the functional dependence of the thermal resistance on the strength of the liquid/solid interactions reveals two distinct regimes. These two regimes are exponential dependence for weak bonding and power law dependence for strong bonding. These two regimes of the Kapitza resistance have profound implications for understanding and designing the thermal properties of nanolayers.

Xue [63] considered the effect of the nanolayer between the solid particle and the base fluid in nanofluids. A new model has been presented for the effective thermal conductivity for nanofluids based on the Maxwell model and average polarisation theory. However, in his model, it is not clear how to determine the depolarisation factor component for the different shapes of particles, and also the thermal conductivity of nanolayers cannot be determined. Another problem with his model is that the predicted thermal conductivity values are matched with experimental data by considering the larger nanolayer thickness, which is unrealistic. Later Yu and Choi [61] showed that Xue's model gave far higher values of thermal conductivity than those given in his work, because Xue used incorrect parameters when comparing his model with that of carbon nanotube-in-oil experimental data. Thus, the validity and accuracy of Xue's model are yet to be established.

Xie *et al* [64] assumed that the interfacial structures formed by liquid molecule layering might play an important role. They investigated the impact of these nanolayers on the effective thermal conductivity of nanofluids and also developed an expression for calculating the enhanced thermal conductivity of nanofluids. They proposed a new formula for the effective thermal conductivity derived from the general solution of the heat conduction equation in spherical coordinates. Although by

that time, there was no available expression for calculating the thermal conductivity of nanolayers, they proposed a new model for the thermal conductivity of a nanolayer as well. For this purpose, they assumed that the thermal conductivity variation in a nanolayer is linear and derived the following equation for the thermal conductivity of a nanolayer:

$$k_{nl} = \frac{k_{bf}\left[\frac{k_p}{k_{bf}}\left(1+\frac{\delta_{nl}}{r_p}\right)-1\right]^2}{\left(\left[\frac{k_p}{k_{bf}}\left(1+\frac{\delta_{nl}}{r_p}\right)-1\right]-\frac{\delta_{nl}}{r_p}\right)\ln\left(1+\left[\frac{k_p}{k_{bf}}\left(1+\frac{\delta_{nl}}{r_p}\right)-1\right]\right)+\frac{\delta_{nl}}{r_p}\left[\frac{k_p}{k_{bf}}\left(1+\frac{\delta_{nl}}{r_p}\right)-1\right]} \tag{2.45}$$

Therefore, the average thermal conductivity of a nanolayer depends on the thermal conductivity of the fluid, the reduced thermal conductivity of the nanoparticle and the ratio of the nanolayer thickness to the original particle radius. They also proposed a formula for the effective thermal conductivity of a nanofluid by applying Fourier's law of heat conduction based on the assumption that a nanofluid is statistically homogeneous and isotropic. It is obtained as

$$\frac{k_{eff}-k_{bf}}{k_{bf}} = 3\Theta\phi_{eff} + \frac{3\Theta^2\phi_{eff}^2}{1-\Theta\phi_{eff}} \tag{2.46}$$

with

$$\Theta = \frac{\left(\frac{k_{nl}-k_{bf}}{k_{nl}+2k_{bf}}\right)\left[(1+\frac{\delta_{nl}}{r_p})^3-\left[\frac{(k_p-k_{nl})(k_{bf}+2k_{nl})}{(k_p+2k_{nl})(k_{bf}-k_{nl})}\right]\right]}{(1+\frac{\delta_{nl}}{r_p})^3+2\left[\left(\frac{k_{nl}-k_{bf}}{k_{nl}+2k_{bf}}\right)\left(\frac{k_p-k_{nl}}{k_p+2k_{nl}}\right)\right]} \tag{2.47}$$

This equation is the proposed model deduced for evaluating the effect of the nanolayer on the effective thermal conductivity of nanoparticle/fluid mixtures. In order to check the validity, they used experimental data of Cu-in-EG, CuO-in-EG, and alumina-in-water and the results show that the proposed model predicts these experimental data quite well. However, similar to the Yu and Choi [59, 61] and Xue [63] models, this empirical model has to be fitted with experimental data by adjusting two fitting parameters. They did not also consider any dynamic mechanism like the Brownian motion.

Leong *et al* [65] also proposed a new model for the effective thermal conductivity of a nanofluid according to the heat conduction in a nanofluid based on Fourier's law of considering the effect of the interfacial layer as

$$k_{eff} = \frac{(k_p - k_{nl})\phi_{nl}k_{nl}\left[2\left(1+\frac{\delta_{nl}}{2r_p}\right)^3 - \left(1+\frac{\delta_{nl}}{r_p}\right)^3 + 1\right] + (k_p + 2k_{nl})\left(1+\frac{\delta_{nl}}{2r_p}\right)^3\left[\phi_{nl}\left(1+\frac{\delta_{nl}}{r_p}\right)^3(k_{nl} - k_{bf}) + k_{bf}\right]}{\left(1+\frac{\delta_{nl}}{2r_p}\right)^3(k_p + 2k_{nl}) - (k_p - k_{nl})\phi_{nl}\left[\left(1+\frac{\delta_{nl}}{2r_p}\right)^3 + \left(1+\frac{\delta_{nl}}{r_p}\right)^3 - 1\right]} \tag{2.48}$$

where $\phi_{nl} = \phi_p\left[\left(1+\frac{\delta_{nl}}{r_p}\right)^3 - 1\right]$

They compared their model with some experimental data of alumina-in-DI water, alumina-in-EG, CuO-in-DI water and CuO-in-EG and concluded that the present model can predict the effective thermal conductivity of nanofluids better than previous models. The improved results come from the point where the temperature gradient at the boundary of the nanolayer is discontinuous. However, a limitation of their model is that they have to set the thermal conductivity and thickness of the nanolayer to predict the experimental data, and they also assumed that the particles are apart and that no interaction occurs between them.

Li *et al* [66] investigated the molecular layer of liquid/solid interfaces of a nanofluid with an equilibrium molecular dynamic simulation method. They assumed that the nanoparticles are spherical and developed their model by tracking the positions of the nanoparticle and the liquid atoms around the nanoparticles. They estimated that the thickness of the nanolayer is approximately 0.5 nm and will move with the Brownian motion of the nanoparticle. Although this finding is very important to the understanding of the thermal property of a nanofluid, their investigation is, however, not complete. Their nanofluid consisted of 1.5% (volume fraction) of copper nanoparticles in an argon base fluid; therefore, it needs to be evaluated for different cases.

UNIVERSITEIT VAN PRETORIA
UNIVERSITY OF PRETORIA
YUNIBESITHI YA PRETORIA

Zhou and Gao [67] investigated the effect of interfacial nanolayers and the mutual interaction of nearest-neighbouring inclusions on the effective thermal conductivity of nanofluids. Firstly, differential effective dipole approximation was generalised to obtain the equivalent thermal conductivity of the coated nanoparticles with graded nanolayers. The multiple image method was then employed to investigate the effect of mutual interaction between nanoparticles on the thermal conductivity of nanofluids. The dependence of effective thermal conductivity on volume fraction, radius of nanoparticles, thickness of the nanoshell and thermal conductivity of the constituents was shown by an analytical correlation as

$$\frac{k_{eff}}{k_{bf}} = 1 + \frac{3\phi_t b\left[\frac{\mathbf{P}_L + 2\mathbf{P}_T}{3\mathbf{P}_0}\right]}{1 - \phi_t b\left[\frac{\mathbf{P}_L + 2\mathbf{P}_T}{3\mathbf{P}_0}\right]} \tag{2.49}$$

where $b = \left[\bar{k}(r_p + \delta_{nl}) - k_{bf}\right]/\left[\bar{k}(r_p + \delta_{nl}) + 2k_{bf}\right]$ is a dipole factor and ϕ_t is the total volume fraction of the coated particles which include both original nanoparticles and graded nanolayers, expressed as

$$\phi_t = \frac{4}{3}\pi(r_p + \delta_{nl})^3 n_v = \phi_o\left(1 + \frac{\delta_{nl}}{r_p}\right)^3 \tag{2.50}$$

where $\phi_o = 4/3\,\pi r_p^3 n_v$ is the original volume fraction of nanoparticles and n_v is the number of complicated particles per volume.

Lin *et al* [68] conducted a molecular dynamics (MD) simulation for thermal conductivity of Cu- EG (ethylene glycol) by considering the role of the particle/fluid interface effect as the main mechanism of the thermal conductivity enhancement. The Layer-Maxwell model for effective thermal conductivity was developed by taking into account the distinct thermal conductivity in the nanolayers around nanoparticles obtained from MD simulations.

Although the nanolayer effect and its mechanism play an important role in the thermal conductivity enhancement of nanofluids, the experiments and simulations [57, 58 and 66] showed that the thickness of the nanolayer is only in the order of a few atomic

distances (0.5 to 1 nm). Thus, it does not seem to be the only factor for the enhancement [1].

2.3.3. Theoretical models based on clustering

There are two methods for producing nanofluids: the one-step direct evaporation method represents the direct formation of the nanoparticles inside the base fluids; and the two-step method represents the formation of nanoparticles and subsequent dispersion of the nanoparticles in the base fluid. In the two-step method, the nanoparticles are separately produced. Thereafter, when the nanoparticles are being dispersed into the base fluid it should be treated with various physical treatment techniques to ensure a homogeneous dispersion. Different types of physical treatment devices that are being used are the stirrer, the ultrasonic bath, the ultrasonic disruptor and the high-pressure homogeniser [69]. These methods were used for preventing the nanoparticles to get agglomerated at the first step of nanofluid production because the nanoparticles as powder get agglomerated to each other rapidly. When the nanofluid is treated by sonication (high frequency sound waves typically used to aid the dispersion of nanoparticles in a liquid) or other physical techniques, the cluster breaks into primary nanoparticles [70]. There have been some works on the effect of sonication time on the thermal conductivity of nanofluids [20].

Karthikeyan *et al* [70] experimentally studied the effect of clustering on the thermal conductivity of CuO nanoparticles dispersed into water. They had shown that the cluster size has a significant effect on the thermal conductivity of CuO-Water nanofluids and the thermal conductivity of nanofluid decrease with elapsed time due to the clustering of CuO nanoparticles. Furthermore, they indicated that the finer particle size and mono-dispersity of nanoparticles causes larger enhancement in thermal conductivity of nanofluids. They also noted that in general, clustering may exert a negative effect on heat transfer enhancement. The nanoclusters are likely to settle in the fluid due to their larger mass that results in a particle gradient in the fluid, particularly at low volume fractions, by settling small particles out of the liquid and

UNIVERSITEIT VAN PRETORIA
UNIVERSITY OF PRETORIA
YUNIBESITHI YA PRETORIA

creating large regions of particle free-liquid with high thermal resistances. The particle-free zones have higher thermal resistances compared with the particle-rich zone. The suppression of clustering of the nanoparticles is also very important for designing effective heat transfer fluids. There are some reports on the formation of clusters and aggregates in the fluid, which enhances the thermal conductivity of the fluid; however, some others mention that the thermal conductivity decreases with elapsed time due to the clustering of nanoparticles.

According to the report of Wang *et al* [71] in 2003, these cluster structures act like local percolation structures and therefore add to the effective thermal conductivity enhancement of nanofluids (this is contrary to the observation of Karthikeyan *et al* [70]). They proposed a method for modelling the effective thermal conductivity of nanofluids based on the effective medium approximation and the fractal theory for the description of nanoparticle clusters and its radial distributions. They modified the Maxwell model by taking into account the size effect and the surface adsorption of nanoparticles.

Their model, however, requires the thermal conductivity of particle clusters and their radius distribution to be determined numerically [72]. Their fractal model predicts the trend for variation of the effective thermal conductivity with diluted suspensions of nanoparticles well and fits the experimental data for CuO-in-DI water successfully. In addition, this model has yet to be validated with experimental results. The other model was proposed by Prasher *et al* [73], and shows that the thermal conductivity of nanofluids based purely on conduction phenomenon can be significantly enhanced as a result of the aggregation of the nanoparticles. These two groups of researchers believe that the cluster effect can enhance the thermal conductivity of nanofluids because the heat transport can be much faster along the backbone of the clusters. The important thing is that the cluster sizes are critical to the thermal performance of nanofluids. When the cluster sizes increase, the nanoclusters are likely to settle in the fluids due to larger mass, which results in gradients in the particle concentrations.

UNIVERSITEIT VAN PRETORIA
UNIVERSITY OF PRETORIA
YUNIBESITHI YA PRETORIA

Therefore, the cluster size should not be more than its critical size for this purpose. There are two major methods to make the attractive force between particles balanced, and hence to prevent particle aggregation. These two methods are electrostatic stabilisation and steric stabilisation.

Feng *et al* [60] proposed a new model for the effective thermal conductivity of nanofluids by considering the nanolayer and nanoparticle aggregation. The model is expressed as a function of the thickness of the nanolayer, the nanoparticle size, the nanoparticle volume fraction and the thermal conductivities of the suspended nanoparticles and the base fluid. For determining the effect of aggregation, they divided the aggregation into two parts: the first is the coherent fluid and the other is a quarter of the column. The column also includes two parts: the touching particles and the base fluid. They used the thermal-electrical analogy technique and the one-dimensional heat conduction model for calculating. The theoretical predictions of the effective thermal conductivities of nanofluids are shown to be in good agreement with experimental data of CuO-in-water, alumina-in-water, CuO-in-EG, and alumina-in-EG.

Okeke *et al* [74] conducted a numerical investigation into thermal conductivity of water-based nanofluids of Al_2O_3, CuO and TiO_2 considering the particle clustering and interfacial layer thickness as effective parameters. Regardless the type of nanofluid, it has been shown that the mode of aggregation plays a major rule in thermal enhancement by influencing the aggregation rate and compactness of the aggregates. In their study they showed the sensitiveness of thermal conductivity to particle aggregation as a possible mechanism for thermal enhancement and relations between aggregation mode, aggregate size and compactness of the aggregates and thermal enhancement of the surrounding nanofluid.

Witharana *et al* [75], studied aggregation and the settling behaviour of nanofluids near their iso-electric points by using small angle X-ray scattering (SAXS) experiments

and optical microscopy for a rapidly settling poly-disperse spherical alumina (Al_2O_3) nanoparticles in the size range of 10–100 nm were dispersed in water at room temperature. Two settling regimes were observed regarding photographic studies and the corresponding settling curve; one showing the settling of very large ($\sim 22\ \mu m$) objects and the second one showing a slower settling rate of relatively smaller ($\sim 6\ \mu m$) objects. They also indicated that using the SAXS technique provided valuable information for this unstable suspension which was not possible to obtain from any existing mechanism. Optical microscopy images were also produced on drying and dried droplets extracted from the suspension at various times. Dried deposits showed the rapid decrease in the number of very large particles with time which qualitatively validates the SAXS prediction, and therefore its suitability as a tool to study unstable poly-disperse colloids.

2.3.4. Hybrid models

There is a lack of reported research on hybrid-combined models for the effective thermal conductivity that takes into consideration all major mechanisms plus other important recognised effects like particle settling down time [76–79], temperature [80], pH [81–83], dispersion [84] and the particle size effect on surface contact of liquid/particle interaction [46, 85–87]. However, the following models are valuable because they included some of these effects.

Avsec [88] developed a combined model based on statistical nanomechanics. His model accounts for influences such as the formation of the nanolayer around nanoparticles and the Brownian motion. He modified the model of Yu and Choi [59] for the nanolayer part of his model by expressing the effective volume fraction as

$$\phi_{eff} = \phi\left(1 + \frac{\delta_{nl}}{r_p}\right)^3 \tag{2.51}$$

However, it has been assumed that the equivalent thermal conductivity of the equivalent particles had the same value as the thermal conductivity of the particle. He

also modified Prasher's equation [89] for influence of the Brownian motion and then offered the thermal conductivity for nanofluids as

$$k_{eff} = k_{bf}\left[\frac{k_p + \left(\frac{3}{\Psi}-1\right)k_{bf} - \left(\frac{3}{\Psi}-1\right)\phi_{eff}(k_{bf}-k_p)}{k_p + \left(\frac{3}{\Psi}-1\right)k_{bf} + \phi_{eff}(k_{bf}-k_p)}\right]\left(1 + C_{ft}\mathrm{Re}^{O_{co}}\mathrm{Pr}^{S_{co}}\right) \tag{2.52}$$

The model is compared with the experimental works from literature for copper nanoparticles (10 nm) in an ethylene-glycol base and also for aluminium oxide nanoparticles in a water base. Although he found good agreement with those two cases, working with the equation including fitting parameter is hard in general.

Murshed *et al* [50] offered a combined model, which included the effects of particle size, nanolayer, Brownian motion, and particle surface chemistry and interaction potential which are the static and dynamic mechanisms responsible for the enhanced effective thermal conductivity of nanofluids. They divided the effective thermal conductivity into two parts consisting of the static-based and the dynamic part (particle Brownian motion, particle surface chemistry and interparticle interactions), i.e. $k_{eff} = k_{static} + k_{dynamic}$, or

$$\begin{aligned} k_{eff-nf} &= \left\{ k_{bf}\frac{\phi_p\omega(k_p-\omega k_{bf})\left[2\left(1+\frac{\delta_{nl}}{2r_p}\right)^3-\left(1+\frac{\delta_{nl}}{r_p}\right)^3+1\right]+(k_p+2\omega k_{bf})\left(1+\frac{\delta_{nl}}{2r_p}\right)^3\left[\phi_p\left(1+\frac{\delta_{nl}}{r_p}\right)^3(\omega-1)+1\right]}{\left(1+\frac{\delta_{nl}}{2r_p}\right)^3(k_p+2\omega k_{bf})-(k_p-\omega k_{bf})\phi_p\left[\left(1+\frac{\delta_{nl}}{2r_p}\right)^3-\left(1+\frac{\delta_{nl}}{r_p}\right)^3+1\right]}\right. \\ &+\left\{\phi_p^2\left(1+\frac{\delta_{nl}}{2r_p}\right)^6 k_{bf}\left[3\Lambda^2+\frac{3\Lambda^2}{2^2}+\frac{3^2\Lambda^3}{2^4}\left(\frac{k_{cp}+k_{bf}}{2k_{cp}+3k_{bf}}\right)+\frac{3\Lambda^4}{2^6}+\cdots\right]\right\} \\ &\left.+\left\{\frac{1}{2}\rho_{cp}c_{cp}d_p\left[\sqrt{\frac{3K_BT\left[1-1.5\left(1+\frac{\delta_{nl}}{r_p}\right)^3\phi_p\right]}{2\pi\rho_{cp}\left(1+\frac{\delta_{nl}}{r_p}\right)^3 r_p^3}}+\frac{G_T}{6\pi\mu\left(1+\frac{\delta_{nl}}{r_p}\right)r_p d_p}\right]\right\}\right. \end{aligned} \tag{2.53}$$

$$\text{where } k_{cp} = k_{nl}\left[\frac{2(k_p-k_{nl})+\left(1+\frac{\delta_{nl}}{r_p}\right)^3(k_p-k_{nl})}{(k_{nl}-k_p)+\left(1+\frac{\delta_{nl}}{r_p}\right)^3(k_p+2k_{nl})}\right],\ \Lambda = \frac{k_{cp}-k_{bf}}{k_{cp}+2k_{bf}} \tag{2.54}$$

UNIVERSITEIT VAN PRETORIA
UNIVERSITY OF PRETORIA
YUNIBESITHI YA PRETORIA

The third term on the right-hand side of Eq. (2.53) takes into account the effect of the dynamic part on effective thermal conductivity, which is applicable for nanoparticle volume fractions more than 0.5%. They compared their model with their experiments as well as with experiments in literature consisting of TiO_2 (15 nm)/DIW-based, Al_2O_3/DIW-based, Al_2O_3/water-based, CuO/water-based and Fe_3O_4/water-based nanofluids. They found a good agreement. They assumed that the nanolayer thermal conductivity (ω), can be between 1.1 and 2.5 without a sensible logic procedure, however, this model needs to be validated in the case of varying each parameter (particle size, nanolayer, Brownian motion, interaction and particle surface chemistry) when the others stay constant with proper experiments. However, this model could not take into consideration the effect of clustering or settling time.

Li *et al* [90] investigated the mechanisms of thermal conductivity of nanofluids, including particle agglomeration, Brownian motion effects and viscosity as well as the effect of temperature. Their results showed that Brownian motion is not enough to describe the temperature dependence of the thermal conductivity of nanofluids. They indicated that the change of particle agglomeration and viscosity with temperature are also important factors. The reduction of the particle surface energy as a result of temperature increase would decrease the agglomeration of nanoparticles, and the reduction of viscosity would improve the Brownian motion. By taking into account the effects of the nano-scale, the effects of the interfacial interaction between nanoparticles and liquid as well as Brownian motion, the model was expressed as

$$k_{eff} = \frac{k_{pn} + 2\,k_{bf} - 2\phi_{eff}\,(k_{bf} - k_{pn})}{k_{pn} + 2\,k_{bf} + \phi_{eff}\,(k_{bf} - k_{pn})}\,k_{bf} + \frac{\rho\phi_{eff}\,c_p}{2}\sqrt{\frac{k_B T}{3\pi\, r_c \mu_{nf}}} \tag{2.55}$$

Nabi and Shirani [91] introduced a new theoretical model for thermal conductivity of nanofluids by taking into account the Brownian motion and resulted in micro mixing of nanoparticles and clusters, as well as aggregation kinetics of nanoparticles and clusters. The proposed model was expressed as a combination of static and dynamic parts diffusive as

$$k_{eff} = k_{static} + k_{dynamic} \tag{2.56}$$

where Maxwell's was used for the static part k_{static} and $k_{dynamic}$ was evaluated as

$$k_{dynamic} = 9064(\rho c_v) \times \frac{k_{bf} T}{\mu\, r_p}\left[\beta_p\left(\phi - \phi^{\frac{d_l - d_f}{d_f - 3}}\right) + \beta_a \phi^{\frac{d_l - d_f}{d_f - 3}}\left(1 + \frac{t}{t_{br}}\right)^{-\frac{1}{3}}\right] \tag{2.57}$$

where d_l is the fractal dimension of backbones and β_p and β_a are semi-empirical parameters which represent the fraction of the liquid volume travelling respectively with a particle and a cluster.

Li *et al* [92] modified the Li-Qu-Feng [90] model in order to calculate thermal conductivity of CNT nanofluids. They showed that the Li-Qu-Feng [90] model underestimates the experiment results and is unable to predict thermal conductivity of CNT nanofluids while no shape factor was included into the model for the special shape of CNTs. Their model takes into account the effect of liquid layering, particle clustering, particle shape factor, Brownian motion and viscosity of base fluid as

$$k_{eff} = \frac{k_{CNTe} + \left(Q_{esf} - 1\right) k_{bf} + \left(Q_{esf} - 1\right) \phi_{eff}\left(k_{CNTe} - k_{bf}\right)}{k_{CNTe} + \left(Q_{esf} - 1\right) k_{bf} - \phi_{eff}\left(k_{CNTe} - k_{bf}\right)} k_{bf} + \frac{\rho \phi_{eff}\, c_p}{2}\sqrt{\frac{k_B T}{3\pi\, r_c \mu_{nf}}} \tag{2.58}$$

where k_{CNTe} and ϕ_{eff} are effective thermal conductivity of CNTs and effective volume fraction of nanoparticles respectively considering the nanolayer of nanoparticles. Q_{esf} is the empirical shape factor which considered Q_{esf} = 6 for CNTs. The predicted thermal conductivities of VFBN containing CNTs by the modified Li-Qu-Feng model were compared with the experimental data as well as the Maxwell model [93], Hamilton-Crosser model [94], Jang-Choi model [95] and the Li-Qu-Feng model [90]. The results showed an excellent agreement with the measured data. The authors mentioned that their proposed model is more suitable for nanofluids with special shapes other than spherical nanoparticles.

Table 2-1 and Table 2-2 summarise the conventional and dynamic models for the thermal conductivity of nanofluids respectively and show the model equations and key parameters required for determining thermal conductivity and remarks.

UNIVERSITEIT VAN PRETORIA
UNIVERSITY OF PRETORIA
YUNIBESITHI YA PRETORIA

Table 2-1: Summary of the studies on the theoretical models for thermal conductivity of nanofluids – conventional models

Models	Formulation	Remarks
Maxwell [93]	$\frac{k_{nf}}{k_{bf}} = 1 + \frac{3\left(\frac{k_p}{k_{bf}} - 1\right)\phi}{\left(\frac{k_p}{k_{bf}} + 2\right) - \left(\frac{k_p}{k_{bf}} - 1\right)\phi}$	*Spherical particles*
Hamilton-Crosser [94]	$\frac{k_{nf}}{k_{bf}} = 1 + \frac{\frac{k_p}{k_{bf}} + (E_{esf} - 1) - (E_{esf} - 1)\left(1 - \frac{k_p}{k_{bf}}\right)\phi}{\frac{k_p}{k_{bf}} + (E_{esf} - 1) + \left(1 - \frac{k_p}{k_{bf}}\right)\phi}$	*$E_{esf} = 3$ for spherical and $E_{esf} = 6$ for cylindrical-shaped particles*
Wasp [36]	$\frac{k_{nf}}{k_{bf}} = \frac{k_p + 2\,k_{bf} - 2\phi(k_{bf} - k_p)}{k_p + 2\,k_{bf} + \phi(k_{bf} - k_p)}$	*Wasp's model is a special case with the sphericity 1.0 of the Hamilton-Crosser's model.*
Bruggeman [96]	$\left(\frac{1}{\phi + 1} - 1\right)\left(\frac{k_p - k_{eff}}{k_p + 2\,k_{eff}}\right) = \left(\frac{k_{bf} - k_{eff}}{k_{bf} + 2\,k_{eff}}\right)$	
Lu-Lin [97]	$\frac{k_{nf}}{k_{bf}} = 1 + \left(\frac{k_p}{k_{bf}}\right)\phi + b\,\phi^2$	*Spherical and non-spherical particles*
Li *et al* [90]	$k_{eff} = \frac{k_{CNTe} + 2\,k_{bf} + 2\,\phi_{eff}\,(k_{CNTe} - k_{bf})}{k_{CNTe} + 2\,k_{bf} - \phi_{eff}\,(k_{CNTe} - k_{bf})}\,k_{bf} + \frac{\rho\phi_{eff}\,c_p}{2}\sqrt{\frac{k_B T}{3\pi\, r_c \mu_{nf}}}$	
Jeffrey [98]	$\frac{k_{nf}}{k_{bf}} = 1 + 3\left(\frac{\frac{k_p}{k_{bf}} - 1}{\frac{k_p}{k_{bf}} + 2}\right)\phi + \left(3\left(\frac{\frac{k_p}{k_{bf}} - 1}{\frac{k_p}{k_{bf}} + 2}\right)^2 + \frac{3}{4}\left(\frac{\frac{k_p}{k_{bf}} - 1}{\frac{k_p}{k_{bf}} + 2}\right)^2 + \frac{9}{16}\left(\frac{\frac{k_p}{k_{bf}} - 1}{\frac{k_p}{k_{bf}} + 2}\right)^3\left(\frac{\frac{k_p}{k_{bf}} + 2}{\frac{k_p}{k_{bf}} + 3}\right) \ldots .\right)\phi^2$	
Davis [99]	$\frac{k_{nf}}{k_{bf}} = 1 + \frac{3\left(\frac{k_p}{k_{bf}} - 1\right)\phi}{\left(\frac{k_p}{k_{bf}} + 2\right) - \left(\frac{k_p}{k_{bf}} - 1\right)\phi}\left(\phi + f\left(\frac{k_p}{k_{bf}}\right)\phi^2 + O(\phi^3)\right)$	

UNIVERSITEIT VAN PRETORIA
UNIVERSITY OF PRETORIA
YUNIBESITHI YA PRETORIA

Sastry *et al* [100]	$k_{eff} = \frac{L_{cell}}{A_{cell}} \left\{ \sum_{j=1}^{n_{c-n}} \frac{\left[\frac{\left(\frac{4L_{cell}}{k_{CNT}\pi d_o^2} \right) + 2R_C}{N_{p-c}} \right] R_{Fi,P}}{\left[\frac{\left(\frac{4L_{cell}}{k_{CNT}\pi d_o^2} \right) + 2R_C}{N_{p-c}} \right] + R_{Fi,P}} \right\}$	
Li *et al* [92]	$k_{eff} = \frac{k_{CNTe} + (Q_{esf} - 1)\, k_{bf} + (Q_{esf} - 1)\phi_{eff}\,(k_{CNTe} - k_{bf})}{k_{CNTe} + (Q_{esf} - 1)\, k_{bf} - \phi_{eff}\,(k_{CNTe} - k_{bf})}\, k_{bf} + \frac{\rho \phi_{eff}\, c_p}{2} \sqrt{\frac{k_B T}{3\pi\, r_c \mu_{nf}}}$	*Q_{esf} is the empirical-shaped factor (for carbon nanotubes, Q_{esf} = 6)*
Syam Sundar *et al* [101]	$k_{nf} = k_{bf}(1 + 10.5\phi)^{0.1051}$ Fe_2O_3 where $0 < \phi < 2\%$ and $20\ ^oC < T < 60\ ^oC$	

UNIVERSITEIT VAN PRETORIA
UNIVERSITY OF PRETORIA
YUNIBESITHI YA PRETORIA

Table 2-2: Summary of the studies on the theoretical models for thermal conductivity of nanofluids – dynamic models

Models	Formulation	Remarks
Xuan *et al.* [34]	$\frac{k_{eff}}{k_{bf}} = \frac{k_p + 2k_{bf} - 2\phi(k_{bf} - k_p)}{k_p + 2k_{bf} + \phi(k_{bf} - k_p)} + \frac{\rho_p \phi\, c_p}{2k_{bf}}\sqrt{\frac{K_B T}{3\pi\mu r_c}}$	
Jang-Choi [95]	$k_{eff} = k_{bf}(1-\phi_{eff}) + Bk_p\phi_{eff} + C_{pco}\frac{d_{bf}}{d_p}k_{bf}\mathrm{Re}_{d_p}{}^2\phi_{eff}$	*where B is a constant for considering the Kapitza resistance per unit area and the Reynolds number is* $Re_{d_p} = \frac{D_0\, d_p}{l_{bf}\,\nu}$
Kumar *et al.* [102]	$\frac{k_{eff}}{k_{bf}} = 1 + C_{co}\bar{u}_p\frac{\phi\, r_{bf}}{k_{bf}(1-\phi)r_p}$	
Koo and Kleinstreuer [35]	$k_{eff} = \left[\frac{k_p + 2k_{bf} - 2\phi(k_{bf} - k_p)}{k_p + 2k_{bf} + \phi(k_{bf} - k_p)}\right]k_{bf} + \left[5\times 10^4 \beta\phi_p\rho_{bf}c_{bf}\sqrt{\frac{K_B T}{\rho_p d_p}}f(T,\phi_p,etc.)\right]$	*For Al_2O_3-water nanofluids ($1\% < \phi_p$),* $\beta = 0.0017(100\phi_p)^{-0.0841}$ $f(T,\phi) = (-6.04\phi_p + 0.4705)T + (1722.3\phi_p - 134.63)$ *and it is valid for* $1\% < \phi_p < 4\%$ *and* $300\ K < T < 325\ K$.
Prasher *et al.* [37]	$k_{eff} = (1 + A_{eco}\,\mathrm{Re}^{M_{eco}}\,\mathrm{Pr}^{0.333}\,\phi)\left[\frac{k_p + 2k_{bf} + 2(k_p - k_{bf})\phi}{k_p + 2k_{bf} - (k_p - k_{bf})\phi}\right]k_{bf}$	
Bhattacharya *et al.* [38]	$k_{eff} = (1 + A_{eco}\,\mathrm{Re}^{M_{eco}}\,\mathrm{Pr}^{0.333}\,\phi)\left(\frac{[k_p(1+2\alpha) + 2k_m] + 2\phi[k_p(1-\alpha) - k_m]}{[k_p(1+2\alpha) + 2k_m] - \phi[k_p(1-\alpha) - k_m]}\right)k_{bf}$	
Xu *et al.* [39]	$\frac{k_{eff}}{k_{bf}} = \frac{k_p + 2k_{bf} - 2\phi(k_{bf} - k_p)}{k_p + 2k_{bf} + \phi(k_{bf} - k_p)} + H_{co}\frac{Nu\, d_{bf}}{\mathrm{Pr}}\cdot\frac{(2-D_f)D_f}{(1-D_f)^2}\frac{\left[\left(\frac{d_{max}}{d_{min}}\right)^{1-D_f} - 1\right]^2}{\left[\left(\frac{d_{max}}{d_{min}}\right)^{2-D_f} - 1\right]}\frac{1}{\bar{d}_p}$	
Vladkov and Barrat [40]	$\frac{k_{eff}}{k_{bf}} = \frac{\left(\frac{k_p}{k_{bf}}(1+2\Omega)+2\right) + 2\phi\left(\frac{k_p}{k_{bf}}(1-\Omega)-1\right)}{\left(\frac{k_p}{k_{bf}}(1+2\Omega)+2\right) - \phi\left(\frac{k_p}{k_{bf}}(1-\Omega)-1\right)}$	*$\Omega = \varsigma k_{bf}/r_p$ is the ratio between the Kapitza length (equivalent thermal thickness of the interface) and the particle radius.*
Yu-Hua *et al.* [43]	$\frac{k_{eff}}{k_{bf}} = \frac{k_{p_{eff}} + 2k_{bf} - 2\phi_{eff}(k_{bf} - k_{p_{eff}})}{k_{p_{eff}} + 2k_{bf} + \phi_{eff}(k_{bf} - k_{p_{eff}})} + \frac{\rho_p\phi_{eff}\, c_p}{2k_{bf}}\sqrt{\frac{K_B T}{3\pi\mu r_c}}$	

UNIVERSITEIT VAN PRETORIA
UNIVERSITY OF PRETORIA
YUNIBESITHI YA PRETORIA

Shukla and Dhir [44]	$k_{eff} = \left\{\frac{k_p + 2k_{bf} + 2\phi(k_p - k_{bf})}{k_p + 2k_{bf} - \phi(k_p - k_{bf})}\right\} k_{bf} + \phi\frac{\rho_p c_p K_B T}{\gamma} + \left\{\frac{nK_B^2 T}{\gamma}\right\} \times \left\{\frac{(1-\phi)Z}{8(1+(\rho_i/nZ))}\right\}\left\{\frac{3.29(r_p\kappa_D)^2 + 3.61(r_p\kappa_D) + 1.89}{a\kappa_D(1+r_p\kappa_D)^2}\right\} + \left\{\frac{\rho_p c_p K_B T}{\gamma}\right\}\left\{\frac{(1-\phi)Z}{16(1+(\rho_i/nZ))}\right\} \times \left\{\frac{9.87(r_p\kappa_D)^2 + 21.64(r_p\kappa_D) + 17.05}{r_p\kappa_D(1+r_p\kappa_D)^2}\right\} + \left\{\frac{\rho_p c_p K_B T}{\gamma}\right\}\left\{\frac{(1-\phi)^2 Z^2}{48(1+(\rho_i/nZ))^2}\right\} \times \left\{\frac{1.92(r_p\kappa_D)^4 + 1.80(r_p\kappa_D)^3 + 1.05(r_p\kappa_D)^2 + 0.29(r_p\kappa_D)}{(1+r_p\kappa_D)^4}\right\}$	
Yang [45]	$k_{eff} = \left[1 + 3\phi_p \frac{\left(\frac{r_p}{R_{tr}k_{bf}}\right) - 1}{\left(\frac{r_p}{R_{tr}k_{bf}}\right) + 2}\right] k_{bf} + 157.5\phi_p c_f u_p \tau$	
Murshed *et al*. [103]	$k_{eff} = \frac{(k_p - k_{nl})\phi_p k_{nl}(2\Pi_2{}^3 - \Pi_1{}^3 + 1) + (k_p + 2k_{nl})\Pi_2{}^3\{\phi_p\Pi_1{}^3(k_{nl} - k_p) + k_{bf}\}}{(k_p + 2k_{nl})\Pi_2{}^3 - (k_p - k_{nl})\phi_p(\Pi_2{}^3 + \Pi_1{}^3 - 1)}$	*spherical nanoparticles* $\Pi_1 = 1 + \frac{\delta_{nl}}{r_p}$, $\Pi_2 = 1 + \frac{\delta_{nl}}{2r_p}$
Murshed *et al*. [103]	$k_{eff} = \frac{(k_p - k_{nl})\phi_p k_{nl}(\Pi_2{}^2 - \Pi_1{}^2 + 1) + (k_p + 2k_{nl})\Pi_2{}^2\{\phi_p\Pi_1{}^2(k_{nl} - k_p) + k_{bf}\}}{(k_p + 2k_{nl})\Pi_2{}^2 - (k_p - k_{nl})\phi_p(\Pi_2{}^2 + \Pi_1{}^2 - 1)}$	*cylindrical nanoparticles* $\Pi_1 = 1 + \frac{\delta_{nl}}{r_p}$, $\Pi_2 = 1 + \frac{\delta_{nl}}{2r_p}$
Shima *et al.* [104]	$\frac{k_{nf}}{k_{bf}} = (1 + p_{co}Re^{p_{sde}}Pr^{0.333}\phi)\left[\frac{1 + 2\left(\frac{k_p - k_{bf}}{k_p + 2k_{bf}}\right)\phi}{1 - \left(\frac{k_p - k_{bf}}{k_p + 2k_{bf}}\right)\phi}\right]$	

Jung and Yoo [49]	$$k_{eff} = \left[1 + \frac{3\left(\frac{k_p}{k_{bf}} - 1\right)\phi}{\left(\frac{k_p}{k_{bf}} + 2\right) - \left(\frac{k_p}{k_{bf}} - 1\right)\phi}\right] k_{bf} + \left(\frac{Nl_p c_v}{3} \cdot \frac{K_B T}{3\pi\mu d_p l_{bf}}\right)\left[1 + \frac{\frac{Nl_p c_v}{3}\sqrt{\frac{\Gamma q^2 l_p}{\varepsilon_{bf} m_p (r_p \phi_p^{-1/3})^2}}}{\frac{Nl_p c_v}{3} \cdot \frac{K_B T}{3\pi\mu_{bf} d_p l_{bf}}}\right]$$	
Yu and Choi [59]	$$k_{eff} = \frac{k_{pe} + 2k_{bf} + 2(k_{pe} - k_{bf})(1 + \frac{\delta_{nl}}{r_p})^3\phi}{k_{pe} + 2k_{bf} - (k_{pe} - k_{bf})(1 + \frac{\delta_{nl}}{r_p})^3\phi} k_f$$ $$k_{pe} = \left[\frac{\left[2\left(1 - \frac{k_{nl}}{k_p}\right) + \left(1 + \frac{\delta_{nl}}{r_p}\right)^3 (1 + 2\frac{k_{nl}}{k_p})\right]\frac{k_{nl}}{k_p}}{-\left(1 - \frac{k_{nl}}{k_p}\right) + \left(1 + \frac{\delta_{nl}}{r_p}\right)^3 (1 + 2\frac{k_{nl}}{k_p})}\right] k_p$$	
Xie *et al.* [64]	$$\frac{k_{eff} - k_{bf}}{k_{bf}} = 3\Theta\phi_{eff} + \frac{3\Theta^2\phi_{eff}^2}{1 - \Theta\phi_{eff}}$$ $$\Theta = \frac{\left(\frac{k_{nl} - k_{bf}}{k_{nl} + 2k_{bf}}\right)\left[(1 + \frac{\delta_{nl}}{r_p})^3 - \left[\frac{(k_p - k_{nl})(k_{bf} + 2k_{nl})}{(k_p + 2k_{nl})(k_{bf} - k_{nl})}\right]\right]}{(1 + \frac{\delta_{nl}}{r_p})^3 + 2\left[\left(\frac{k_{nl} - k_{bf}}{k_{nl} + 2k_{bf}}\right)\left(\frac{k_p - k_{nl}}{k_p + 2k_{nl}}\right)\right]}$$	
Leong *et al.* [65]	$$k_{eff} = \frac{(k_p - k_{nl})\phi_{nl}k_{nl}\left[2\left(1 + \frac{\delta_{nl}}{2r_p}\right)^3 - \left(1 + \frac{\delta_{nl}}{r_p}\right)^3 + 1\right] + (k_p + 2k_{nl})\left(1 + \frac{\delta_{nl}}{2r_p}\right)^3\left[\phi_{nl}\left(1 + \frac{\delta_{nl}}{r_p}\right)^3 (k_{nl} - k_{bf}) + k_{bf}\right]}{\left(1 + \frac{\delta_{nl}}{2r_p}\right)^3 (k_p + 2k_{nl}) - (k_p - k_{nl})\phi_{nl}\left[\left(1 + \frac{\delta_{nl}}{2r_p}\right)^3 + \left(1 + \frac{\delta_{nl}}{r_p}\right)^3 - 1\right]}$$ $$\phi_{nl} = \phi_p\left[\left(1 + \frac{\delta_{nl}}{r_p}\right)^3 - 1\right]$$	
Lin et al. [68]	$$k_{eff} = k_{bf} + \frac{(k_p - k_{bf})\left[\frac{(1 - \Xi_1)(1 - \Xi_2)}{1 + 2\rho_{nf}\Xi_1\Xi_2}\right]\phi_p + (k_l - k_{bf})\left[\frac{(1 - \Xi_1)}{1 + 2\rho_{nf}\Xi_1\Xi_2}\right](\phi_{pl} - \phi_p)}{\left[\frac{(1 - \Xi_1)(1 - \Xi_2)}{1 + 2\rho_{nf}\Xi_1\Xi_2}\right]\phi_p + \left[\frac{(1 - \Xi_1)}{1 + 2\rho_{nf}\Xi_1\Xi_2}\right](\phi_{pl} - \phi_p) + (1 - \phi_{pl})}$$	$$\Xi_1 = \frac{k_p - k_{nl}}{k_p + 2k_{nl}}$$ $$\Xi_2 = \frac{k_{nl} - k_{bf}}{k_{nl} + 2k_{bf}}$$

Nabi- Shirani [91]	$k_{eff} = \left[1 + \frac{3\left(\frac{k_p}{k_{bf}} - 1\right)\phi}{\left(\frac{k_p}{k_{bf}} + 2\right) - \left(\frac{k_p}{k_{bf}} - 1\right)\phi}\right] k_{bf} + 9064(\rho c_v) \times \frac{k_{bf} T}{\mu r_p}\left[\beta_p\left(\phi - \phi^{\frac{d_l - d_f}{d_f - 3}}\right) + \beta_a \phi^{\frac{d_l - d_f}{d_f - 3}}\left(1 + \frac{t}{t_{br}}\right)^{-\frac{1}{3}}\right]$	

2.4. EXPERIMENTAL DATA FOR THERMAL CONDUCTIVITY OF Al_2O_3-WATER NANOFLUIDS

Masuda *et al* [105] were the first researchers who used nanoparticles for the enhancement of heat transfer in a liquid. They used the transient hot wire technique to measure the thermal conductivity ratio of Al_2O_3-water nanofluids. Their experiments included three different temperatures consisted of 32, 47 and 67^{o}C. Lee *et al* [15] experimentally investigated the thermal conductivity of Al_2O_3-water nanofluids prepared with 38.4 nm average diameter of alumina nanoparticle at 21^{o}C temperature for four different volume concentrations (1, 2, 3 and 4%). Wang *et al* [16] measured the effective thermal conductivity of fluids and nanometre-size Al_2O_3 by using a steady-state parallel-plate technique. They dispersed Al_2O_3 powder (γ phase) with an average diameter of 28 into water with a vacuum pump fluid and measured the thermal conductivity ratio at 24^{o}C in three different volume concentrations. Das *et al* [13] investigated the thermal conductivity ratio of Al_2O_3-water nanofluids with a thermal oscillation method. They studied the temperature effect of the thermal conductivity ratio of Al_2O_3 nanoparticles with an average diameter of 38.4 nm. Their experiments consisted of seven different temperatures (21, 26, 31, 36, 41, 46 and 51^{o}C) for four nanoparticle volume concentrations (1, 2, 3 and 4%). Putra *et al* [14] reported some experimental data for thermal conductivity ratio of Al_2O_3 (with an average diameter of 131.2 nm) in a water-based nanofluid over a temperature range from 21 to 51^{o}C at volume concentrations of 1 and 4%. Chon *et al* [9] measured the thermal conductivity of Al_2O_3-water nanofluids in 11, 47 and 150 nm nanoparticle sizes over a wide range of temperatures (from 21 to 71^{o}C) at 1 and 4% volume concentrations. Li and Peterson [10, 17] published their experimental investigation

into the effect of variations in temperature and volume concentration on steady-state effective thermal conductivity of Al_2O_3-water suspensions. Al_2O_3 nanoparticles with 36 and 47 nm average diameters were blended with water at 0.5, 2, 4, 6 and 10% volume concentrations and the resulting suspensions were evaluated at temperatures ranging from 27.5 to 35.5^oC. Kim *et al* [18] measured the thermal conductivity of alumina-water nanofluids by using the transient hot wire method. They used alumina nanoparticles with an average diameter of 38 nm for their work and reported the results for 0.3, 0.5, 0.8, 1.5, 2 and 3% of volume concentrations at 25^oC. Timofeeva *et al* [106] investigated Al_2O_3-water nanofluids thermal conductivity for a series of nanofluids consisting of 11, 20 and 40 nm and volume concentrations of 2.5, 5, 7.5 and 10% at 23^oC. Zhang *et al* [107] used a short hot wire probe to measure the thermal conductivity ratio of Al_2O_3-water nanofluids for 10, 30 and 50^oC. Ju *et al* [108] reported their measurements for thermal conductivity of Al_2O_3-water suspensions with nominal diameters of 20, 30 and 45 nm for volume concentrations up to 10%. Murshed *et al* [103] conducted an experimental investigation into the effective thermal conductivity of Al_2O_3 nanoparticles with average diameters of 80 and 150 nm in a water-based suspension. In their work, the transient hot wire technique was used to measure the thermal conductivity ratio of nanofluids at different temperatures ranging from 21 to 60^oC. Patel *et al* [11] measured thermal conductivity enhancement of Al_2O_3-water nanofluids in 11, 45 and 150 nm nanoparticle sizes for four different temperatures (20, 30, 40 and 50^oC) at 0.5, 1, 2 and 3% volume concentrations.

2.5. SUMMARY

In order to use nanofluids efficiently in industrial applications as well as understanding thermal conductivity enhancement of base fluid in the presence of nanoparticles, investigation into the heat transport mechanisms of nanofluids is essential.

UNIVERSITEIT VAN PRETORIA
UNIVERSITY OF PRETORIA
YUNIBESITHI YA PRETORIA

Section 2.2 has provided a review on possible mechanisms which could potentially influence the thermal conductivity enhancement of nanofluids. The Brownian motion of nanoparticles, nano particle size, concentration, distribution and formation of aggregates, nanolayering of the liquid at the liquid/particle interface, electric charge on the surface of nanoparticle, thermophoretic effect, preparation and surfactants are different factors which have been introduced and explained.

In section 2.3, theoretical models which have been proposed by different researchers for thermal conductivity of nanofluids are reviewed based on the influence of Brownian motion, nanolayering as well as clustering. Furthermore, some hybrid models that are taking into account the Brownian motion and nanolayering simultaneously are presented.

In section 2.4, experimental investigations of different researchers on thermal conductivity of Al_2O_3-water nanofluids are reviewed. The experimental data as data points divided into two set of train and test data which they have used for modelling and benchmark in chapter three.

The different factors that may influence the thermal conductivity of nanofluids are molecular-level layering of the liquid at the liquid/particle interface (nanolayer), Brownian motion of the nanoparticle, clustering, nanoparticle size, pH, temperature and the nature of heat transport in the nanoparticles. It seems that none of these factors could be merely responsible for the enhancement in thermal conductivity. In order to have more accurate models, the hybrid models which are considering more effective factors into account are the best options.

3

CHAPTER 3: THERMAL CONDUCTIVITY OF NANOFLUIDS BASED ON ARTIFICIAL INTELLIGENCE TECHNIQUES[5]

3.1. INTRODUCTION

In this chapter, the application of FCM-based Neuro-Fuzzy Inference System (FCM-ANFIS) and Genetic Algorithm-Polynomial Neural Network (GA-PNN) methods is introduced for predicting the effective thermal conductivity of nanofluids as a function of nanoparticle volume concentration, temperature and nanoparticle size. In order to show the ability of proposed models to predict the thermal conductivity of nanofluids, the results have been compared with Al_2O_3-water nanofluids experimental data as well as Xuan *et al* [34] and Hamilton-Crosser [94] correlations. In section 3.2 the FCM-ANFIS method has been introduced in detail as a method that uses neural network and fuzzy method approaches simultaneously to model engineering problems based on input-output experimental data.

Detailed information about the GA-PNN hybrid system has been given in section 3.3. In this section after introducing the GMDH polynomial neural networks which is a polynomial neural network that uses the group method of data handling learning algorithm, the application of genetic algorithm to determine the GMDH polynomial neural network weights, hidden layers and bias coefficients has been described.

Furthermore, after introducing some experimental data available in literature for thermal conductivity of Al_2O_3-water nanofluids, the proposed models based on FCM-

[5] This chapter has been published in part: M. Mehrabi, M. Sharifpur and J.P. Meyer, "Application of the FCM-based neuro-fuzzy inference system and genetic algorithm-polynomial neural network approaches to modelling the thermal conductivity of alumina-water nanofluids", *International communications in heat and mass transfer,* Vol. 39 (7), pp. 971–977, 2012 and M. Mehrabi, M. Sharifpur and J.P. Meyer, "Adaptive neuro-fuzzy modelling of the thermal conductivity of alumina-water nanofluids", *Proc. ASME, 54778; ASME, 2012 Third International Conference on Micro/Nanoscale Heat and Mass Transfer,* pp.155–161, March 03, 2012.

UNIVERSITEIT VAN PRETORIA
UNIVERSITY OF PRETORIA
YUNIBESITHI YA PRETORIA

ANFIS and GA-PNN techniques have been compared against experimental data as well as Xuan *et al* [34] and Hamilton-Crosser [94] correlations.

3.2. ADAPTIVE NEURO-FUZZY INFERENCE SYSTEM (ANFIS)

Artificial neural networks are among the systems which transfer the knowledge and rules existing beyond the empirical data into the network structure by their processing. Because artificial neural network does not consider any presupposition about statistical distribution and characteristics of the data, they are practically more efficient than common statistical methods. On the other hand, they use a non-linear approach to create a model, so when encountered with the complicated and non-linear data, these networks may express such data much more accurately as a defined model. High learning abilities of artificial neural network has converted the method into a superior choice when combined with fuzzy systems. The combination of artificial neural network with the fuzzy method can create an efficient approach for various modelling systems, so that each of these two methods may recover the weakness of another and increase the efficiency of the neuro-fuzzy system. A neuro-fuzzy system uses learning methods derived from artificial neural network in order to find the parameters of the fuzzy system which includes appropriate membership functions and fuzzy rules. One of the neuro-fuzzy systems in which learning algorithm is coincided with integrates learning approaches in the ANFIS system. In recent years, many investigations have been performed to apply the ANFIS system for modelling of the engineering processes [109-111].

In general, artificial neural networks have no ability to develop a model during a logical time. In addition, fuzzy modelling needs an approach to learn from experiences (empirical data) in order to apply the integrated decisions resulted from different variables. Therefore, regarding the advantages and deficiencies existing in both methods, a successful combination of these approaches has created the neuro-fuzzy modelling.

UNIVERSITEIT VAN PRETORIA
UNIVERSITY OF PRETORIA
YUNIBESITHI YA PRETORIA

3.2.1. Neuro-fuzzy networks

Artificial neural network is a calculation tool which is used to test the data and to create a model by these data. When neural network applies the training data for learning latent patterns existing within the data, it may use them to access the outputs. Regarding the researcher's objectives, various kinds of artificial neural networks may be used. One of the most well-known artificial neural networks is the multilayer feed-forward neural network which is a neural network instructed by the supervisor. This neural network is useful for solving the problems that include learning the relationship between definite input and output sets. In fact, this is a method of instruction by a supervisor to learn the relationships between data by training data sets. In the error-back propagation algorithm, the network creates an output (or an output set) for the provided input criterion and compares the reaction with appropriate reaction of each neuron. Thereafter, the weights of the network are corrected to reduce the error and the next criterion is emerging. The weights will be corrected continuously until the total errors are less than the authorised error value. Since this algorithm has a descending gradient in the error function, the input correction gradually minimises the mean square error [112,113].

While moving forward, the neuro-fuzzy networks normally calculate the nodes outputs up to the last layer in every period of instruction. Thus, the resulted parameters are calculated by the least square error method. After calculation of error in the returning backward route, the error ratios are distributed on condition that parameters and their values are corrected by the error descending gradient method. Various structures have been suggested to establish a fuzzy system by neural networks. One of the most powerful structures which has been developed by Jang [114] is known as adaptive neuro-fuzzy inference system (ANFIS). The main instruction approach in this structure is error-back propagation which scatters the error value towards inputs by algorithm of the steepest gradient descent and corrects the parameters [114].

3.2.2. Architecture of ANFIS

An ANFIS system uses two neural network and fuzzy logic approaches. When these two systems are combined, they may qualitatively and quantitatively achieve a proper result that will include either fuzzy intellect or calculative abilities of a neural network. As other fuzzy systems, the ANFIS structure is organised into two introductory and concluding parts which are linked together by a set of rules. Five distinct layers may be recognised in the structure of an ANFIS network which makes it a multi-layer network. A Sugeno type fuzzy system with two inputs and one output is showed in Figure 3.1.

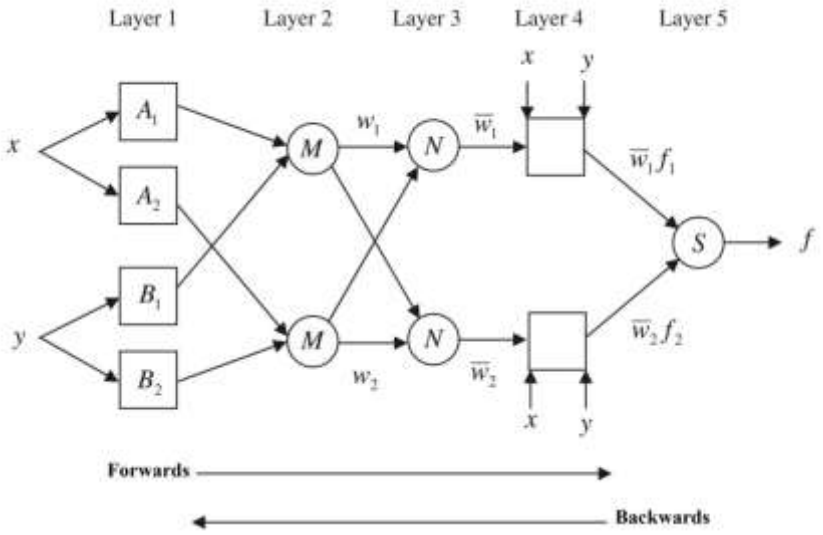

Figure 3.1: Architecture of ANFIS

As shown in Figure 3.1, this system contains two inputs x and y and an output or f which is associated with the following rules:

Rule 1: If (x is A_1) and (y is B_1) then $f_1=p_1x+q_1y+r_1$

Rule 2: If (x is A_2) and (y is B_2) then $f_2=p_2x+q_2y+r_2$

In this system, A_i, B_i and f_i are fuzzy sets and systems output respectively. p_i, q_i and r_i are design parameters which are produced during the learning process. If the output of each layer in the ANFIS network has been considered as O_i^j (i_{th} node output in j_{th}

layer) then the various layer functions of this network may have been explained as follows:

- Layer 1: In this layer, each node is equal to a fuzzy set and the output of a node in the respective fuzzy set is equal to the input variable membership grade. The parameters of each node determine the membership function form. Because the Gaussian membership function is used in this study:

  $$\mu_{Ai}(x) = exp\left\{-\frac{1}{2}\left(\frac{x-C_i}{\sigma_i}\right)^2\right\} \quad (3.1)$$

  the input value of the node is x and C_i and σ_i are membership function parameters of this set which explain Gaussian membership function centre and Gaussian membership function width respectively.

- Layer 2: In this layer input signal values into each node are multiplied by each other and a rule firing strength is calculated.

  $$O_i^2 = \omega_i = \mu_{Ai}(x)\,\mu_{Bi}(y) \qquad i = 1,2 \quad (3.2)$$

  in which μ_{Ai} is the membership grade of x in A_i fuzzy set and μ_{Bi} is the membership of y in fuzzy set of B_i.

- Layer 3: This layer nodes calculate rules relative weight, in which ω_i^n is the normalised firing strength of i_{th} rule.

  $$O_i^3 = \omega_i^n = \frac{\omega_i}{\omega_1 + \omega_2} \qquad i = 1,2 \quad (3.3)$$

- Layer 4: This layer is named the rules layer which is from multiplication of the normalised firing strength (has been resulted in the previous layer) by the first order Sugeno fuzzy rule.

  $$O_i^4 = \omega_i^n f_i = \omega_i^n\,(p_i x + q_i y + r_i) \qquad i = 1,2 \quad (3.4)$$

- Layer 5: This layer is the last layer of the network and is composed of one node and adds up all inputs of the node.

  $$O_i^5 = \sum_{i=1}^{2} \omega_i^n f_i = \frac{\omega_1 f_1 + \omega_2 f_2}{\omega_1 + \omega_2} \quad i = 1,2 \quad (3.5)$$

Briefly, the first layer in the ANFIS structure performs fuzzy formation and the second layer performs fuzzy AND and fuzzy rules. The third layer performs normalisation of membership functions and the fourth layer is the conclusive part of

fuzzy rules. The last layer calculates network output. The first and fourth layers in the ANFIS structure are adaptive layers in which C_i and σ_i in layer 1 are known as premise parameters that relate to the membership function of the fuzzy input. In layer 4, r_i, q_i and p_i are adaptive parameters of the layer and called consequent parameters [115, 116].

3.2.3. Fuzzy C-means Clustering Based Neuro-Fuzzy Inference System (FCM-ANFIS) Modelling Technique

Structure identification in fuzzy modelling involves selecting the input variables, input space partitioning, choosing the number and kinds of membership functions for inputs, creating fuzzy rules, premise and conclusion parts of fuzzy rules and selecting initial parameters for membership functions. For a given data set, different ANFIS models can be constructed using three different identification methods such as grid partitioning, subtractive clustering method and fuzzy C-means clustering [117]. In the present work, the fuzzy C-means clustering (FCM) method is used to identify the premise membership functions for the ANFIS model.

Fuzzy C-means clustering as proposed by Bezdek [118] is a data clustering technique in which each data point belongs to two or more clusters. Fuzzy C-means is an iterative algorithm, which wants to find cluster centres based on minimisation of an objective function. The objective function is the sum of square distance between each data point and the cluster centres and is weighted by its membership.

In the first step, the number of clusters v $(1 \leq v \leq n)$ and weighting exponent (fuzziness index) m $(1 \leq m < \infty)$ are randomly selected. Thereafter, the algorithm starts by initialising the cluster centres $c_j, j = 1, 2, \ldots, v$ to a random value at first time from the n data points $\{x_1, x_2, \ldots, x_n\}$. In the next step, the membership matrix $u_{ij} = [U]$ is computed by using the following equation:

$$u_{ij} = \frac{1}{\sum_{k=1}^{v} \left(\frac{\|x_i - c_j\|}{\|x_i - c_k\|} \right)^{\frac{2}{m-1}}} \tag{3.6}$$

where $\|*\|$ is any norm expressing the similarity between any measured data and the centre, so $\|x_i - c_j\|, \|x_i - c_k\|$are the Euclidean distance between the *j*-th and *k*-th cluster centres and the *i*-th data point. In the fourth step, the objective function *J* is computed according to Eq. (3.7)

$$J(U, c_1, c_2, \dots, c_v) = J_m = \sum_{i=1}^{n} \sum_{j=1}^{v} u_{ij}^m . \|x_i - c_j\|^2 \quad 1 \le m < \infty \tag{3.7}$$

In the final step, by using Eq. (3.8), the new fuzzy cluster centres $c_j , j = 1, 2, \dots, v$ are computed [119-121].

$$c_j = \frac{\sum_{i=1}^{n} u_{ij}^m . x_i}{\sum_{i=1}^{n} u_{ij}^m} \tag{3.8}$$

3.3. POLYNOMIAL NEURAL NETWORKS[6]

The objective of inductive modelling is to extract a general model by instruction data set. The obtained model may be used to explain unseen data in the training phase. This model should have an appropriate complexity as well as useful structure; i.e. it should be exact enough to be able to estimate instruction data, but should also be wide-ranging to be able to test data. Inductive modelling can be categorised into two methods, parametric and non-parametric. In parametric methods, training data are only used to construct the model. In these methods, the model structure is known previously and model parameters are estimated by training data. In other words, in parametric methods training data are abstracted into the model parameters and when these parameters are determined, the data presence will not be necessary. The most

[6] This section has been published in part: M. Mehrabi, M. Sharifpur and J.P. Meyer, "Application of the FCM-based neuro-fuzzy inference system and genetic algorithm-polynomial neural network approaches to modelling the thermal conductivity of alumina-water nanofluids", *International Communications in Heat and Mass Transfer*, Vol. 39 (7), pp. 971– 977, 2012.

well-known parametric modelling method is linear regression. In this method, polynomial terms or the structure of the model are determined and the objective of the modelling is to estimate the model parameters. Artificial neural networks are also among this group. In most known neural networks the structure of the model (number of neurons and layers) are considered constant and the model parameters are supposed as the network manes. Another group of neural networks named polynomial networks are formed from the combination of the linear regression method and artificial neural network. Each layer in this network is composed of a number of units (identical to neurons) which are considered as a polynomial. Polynomial networks have a pioneer structure and are formed by a number of layers. Each layer is composed of several units in which every unit is defined as a polynomial. Therefore, the parameters of this modelling method are considered as coefficients of units' polynomial [122].

3.3.1. Polynomial networks training algorithms

Different algorithms have been suggested to train the polynomial neural networks. The most popular ones are GMDH[7], PNTR[8] and ASPN[9]. Among them GMDH, which is the most important one to use, has been chosen in this thesis.

3.3.2. Training the polynomial networks by GMDH algorithm

GMDH algorithm was first introduced by Ivakhnenko as a learning method for modelling the complex and non-linear systems. This algorithm considers many simple models to construct and instruct polynomial networks. Based on the reinstructing the most appropriate simple models it obtains a final model as a pioneer network from a mixture of new models. Every unit of network processor in the resultant network contains two inputs and one output. A typical processor unit is indicated in Figure 3.2.

[7] Group Method of Data Handling
[8] Polynomial Network Training Routine
[9] Algorithm for Synthesis of Polynomial Networks

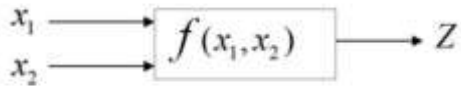

Figure 3.2: A GMDH typical processor unit

The model blocks (polynomial units) are usually in the second order as showed in the following relationship:

$$z = f(x_1, x_2) = a_0 + a_1 x_1 + a_2 x_2 + a_3 x_1^2 + a_4 x_2^2 + a_5 x_1 x_2 \tag{3.9}$$

in which x_1 and x_2 are the unit's input, a_i is coefficient (weight) and Z is the output. The coefficients of Eq. (3.9) are obtained by solving the linear regression equation (Z=Y), in which Y is the vector for training data output. If the numbers of inputs are M_0, all their $\binom{M_0}{2}$ states are analysed at first and their more appropriate M_1s are considered as the first layer of units. This procedure continues with considering M_1 selected units as inputs in the second layer. In this manner, increasing the layers continues so much that the complexity of the model reaches an optimum level and error decreases to a minimum. Figure 3.3 illustrates how the output of the second layer can be determined from the input variables. Thus, the last layer and its joined units, which are formed as returning, will establish the final model. Figure 3.4 gives an illustration of how a GMDH model is structured.

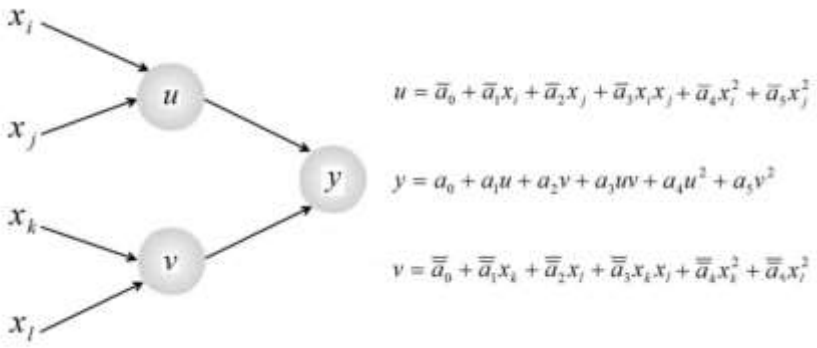

Figure 3.3: The second generation output y as a function of the input parameters x_i, x_j, x_k, and x_l

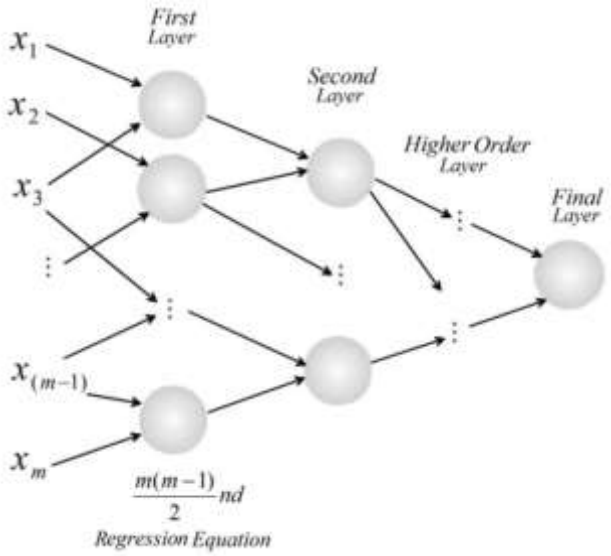

Figure 3.4: A complete GMDH model, showing the relationship between the input variables and the output

GMDH training algorithm includes two steps: in the first step the network units are instructed, in the second step the best unit is selected. Identical to these two steps in the training data are also divided into two sets: firstly, the instruction of the models (to find the units parameters) by linear regression, whereas the second set is used to compare models and select the more appropriate ones.

According to regularity criterion the models which will affect the second sets are retained and the remainders are abandoned. When the best unit of a layer (a unit with minimum error) is worse than the best unit of the previous layer, the addition of layers is stopped. The best unit of the previous layer is introduced as the final output of the model and all joints that do not lead to the output unit are eliminated [123, 124].

3.3.3. GMDH polynomial neural networks

By using a GMDH learning algorithm to train a polynomial neural network, a new class of polynomial neural network, which is called a GMDH-type polynomial neural network, is introduced. In a GMDH-type polynomial neural network, all neurons contain an identical structure with two inputs and one output. Each neuron performs

processing with five weights and one bias between the input and output data. The relationship which is established between input and output variables by a GMDH-type polynomial neural network is a non-linear function as Eq. (3.10):

$$z = a_0 + \sum_{i=1}^{M} a_i x_i + \sum_{i=1}^{M}\sum_{j=1}^{M} a_{ij} x_i x_j + \sum_{i=1}^{M}\sum_{j=1}^{M}\sum_{k=1}^{M} a_{ijk} x_i x_j x_k + \cdots \quad (3.10)$$

This is named a Volterra functions series. The GMDH algorithm is founded on the basis of Volterra functions series disintegration into second-rate two-variable polynomials. In fact, the algorithm objective is to find the unknown coefficients or weights of $[\mathbf{a}_{i,j}]$ in the Volterra functions series. Volterra functions series with definite weights can be obtained from Lemke and Müller [125].

In this manner, unknown coefficients are distributed among disintegrated factors and regulated as second-rate polynomials (Eq. (3.11)) to specify weights and algebraic substitution of any returning factors:

$$f(x_i, x_j) = a_0 + a_1 x_i + a_2 x_j + a_3 x_i^2 + a_4 x_j^2 + a_5 x_i x_j \quad (3.11)$$

Prior to instruction, the number of layers and neurons are not clear and regarding the problem, solution and answer are obtained during the instruction pace. In other words, GMDH is a self-organising network, which in the planning of second-rate polynomial coefficient neurons are obtained for all instruction couples by the linear fitting analysis method. Considering either the disability of neurons to comply with or to prevent the network divergence, a number of neurons are eliminated. Thus, the instruction process constructs the pioneer layer neurons with remaining neurons. This expansion process continues until a desirable answer is found.

3.3.4. Application of genetic algorithm in optimisation of GMDH-type polynomial neural networks design[10]

In this research work a genetic algorithm was applied to determine the GMDH polynomial neural network weights, hidden layers and bias coefficients for minimising the training error and finding the optimal structure. The hidden layers and bias coefficients were different chromosomes that the genetic algorithm tried to find. Figure 3.5, shows the combination of GMDH polynomial neural network and genetic algorithm that were used to model the effective thermal conductivity.

By using a group method of data handling learning algorithm to instruct the polynomial neural network, the GMDH polynomial neural network was introduced which created the neural network part. On the other hand, the genetic algorithm was used to find the GMDH polynomial neural network hidden layers and bias coefficients. These three different approaches built a genetic algorithm-GMDH type polynomial neural network hybrid system that is called GA-PNN. This hybrid system approach steps are described below:

- Step 1: The number of chromosome strings was selected randomly and each of them was divided into several sections. Each chromosome string was represented as a set of the connection weights (hidden layer and bias coefficients) for the GMDH polynomial neural network.

[10] This section has been published in part: M. Mehrabi, S. Rezazadeh, M. Sharifpur and J.P. Meyer "Modelling of proton exchange membrane fuel cell (PEMFC) performance by using genetic algorithm-polynomial neural network (GA-PNN) hybrid system", *Proc. ASME. 44823; ASME 2012 10th International Conference on Fuel Cell Science, Engineering and Technology Collocated with the ASME 2012 6th International Conference on Energy Sustainability, FUELCELL 2012,* pp.447–452, July 23, 2012.

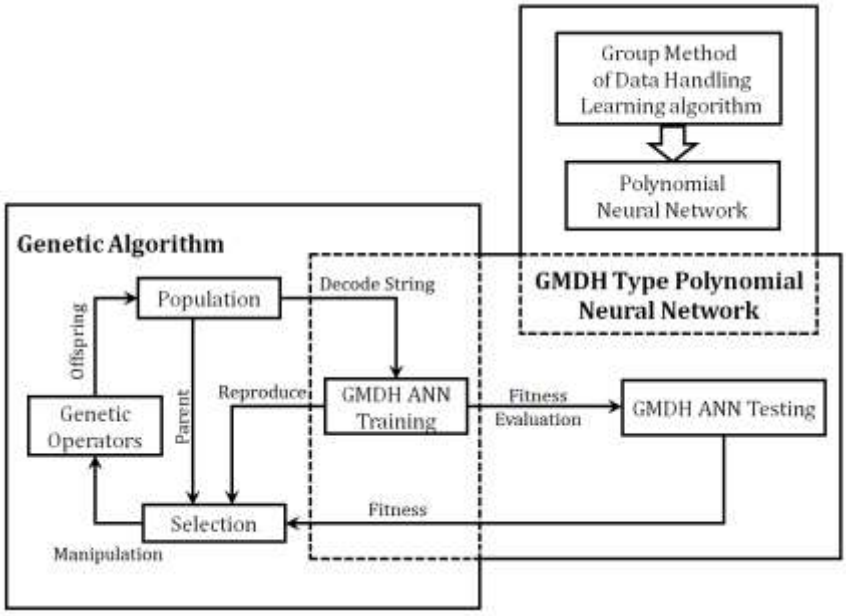

Figure 3.5: Combination of genetic algorithm and GMDH type polynomial neural network approaches in a hybrid system

- Step 2: For each string that was established with the training data, fitness was measured. A string's probability of being selected for reproduction was proportional to its fitness value.

- Step 3: The crossover, mutation and mating operators created the offspring that constituted the new generation. By decoding these new chromosomes, a new set of weights was gained which was submitted to the network. When the training error met the demand mentioned in the program this step stopped.

- Step 4: In the last step, the chromosome string with the smallest error in the training procedure was selected to provide the final network structure. After each run, a new set of weights was obtained and replaced with the old ones. Finally, one could get a best set of weights (layer coefficients), and obtained a well-trained GMDH polynomial neural network [126, 127].

3.4. APPLICATION OF THE NEURO-FUZZY INFERENCE SYSTEM (ANFIS) AND THE GENETIC ALGORITHM-POLYNOMIAL NEURAL NETWORK (GA-PNN) METHODS FOR MODELLING THE THERMAL CONDUCTIVITY OF Al_2O_3-WATER NANOFLUID[11]

There are different effective parameters on enhancement of nanofluids thermal conductivity reported in literature, which can be used for modelling of the effective thermal conductivity. Among these parameters, three important and measurable ones namely particle size, volume concentration and temperature were chosen for the modelling of the thermal conductivity of nanofluids.

Experimental data were addressed in section 2.4 have been used to model the thermal conductivity ratio (k_{eff}/k_{bf}) of Al_2O_3-water nanofluids, employing the FCM-ANFIS and GA-PNN approaches.

A total number of 232 input-output experimental data points obtained from literature [10, 11, 13-18, 103, 105-108] were used to establish a FCM-ANFIS and a GA-PNN prediction models for thermal conductivity of Al_2O_3-water nanofluids. For both models (GA-PNN model and FCM-ANFIS), Al_2O_3-water nanofluid experimental data were used to create models for predicting the effective thermal conductivity of Al_2O_3-water nanofluids. The experimental data were divided into two subsets as 80% for training and 20% for testing (benchmark) purposes.

8 different membership functions, namely: , “trimf”, “trapmf”, “gbellmf”, “gaussmf”, “gauss2mf”, “pimf”, “dsigmf” and “psigmf” have been used to model a case study. By using the experimental of Ju et al [108], 8 models with different membership functions have been proposed for thermal conductivity of nanofluids. The experimental data (volume concentrations between 1 and 5.6%, particle size of 30 nm and temperature of 23^{o}C) and proposed models were compared and the Gaussian

[11] This section has been published in part: M. Mehrabi, M. Sharifpur and J.P. Meyer, “Application of the FCM-based neuro-fuzzy inference system and genetic algorithm-polynomial neural network approaches to modelling the thermal conductivity of alumina-water nanofluids”, *International Communications in Heat and Mass Transfer*, Vol. 39 (7), pp. 971–977, 2012.

curve membership function ("gaussmf") has been chosen as the membership function due to least modelling error.

Beside the membership function for FCM-clustering, identification method is necessary to define the number of clusters, the fuzziness exponent and the termination tolerance. In most of the cases the equal number of clusters with number of groups that actually exist in the data, gave an acceptable result and identified the input-output data correctly. Furthermore, the fuzziness exponent and the termination tolerance have been chosen 2 and 0.001, respectively.

An unsupervised clustering algorithm called topology based fuzzy clustering has been used to determine the number of nodes, node positions and node conductivity of the ANFIS system.

3.5. RESULTS AND DISCUSSION

The performance of the FCM-ANFIS and the GA-PNN proposed models was tested with the sum of the squares due to the error or summed squares of residuals (*SSE*) and root mean square errors (*RMSE*). If Q_1, Q_2 , Q_3 , …, Q_n are n observed values, P_1, P_2 , P_3 , …, P_n are n predicted values, then *SSE* and *RMSE* values are as follows:

$$SSE = \sum_{i=1}^{n} (Q_i - P_i)^2 \tag{3.12}$$

$$RMSE = \sqrt{\frac{1}{n} . \sum_{i=1}^{n} (Q_i - P_i)^2} \tag{3.13}$$

Experimental data points obtained from literature were divided into two subsets as 80% for training and 20% for testing purposes. In this thesis the data points that have been used for testing (benchmark) purpose have not been entered to the training (modelling) section at all. It means that at the beginning, the experimental data sets were divided to training and testing (benchmark) sets and the models have been trained with the training set. When the training process completed and the final model

is produced, the testing set (which not used for modelling) was applied for benchmark.

The structure of the GA-PNN model is shown in Figure 3.6 corresponding to the genome representation of ***2312332311231322*** for thermal conductivity ratio (k_{eff}/k_{bf}) in which ***1, 2*** and ***3*** stand for volume concentration ϕ (%), temperature T (^{o}C) and nanoparticle diameter d_p (nm), respectively.

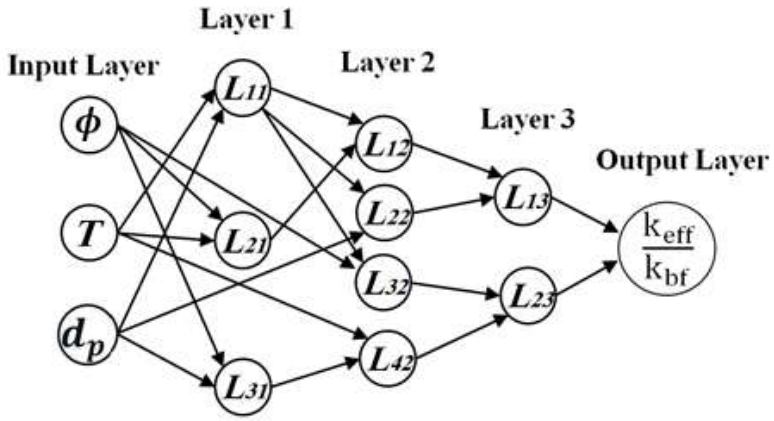

Figure 3.6: Structure of GA-PNN-type neural network for thermal conductivity ratio (k_{eff}/k_{bf}) modelling

The corresponding polynomial representation of model for k_{eff}/k_{bf} is as follows:

$$L_{11} = a_{1,0} + a_{1,1}.T + a_{1,2}.d_p + a_{1,3}.T.d_p + a_{1,4}.T^2 + a_{1,5}.{d_p}^2$$

$$L_{21} = a_{2,0} + a_{2,1}.\phi + a_{2,2}.T + a_{2,3}.\phi.T + a_{2,4}.\phi^2 + a_{2,5}.T^2$$

$$L_{31} = a_{3,0} + a_{3,1}.\phi + a_{3,2}.d_p + a_{3,3}.\phi.d_p + a_{3,4}.\phi^2 + a_{3,5}.{d_p}^2$$

$$L_{12} = a_{4,0} + a_{4,1}.L_{11} + a_{4,2}.L_{21} + a_{4,3}.L_{11}.L_{21} + a_{4,4}.{L_{11}}^2 + a_{4,5}.{L_{21}}^2$$

$$L_{22} = a_{5,0} + a_{5,1}.d_p + a_{5,2}.L_{11} + a_{5,3}.d_p.L_{11} + a_{5,4}.{d_p}^2 + a_{5,5}.{L_{11}}^2$$

$$L_{32} = a_{6,0} + a_{6,1}.\phi + a_{6,2}.L_{11} + a_{6,3}.\phi.L_{11} + a_{6,4}.\phi^2 + a_{6,5}.{L_{11}}^2$$

$$L_{42} = a_{7,0} + a_{7,1}.L_{31} + a_{7,2}.T + a_{7,3}.L_{31}.T + a_{7,4}.{L_{31}}^2 + a_{7,5}.T^2$$

$$L_{13} = a_{8,0} + a_{8,1}.L_{12} + a_{8,2}.L_{22} + a_{8,3}.L_{12}.L_{22} + a_{8,4}.{L_{12}}^2 + a_{8,5}.{L_{22}}^2$$

$$L_{23} = a_{9,0} + a_{9,1}.L_{32} + a_{9,2}.L_{42} + a_{9,3}.L_{32}.L_{42} + a_{9,4}.{L_{32}}^2 + a_{9,5}.{L_{42}}^2$$

$$\frac{k_{eff}}{k_{bf}} = a_{10,0} + a_{10,1}.L_{13} + a_{10,2}.L_{23} + a_{10,3}.L_{13}.L_{23} + a_{10,4}.{L_{13}}^2 + a_{10,5}.{L_{23}}^2$$

$$[\mathbf{a}_{i,j}]$$

$$= \begin{bmatrix} 1.0735962 & -0.0020244 & 0.0605055 & 8.35 \times 10^{-6} & -0.0064905 & 0.0001505 \\ 0.8718401 & 0.0098069 & 0.0011233 & -7.83 \times 10^{-5} & -7.14 \times 10^{-6} & -7.75 \times 10^{-6} \\ 0.8733007 & 0.0069859 & 0.0177932 & -7.08 \times 10^{-5} & -2.67 \times 10^{-3} & 7.96 \times 10^{-4} \\ 10.668079 & -15.644669 & -3.3349184 & 3.9400101 & -1.6277918 & 7.0065401 \\ -2.6847113 & -0.3084822 & 6.3004023 & -1.26 \times 10^{-3} & -2.5900101 & 0.2760002 \\ 3.4734893 & -0.0050944 & -5.2272048 & -9.32 \times 10^{-5} & 2.5841052 & 0.0140529 \\ 0.4093305 & 0.4501285 & -0.0042521 & 0.1989611 & 6.83 \times 10^{-6} & 0.0025185 \\ 0.9721418 & -2.0553909 & 1.2665332 & -2.3233686 & -4.1070767 & 7.2531441 \\ 0.2394494 & 2.1513521 & -1.5733885 & 13.480884 & 15.199995 & -28.498592 \\ -0.0477731 & 1.0660376 & -0.0012041 & 0.0495427 & 0.7246142 & -0.7942074 \end{bmatrix}$$

Two statistical criteria which were mentioned before were used to determine how well the FCM-ANFIS and GA-PNN models could predict the thermal conductivity ratio k_{eff}/k_{bf} of Al_2O_3-water nanofluids corresponding to various values of inlet variables.

Figure 3.7 to Figure 3.9 show plots comparing the experimental data, FCM-ANFIS and GA-PNN models. These diagrams demonstrate that the predicted values are close to the experimental data and as many of the modelled data points fall very close to the experimental value.

Figure 3.7, shows the experimental results of Lee *et al* [15] compared with the FCM-ANFIS and the GA-PNN models for a particle size of 38.4 nm, temperature of 21^{o}C at four different volume concentrations as well as with Hamilton-Crosser [94] and Xuan *et al* [34] correlations. The FCM-ANFIS model shows a better agreement with experimental data in comparison with the GA-PNN model and is well matched with the experimental data ($SSE = 1.527 \times 10^{-5}$ and $RMSE = 0.002$). However, the GA-PNN ($SSE = 2.237 \times 10^{-6}$ and $RMSE = 0.0011$) model is not as good as the FCM-ANFIS model. Hamilton-Crosser [94] and Xuan *et al* [34] correlations are in a good agreement with the experimental data for volume concentrations less than 2% and when the volume concentration increases these correlations are unable to predict the thermal conductivity with a good accuracy.

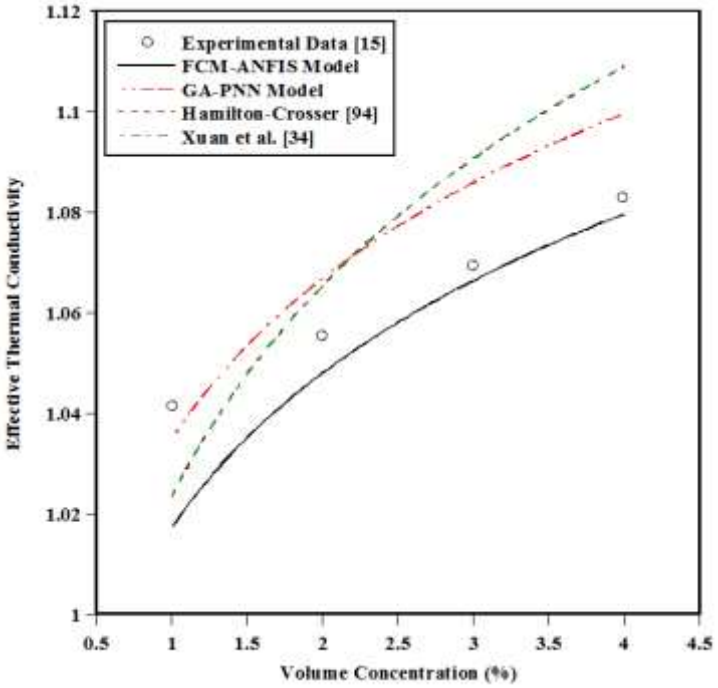

Figure 3.7: Comparison between the experimental data of Lee *et al* [15] and the proposed models for d_p= 38.4 nm and T= 21 ^{o}C and Hamilton-Crosser [94] and Xuan et al [34] correlations

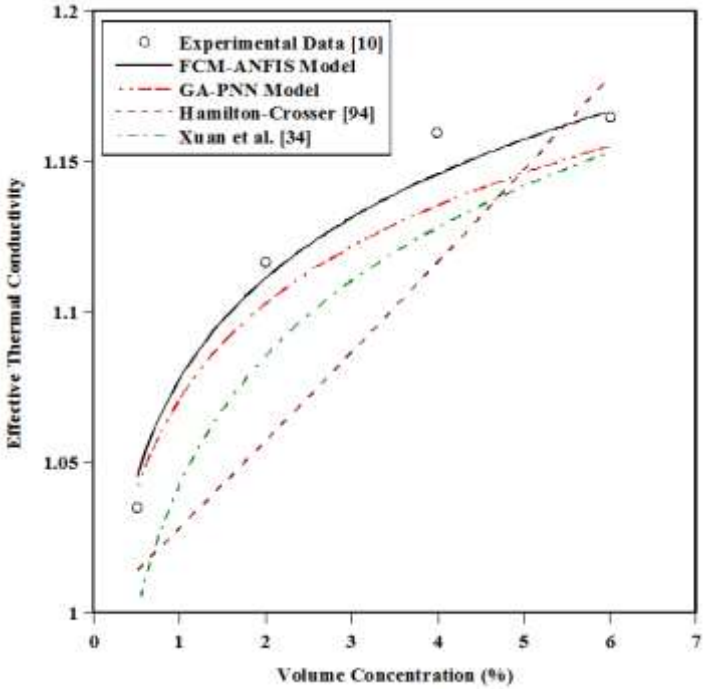

Figure 3.8: Comparison between the experimental data of Li and Peterson [10] and the proposed models for d_p = 36 nm and T= 30.5 ^{o}C and Hamilton-Crosser [94] and Xuan et al [34] correlations

In Figure 3.8, the experimental results of Li and Peterson [10] compared with the FCM-ANFIS and the GA-PNN models for a particle size of 36 nm, temperature of 30.5^{o}C at four different volume concentrations as well as Hamilton-Crosser [94] and Xuan *et al* [34] correlations. The FCM-ANFIS model ($SSE = 3.582 \times 10^{-5}$ and $RMSE = 0.0004$) is well-matched and the GA-PNN model ($SSE = 6.132 \times 10^{-4}$ and $RMSE = 0.0018$) is also in good agreement with the experimental data better than Hamilton-Crosser [94] and Xuan *et al* [34] correlations. For the FCM-ANFIS model at ϕ= 2% and ϕ=6%, the model is approximately the same as the experimental data.

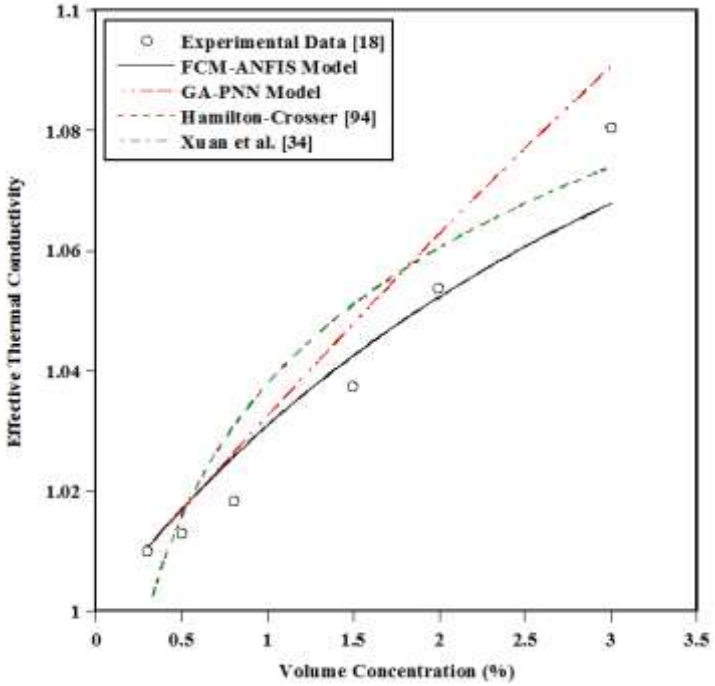

Figure 3.9: Comparison between the experimental data of Kim *et al* [18] and the proposed models for d_p = 38 nm and T= 25 ^{o}C and Hamilton-Crosser [94] and Xuan et al [34] correlations

Figure 3.9 shows the experimental results of Kim *et al* [18] compared with the FCM-ANFIS and the GA-PNN models for a particle size of 38 nm, temperature of 25 ^{o}C at five different volume concentrations and also with Hamilton-Crosser [94] and Xuan *et al* [34] correlations. The FCM-ANFIS model ($SSE = 8.39 \times 10^{-5}$ and $RMSE = 0.0046$) and the GA-PNN model ($SSE = 3.576 \times 10^{-5}$ and $RMSE = 0.0029$) are in good agreement with the experimental data. However, as the volume concentration

increases, the accuracy of the FCM-ANFIS is better than that of the GA-PNN model. In this case the FCM-ANFIS model delivers a better agreement with the experimental data set.

3.6. CONCLUSION AND RECOMMENDATIONS

In the FCM-ANFIS method, which consists of a neural network combined with a fuzzy logic approach, the fuzzy C-means clustering is used as an identification method. The Adaptive Neuro-Fuzzy Inference System (ANFIS) uses neural network and fuzzy logic approaches at the same time to combine the advantages of each method to achieve a better performance. In the GA-PNN hybrid system, which consists of neural network and genetic algorithm parts, the genetic algorithm is used to find the best network weights for minimising the training error and finding the optimal structure for a GMDH-type polynomial neural network. In the neural network part of this hybrid system the Group Method of Data Handling (GMDH) learning approach is used to learn a second-rate polynomial neural network.

232 input-output experimental data sets of Al_2O_3-water nanofluids from literature have been used for modelling and benchmarking proposes of the thermal conductivity ratio by using the FCM-ANFIS and GA-PNN approaches. The detailed information about the proposed models has been addressed in section 3.4 and 3.5.

Based on the result of this chapter, the proposed models based on GA-PNN and FCM-ANFIS techniques have shown a good agreement with experimental data for modelling the effective thermal conductivity of Al_2O_3-water nanofluids, so these methods show to be good candidates to model the effective thermal conductivity of other nanofluids.

4

CHAPTER 4: VISCOSITY OF NANOFLUIDS BASED ON AN ARTIFICIAL INTELLIGENCE MODEL[12]

4.1. INTRODUCTION

Viscosity of nanofluid is one of the most important thermophysical properties of nanofluids for practical applications due to its direct effects on the pressure drop in forced convection. Changes in viscosity properties in industrial applications influence the pumping power required as well as the convective heat transfer coefficients. Therefore, in order to being able to use nanofluids in practical applications, accurate information on the viscosity properties of nanofluids is essential [128, 129]. Due to hydrodynamic interactions and particle-particle interactions of nanoparticles in dispersions, it is challenging to determine the viscosity of nanofluids.

In this chapter, by using an FCM-based adaptive neuro-fuzzy inference system (FCM-ANFIS) and a set of experimental data, models were developed to predict the viscosity of nanofluids. The viscosity has been selected as the target parameter, and the volume concentration, temperature and size of the nanoparticles are considered as the input (design) parameters. To model the viscosity, experimental data from literature were divided into two sets: a train and a test data set. The model is instructed by the train data set and the results are compared against the experimental test data set. The predicted viscosities have been compared with experimental data for four nanofluids, which are Al_2O_3, CuO, TiO_2 and SiO_2 with water as base fluid. The proposed models outputs are also compared with several of the most cited correlations in literature.

[12] This chapter has been published in part: M. Mehrabi, M. Sharifpur and J.P Meyer, "Viscosity of nanofluids based on an artificial intelligence model", *International Communications in Heat and Mass Transfer*, Vol. 43, pp. 16–21, 2013.

4.2. APPLICATION OF THE FUZZY C-MEANS CLUSTERING NEURO-FUZZY INFERENCE SYSTEM (FCM-ANFIS) FOR MODELLING THE VISCOSITY OF NANOFLUIDS

There are several parameters that influence the viscosity of nanofluids; namely temperature, volume concentration and thickness of the nanolayer, as well as the nanoparticle geometrical properties such as nanoparticle size, shape, aspect ratio and interparticle spacing. Empirical investigations have been conducted on the effect of electromagnetic fields, electro-viscous, dispersion energy and settling time on the viscosity of nanofluids as well as the influence of base fluid properties such as density and polarity [130]. Among these parameters, the three important and measurable ones which were chosen for this study are particle size, volume concentration and temperature.

- **Effect of particle size**

Namburu *et al* [131] measured the viscosity of nanofluids containing three different sizes of silicon dioxide nanoparticles with diameters of 20, 50 and 100 nm over a temperature range from -35 to 50°C at volume concentrations of 2, 4, 6 and 10%. Their results showed that the viscosity decreased as the particle size increased. Lu and Fan [132] conducted an experimental and numerical investigation into the viscosity of Al_2O_3- nanoparticles with average diameters of 35, 45 and 90 nm in water and ethylene glycol- based suspensions. They observed the same results as Namburu *et al* [131], namely that the viscosity decreased as the particle sizes increased. Pastoriza-Gallego *et al* [86] reported viscosity measurements of water containing CuO nanoparticles with average diameters of 33±13 and 11±3 nm, temperatures from 10 to 50ºC, and volume concentrations from 0.16 to 1.17%. They also observed that for a constant volume concentration, the nanofluid samples with smaller average particle sizes had a larger viscosity.

- **Effect of volume concentration**

Most of the viscosity data of nanofluids in the literature exhibited the trend that as the volume concentration of the particles increased, the effective viscosity also increased [14, 80 and 131–134]. Chevalier *et al* [135] measured the relative viscosity of nanofluids containing three different sizes of silicon dioxide nanoparticles with diameters of 35±3, 94±5 and 190±8 nm at different volume concentrations up to 7%. They also observed that the relative viscosity increased as the volume concentration increased. Duangthongsuk and Wongwises [79] reported viscosity measurements of water containing TiO_2 nanoparticles with average particle diameters of 21 nm at three different temperatures, which were 15, 25 and 35°C. They conducted their experimental work with a parallel-plate rotational rheometer at five different volume concentrations ranging from 0.2 to 2%. They observed the same result as Chevalier *et al* [135], namely that the relative viscosity increased as the volume concentration increased.

- **Effect of temperature**

Chen *et al* [136] measured the viscosity of distilled water, ethylene glycol, glycerol and silicone oil suspensions with different multi-wall carbon nanotube volume fractions as a function of temperature by using a plate-and-cone viscometer. They studied the temperature effect on the viscosity at temperatures from 5 to 65ºC and they observed that the viscosity decreased as the temperature increased. Lee et al [137] reported viscosity measurements of distilled water containing silicon carbide nanoparticles at temperatures between 28 and 72ºC. They observed that the viscosity decreased as the temperature increased. The experimental results published by Prasher *et al* [138] and Chen *et al* [139 and 140] showed that the relative viscosity of Al_2O_3-propylene glycol and TiO_2-water nanofluids is independent of temperature at temperatures between 30 and 60 ºC and 20 and 60ºC, respectively. However, the observations of Prasher *et al* [138] and Chen *et al* [139, 140] do not correspond with the most experimental data available in literature. Furthermore, there is no discussion

on the effect of temperature on the effective viscosity of nanofluids which decreased as temperature increased.

4.3. EXPERIMENTAL DATA USED FOR THE TRAINING AND TESTING PROCEDURE

Nguyen *et al* [80] investigated the viscosity of Al_2O_3-water and CuO-water nanofluids with a piston-type viscometer. They studied the temperature and volume concentration effects of the viscosity of Al_2O_3-water nanofluids with average diameters of 36 and 47 nm as well as CuO-water nanofluids with an average diameter of 29 nm. Their experiments covered a wide range of temperatures from 21 to 70°C for four nanoparticle volume concentrations.

Tavman *et al* [141] experimentally investigated the viscosity of SiO_2-water and Al_2O_3-water nanofluids prepared with 12 and 30 nm average diameters of silicon dioxide and alumina nanoparticle, respectively. They conducted their experimental work at seven temperatures from 20 to 50°C for different volume concentrations. Lee *et al* [142] measured the viscosity of Al_2O_3-water nanofluid by using an oscillation-type viscometer. They dispersed Al_2O_3-powder with an average diameter of 30 nm into water and measured the viscosity of Al_2O_3-water nanofluid sizes over a range of temperatures from 21 to 39°C at low volume concentrations.

Duangthongsuk and Wongwises [79] reported some experimental data for viscosity of TiO_2, with an average diameter of 21 nm, in a water-based nanofluid for three different temperatures of 15, 25 and 35°C, at volume concentrations of 0.2, 0.6, 1, 1.5 and 2%. Turgut *et al* [143] reported their measurements for the viscosity of TiO_2-water suspensions with a nominal diameter of 21 nm for four different volume concentrations up to 3% over a temperature range from 13 to 55°C.

Anoop *et al* [144] measured the viscosity of alumina-water nanofluids by using a cone-plate viscometer. They used alumina nanoparticles with an average diameter of

95 nm for their experiments and reported the results for volume concentrations of 1, 2, 4 and 6% for the temperature range of 20 to 50°C.

Pastoriza-Gallego *et al* [86 and 145] published their experimental investigation of the effect of temperature variation and volume concentration on viscosity of Al_2O_3-water suspensions. Al_2O_3-nanoparticles with 8 and 43 nm average diameters were mixed with water at seven different volume concentrations ranging from 0.13 to 2.9% and the resulting suspensions were evaluated at temperatures ranging from 10 to 60°C. Furthermore, they measured the viscosity of CuO-water nanofluids with 33 and 11 nm nanoparticle sizes for eight different temperatures (10, 15, 20, 25, 30, 40 and 50°C) at low volume concentrations ranging from 0.16 to 1.17%.

Kwek *et al* [146] conducted an experimental investigation into the variation in temperature and volume concentration on the viscosity of Al_2O_3-water suspensions. Al_2O_3-nanoparticles with an average diameter of 25 nm were used at 2 and 3% volume concentrations and the results were given at five temperatures ranging from 15 to 55°C.

Fedele *et al* [147] experimentally measured the viscosity of titanium oxide nanoparticles with an average diameter of 76 nm in a water-based suspension. A cone-plate-type viscometer was used to measure the viscosity at different temperatures ranging from 10 to 70°C.

In this section, all the above-mentioned experimental results were used to model the viscosity of nanofluids using the FCM-ANFIS approach. The design variables (input parameters) chosen for the nanoparticles were the average diameter, volume concentration and temperature. The results of the FCM-ANFIS models were compared against experimental data [86, 141 and 144-147] and the most cited correlations from literature that are shown in Table 4-1.

Table 4-1: The most cited correlations of nanofluids viscosity

Model	Correlation	Remark
Einstein [148]	$\mu_{nf} = \mu_{bf}.(1 + 2.5\,\phi)$	Valid for very low volume concentrations ($\phi \leq 0.02$) and spherical particles
Brinkman [149]	$\mu_{nf} = \mu_{bf}.\left(\frac{1}{(1-\phi)^{2.5}}\right)$	
Batchelor [150]	$\mu_{nf} = \mu_{bf}.(1 + 2.5\,\phi + 6.5\,\phi^2)$	
Abu-Nada *et al.* [151]	$\mu_{Al_2O_3} = \exp(3.003 - 0.04203\,T - 0.5445\,\phi + 0.0002553\,T^2 + 0.0524\,\phi^2 - \frac{1.622}{\phi})$ $\mu_{CuO} = -0.6967 + \left(\frac{15.937}{T}\right) + 1.238\,\phi + \left(\frac{1356.14}{T^2}\right) - 0.259\,\phi^2 - 30.88\left(\frac{\phi}{T}\right) - \left(\frac{19652.74}{T^3}\right) + 0.01593\,\phi^3 + 4.38206\left(\frac{\phi^2}{T}\right) + 147.573\left(\frac{\phi}{T^2}\right)$ $\mu_{H_2O} = -81.1 + 98.75\ln(T) - 45.23\ln^2(T) + 9.71\ln^3(T) - 0.946\ln^4(T) + 0.03\ln^5(T)$	The viscosity in these equations is expressed in centi poise (cP), the temperature in ^{o}C.
Abedian and Kachanov [152]	$\mu_{nf} = \mu_{bf}.\left(\frac{1}{1-2.5\,\phi}\right)$	Newtonian fluid with a single rigid spherical particle
Masoud Hosseini *et al.* [153]	$\mu_{nf} = \mu_{bf}.\exp\left[m + \alpha\left(\frac{T}{T_0}\right) + \beta(\phi) + \gamma\left(\frac{d_P}{1+R}\right)\right]$ $\alpha = -0.485\,,\beta = 14.94,\gamma = 0.0105$ $m = 0.72\,,T_0 = 20\,^{o}$C, $R = 1$ nm	For Al_2O_3-Water nanofluids (Based on Nguyen *et al.* [80] experimental data)
Ward model [154]	$\mu_{nf} = \mu_{bf}.[1 + (2.5\,\phi) + (2.5\,\phi)^2 + (2.5\,\phi)^3 + (2.5\,\phi)^4 + \cdots]$	
renewed Ward (RW) model [155]	$\mu_{nf} = \mu_{bf}.[1 + (2.5\,\phi_e) + (2.5\,\phi_e)^2 + (2.5\,\phi_e)^3 + (2.5\,\phi_e)^4 + \cdots]$ $\phi_e = \phi.\left(1 + \frac{h}{r}\right)^3$	

4.4. PREDICTION MODELS

A total of 536 input-output experimental data points obtained from literature [80, 86, 141–147] were used to establish four different prediction models (Model I to Model IV) for viscosity. For the first model (Model I), Al_2O_3-water nanofluid experimental data were used to create a model for predicting the viscosity of Al_2O_3-water nanofluids. The experimental data were divided into two subsets as 80% for training and 20% for testing purposes. The same procedure was used to establish the second and third models (Model II and Model III) for predicting the viscosity of CuO-water and TiO_2-water nanofluids, respectively. For the fourth model (Model IV), the viscosity of SiO_2-water nanofluid was determined, but without any experimental data in the training section. The model was established with the input-output experimental data points for the Al_2O_3-water, CuO-water and TiO_2-water models.
8 different membership functions indicated in subsection 3.4 have been applied to model a case study By using the experimental of Nguyen et al [80], 8 models with different membership functions have been proposed for viscosity of nanofluids. The experimental data (Temperature between 23 and 65 ^oC, particle size of 36 nm and volume concentration of 4.5%)) and proposed models were compared and the Gaussian curve membership function (“gaussmf”) has been chosen as the membership function due to least modelling error.

Same as FCM-ANFIS model for thermal conductivity of nanofluids, topology based fuzzy clustering algorithm has been used to determine the number of nodes, node positions and node conductivity of the ANFIS system. The number of clusters is equal to number of input-output data sets and the fuzziness exponent and the termination tolerance have been chosen 2 and 0.001, respectively.

Three different statistical criteria given in Table 4-2 were used to determine how well the FCM-ANFIS proposed models could predict the viscosity of nanofluids corresponding to various values of inlet variables.

Table 4-2: Statistical criteria used for the analysis of the results

Statistical criterion	Equation
Mean absolute error	$MAE = \frac{1}{n}\sum_{i=1}^{n}\left\|X_p - X_a\right\|$
Mean relative error	$MRE(\%) = \frac{100}{n}\sum_{i=1}^{n}\left(\frac{\left\|X_p - X_a\right\|}{X_a}\right)$
Root mean square error	$RMSE = \sqrt{\frac{1}{n}\sum_{i=1}^{n}\left(X_p - X_a\right)^2}$

4.5. RESULT AND DISCUSSION

Figure 4.1, shows the experimental results of Kwek *et al* [146] compared with the FCM-ANFIS model (Model I) and correlations for an Al_2O_3-water nanofluid with a particle size of 25 nm, volume concentration of 2% at temperature ranging from 15 to 55 ^{o}C. Model I is in good agreement with the experimental data (MAE = 0.10, MRE = 10% and RMSE = 0.11). The proposed FCM-ANFIS model is well-matched with the experimental data in comparison with the correlations, especially in the low temperature range from 15 to 35^{o}C.

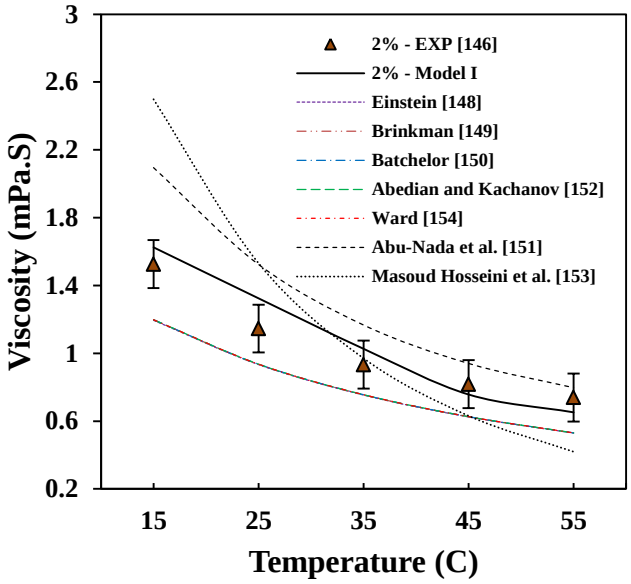

Figure 4.1: Comparison between the experimental data of Kwek *et al* [146] with Model I and correlations from literature for an Al_2O_3-water nanofluid, with an average particle size of 25 nm at a volume concentration of 2%

Figure 4.2, shows the experimental results of Anoop *et al* [144] compared with the FCM-ANFIS model (Model I) and the correlations from literature for a particle size of 95 nm and a volume concentration of 2% for an Al_2O_3-water nanofluid. The FCM-ANFIS model is in very good agreement with the experimental data (MAE = 0.020, MRE = 2.2% and RMSE = 0.026) and predicts the viscosities better than any of the correlations.

Figure 4.3, shows a comparison between the experimental results of Pastoriza-Gallego *et al* [155], the FCM-ANFIS model (Model I) and correlations for an Al_2O_3-water nanofluid with a particle size of 43 nm and a volume concentration of 1.4%. The FCM-ANFIS model (MAE = 0.023, MRE = 2.6% and RMSE = 0.025) corresponds very well with the experimental data although the correlations of Brinkman [149], Batchelor [150], Abedian and Kachanov [152], and Ward [154] also correspond well with the experimental measurements.

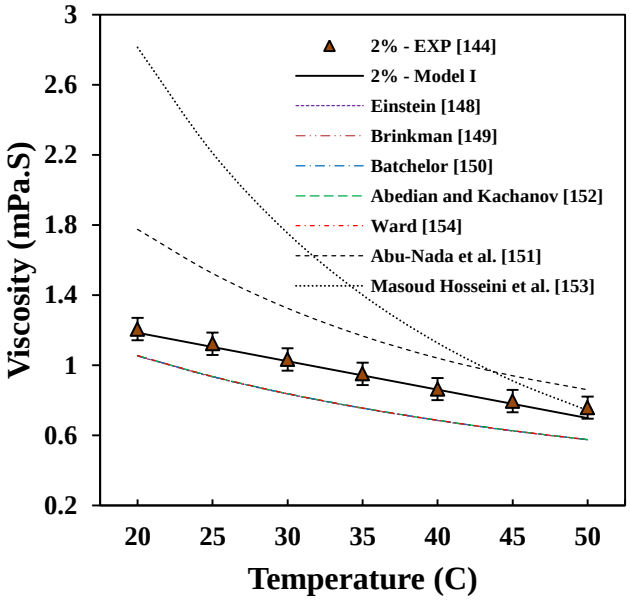

Figure 4.2: Comparison between the experimental data of Anoop *et al* [144] with Model I and correlations from literature for an Al_2O_3-water nanofluid, with an average particle size of 95 nm at a volume concentration of 2%

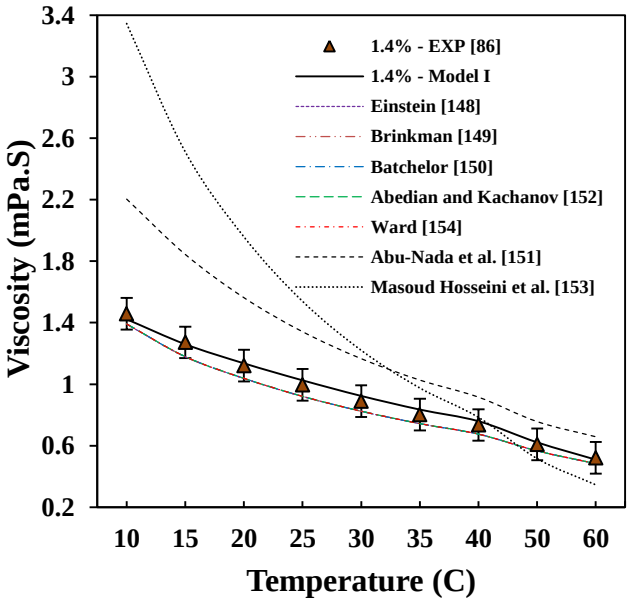

Figure 4.3: Comparison between the experimental data of Pastoriza-Gallego *et al* [86] with Model I and correlations from literature for an Al_2O_3-water nanofluid, with an average particle size of 43 nm at a volume concentration of 1.4%

In Figure 4.4, the experimental results of Tavman *et al* [141] are compared with those of the FCM-ANFIS model (Model I) and the correlations for an Al_2O_3-water nanofluid with a particle size of 30 nm, and a volume concentration of 0.5%. In

general, the FCM-ANFIS model matches the data (MAE = 0.095, MRE = 11% and RMSE = 0.097) better than any of the other correlations.

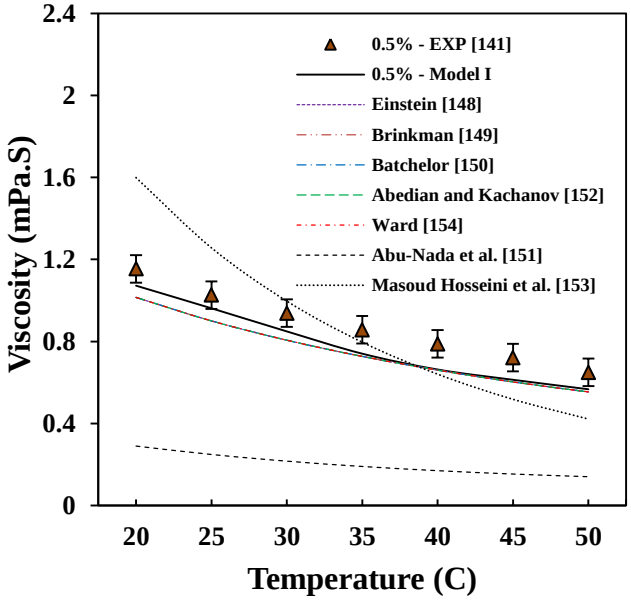

Figure 4.4: Comparison between the experimental data of Tavman *et al* [141] with Model I and correlations from literature for an Al_2O_3-water nanofluid, with an average particle size of 30 nm at a volume concentration of 0.5%

From Figure 4.2 to Figure 4.4 it can be concluded that for Al_2O_3-water nanofluids, in general, the FCM-ANFIS, Model I, predicts the viscosities better than those of the correlations in literature.

In Figure 4.5, the experimental data of Pastoriza-Gallego *et al* [86] is compared with the predictions of the FCM-ANFIS model (Model II) and with correlations for a CuO-water nanofluid with particle sizes of 11±3 nm and a volume concentration of 1.15%. The model predicts the viscosities the best when compared with the measurements (MAE = 0.018, MRE = 1.3% and RMSE = 0.022). All the models significantly under predict the experimental data.

In Figure 4.6, the experimental data of Fedele *et al* [147] are compared with the modelled values of the FCM-ANFIS model (Model III) and correlations for a TiO_2-water nanofluid with a particle size of 76 nm and a volume concentration of 5.54%. The renewed Ward [155] model and Model III (MAE = 0.22, MRE = 20% and RMSE

= 0.24) show a better agreement with the experimental data in comparison with other correlations. The renewed Ward correlation predicts better results than Model III.

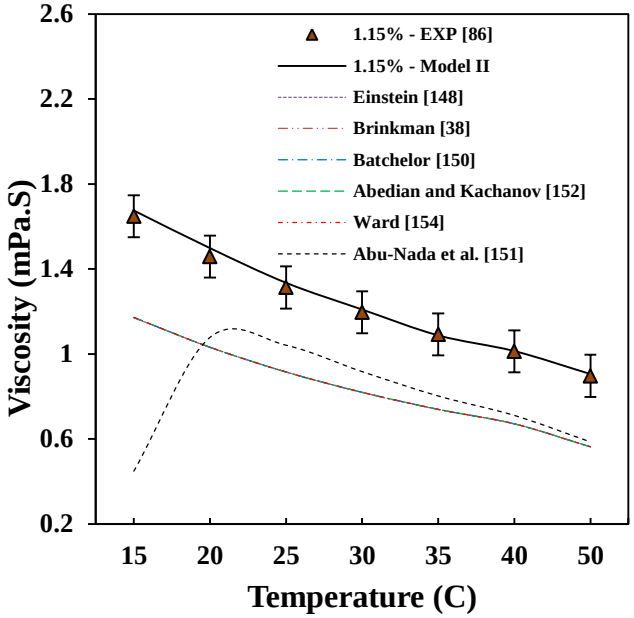

Figure 4.5: Comparison between the experimental data of Pastoriza-Gallego *et al* [86] with Model II and correlations from literature for a CuO-water nanofluid, with an average particle size of 11±3 nm at a volume concentration of 0.5%

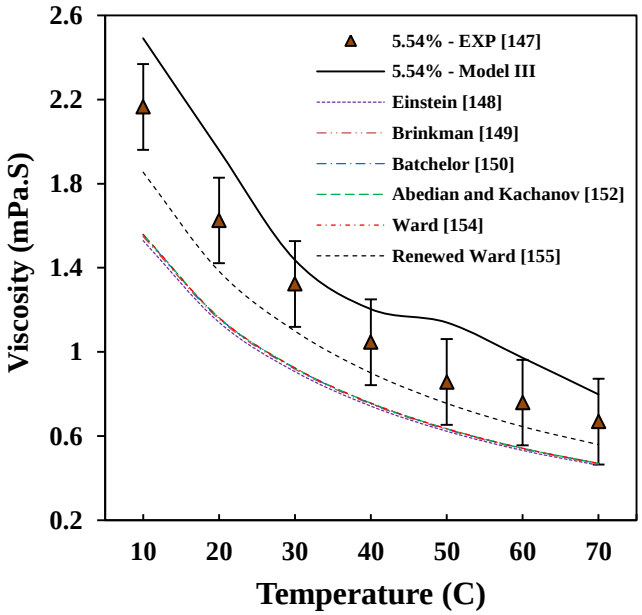

Figure 4.6: Comparison between the experimental data of Fedele *et al* [147] with Model III and correlations from literature for a TiO_2-water nanofluid, with an average particle size of 76 nm at a volume concentration of 5.54%

Figure 4.7, compares the experimental measurements of Tavman *et al* [141] with those of the FCM-ANFIS model (Model IV) and the correlations for SiO_2-water nanofluid with a particle size of 12 nm and a volume concentration of 1.85%. As was mentioned before, there were no experimental data for the viscosity of SiO_2-water nanofluid in the FCM-ANFIS model-training procedure. The FCM-ANFIS model trend matches the experimental data the best, while all the correlations significantly under predicted the experimental data.

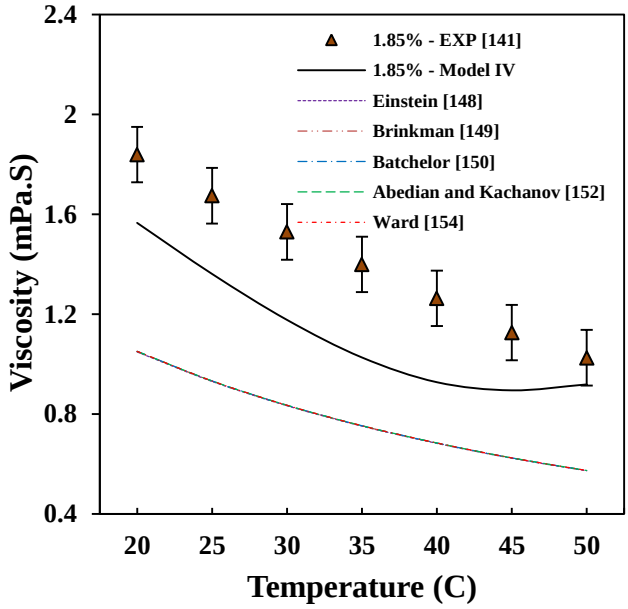

Figure 4.7: Comparison between the experimental data of Tavman *et al* [141] with Model IV and correlations from literature for a SiO_2-water nanofluid, with an average particle size of 12 nm at a volume concentration of 1.85%

4.6. CONCLUSION AND RECOMMENDATIONS

The FCM-ANFIS approach was used for modelling the viscosity of nanofluids as a function of particle size, volume concentration and temperature. The FCM-ANFIS method consists of a neural network combined with a fuzzy logic approach which the fuzzy C-means clustering was used as the fuzzy identification method. The adaptive neuro-fuzzy inference system (ANFIS) used neural network and fuzzy logic

approaches at the same time to combine the advantages of each method to achieve a better performance.

A literature review of experimental data of the viscosity of nanofluids showed that particle size, volume concentration and temperature were the three most important variables that influence on the viscosity. Therefore, 536 experimental data points for Al_2O_3, CuO, TiO_2 and SiO_2 nanoparticles with water as base fluid were obtained from literature for benchmarking the proposed models for the viscosity of nanofluids by using the experimental data point.

The results of the FCM-ANFIS method were compared with the experimental data as well as several well-cited correlations from literature. In almost all cases, the proposed FCM-ANFIS models were in very good agreement with the experimental data. This study showed the ability of FCM-ANFIS technique for modelling engineering problems containing nanofluids based on input-output experimental data.

Since the proposed FCM-ANFIS models for modelling the viscosity of nanofluids has showed a great agreement with experimental data, this method is a very good candidate to model required sonication time and power. Since there is still a challenge to find the optimised sonication power and time to prepare the nanofluids in a two-step procedure, therefore, it can recommend applying FCM-ANFIS technique to model required sonication power and time for nanofluids preparation to be able to use optimisation techniques (like NSGA-II) to find the optimum sonication power and time for the best nanofluid preparation.

5

CHAPTER 5: MULTI-OBJECTIVE OPTIMISATION OF THE CONVECTIVE HEAT TRANSFER CHARACTERISTICS AND PRESSURE DROP OF NANOFLUIDS[13]

5.1. INTRODUCTION

In this chapter, a GA-PNN hybrid system was used for modelling the convective heat transfer characteristics and pressure drop of TiO_2-water nanofluids in a fully developed turbulent flow based on an experimentally obtained train and test data set. Models have been developed for the Nusselt number and the pressure drop of the nanofluids as function of Reynolds and Prandtl numbers, nanofluid volume concentration and average nanoparticle diameter. The results of the proposed models have been compared with experimental data as well as existing correlations. The validity of the proposed models benchmarked by using statistical criteria and after showing a fair agreement with experimental data, the modified non-dominated sorting genetic algorithm (NSGA-II) was used for multi-objective optimisation of the convective heat transfer. In the optimisation procedure, the Nusselt number and pressure drop have been considered as the objective functions. However, when the set of decision variables is selected based on the Pareto set, it ensures the best possible combination of objectives. The Pareto front of multi-objective optimisation of the Nusselt number and pressure drop proposed models has also been shown and discussed.

5.2. GENETIC ALGORITHM-POLYNOMIAL NEURAL NETWORK HYBRID SYSTEM

In this dissertation, a GA-PNN hybrid system was applied for the simulation of the Nusselt number and pressure drop of TiO_2-water nanofluid in fully- developed turbulent flow. The GA-PNN hybrid system was created by a combination of genetic

[13] This chapter has been published in part: M. Mehrabi, M. Sharifpur and J.P. Meyer, "Modelling and multi-objective optimisation of the convective heat transfer characteristics and pressure drop of low concentration TiO2-water nanofluids in the turbulent flow regime", *International Journal of Heat and Mass Transfer*, Vol. 67 (1), pp. 646–653, 2013.

algorithm and GMDH-type polynomial neural network approaches. In this hybrid system, a GMDH learning algorithm was used to instruct the polynomial neural network. The application of this learning algorithm to the polynomial neural network would introduce the GMDH-type polynomial neural network, which would be created for the neural network. On the other hand, the genetic algorithm was used to find the hidden layers and bias coefficients of the GMDH-type polynomial neural network for minimising the training error and finding the optimal structure of the network. Detailed information about the GMDH-type polynomial neural network structure and GA-PNN hybrid system is given in Pesteei and Mehrabi [122] and Mehrabi *et al* [156, 157], respectively.

5.3. CONVECTIVE HEAT TRANSFER OF TiO_2-WATER NANOFLUID

Most of the fluid flow regimes are turbulent in industrial applications. Due to the presence of unsteady vortexes, the turbulent flow has more potential to enhance heat transfer. Therefore, the investigations into turbulent heat transfer of nanofluids are crucial for practical applications. Subsequently, there are several studies in the literature on the convection heat transfer of TiO_2-water nanofluids in fully-developed turbulent flow regime [158–162 and 167]. In the present work, a new model was obtained by using the GA-PNN hybrid system as a function of the Reynolds number, Prandtl number, volume concentration and average particle size, which gives better accuracy for predicting the heat transfer performance of the TiO_2-water nanofluids. In the proposed model, the Nusselt number is related to the parameters as follows:

$$Nu_{nf} = f(Re, Pr, \phi, d_p) \tag{5.1}$$

The results of the proposed model were compared against experimental data [158, 159 and 162] as well as available correlations. The correlations, which were developed by Pak and Cho [163] (Eq. 5.2) and Maiga *et al* [168] (Eq. 5.3), can predict the Nusselt number for the nanofluids in a fully-developed turbulent flow.

$$Nu_{nf} = 0.021\, Re^{0.8} Pr^{0.5} \quad (5.2)$$

$$Nu_{nf} = 0.085\, Re^{0.71} Pr^{0.35} \quad (5.3)$$

The correlations determine the Nusselt numbers as a function of the Reynolds number and the Prandtl number.

Sajadi and Kazemi [159] proposed a correlation for the Nusselt number of TiO_2-water nanofluids in a fully developed turbulent regime as a function of the Reynolds number and the Prandtl number as:

$$Nu_{nf} = 0.067\, Re^{0.71} Pr^{0.35} + 0.0005\, Re \quad (5.4)$$

Duangthongsuk and Wongwises [158] and Abbasian Arani and Amani [167] offered correlations for the Nusselt number of TiO_2-water nanofluids as a function of the Reynolds number, the Prandtl number and volume concentration respectively, as follows:

$$Nu_{nf} = 0.074\, Re^{0.707} Pr^{0.385} \phi^{0.074} \quad (5.5)$$

$$Nu_{nf} = 0.041\, Re^{0.83} Pr^{1.35} (1 + \phi^{0.43}) \quad (5.6)$$

Unlike the present models for the Nusselt number, the dependence of the average particle diameter of the nanoparticles was not considered in these correlations.

5.4. PRESSURE DROP OF TiO_2-WATER NANOFLUIDS

In this chapter, a new model was developed for the pressure drop of TiO_2-water nanofluids in fully-developed turbulent flow by using a GA-PNN hybrid system as a function of Reynolds number, volume concentration and average particle size. In the model, the pressure drop is a function of Reynolds number, nanoparticle volume concentration and the diameter of nanoparticles, thus:

$$\Delta P_{nf} = f(Re, \phi, d_p) \quad (5.7)$$

5.5. PREDICTIVE ABILITY OF THE PROPOSED MODELS

A total of 168 input-output experimental data points obtained from literature [158, 159 and 162] were used in order to predict the Nusselt number for a TiO_2-water nanofluid. The experimental data were divided into two subsets as 75% (127 data points) for training and 25% (41 data points) for testing purposes. In order to model the pressure drop 151 experimental data points from [156, 157 and 160] were divided to subsets as 81% (124 data points) for training and 19% (29 data points) for testing purposes. The mean absolute error (*MAE*), mean relative error (*MRE*) and root mean square errors (*RMSE*) criteria were used. It shows the accuracy of the GA-PNN models in order to predict the Nusselt number and pressure drop of TiO_2-water nanofluid for various values of inlet variables.

5.5.1. Nusselt Number Prediction

The structure of the GA-PNN model for predicting the Nusselt number of TiO_2-water nanofluid is shown In Figure 5.1, corresponds to the genome representation of ***3312141411342222,*** in which ***1, 2, 3*** and ***4*** stand for volume concentration ϕ (%), average particle diameter d_p (nm) , the Reynolds number *Re* and the Prandtl number *Pr* respectively.

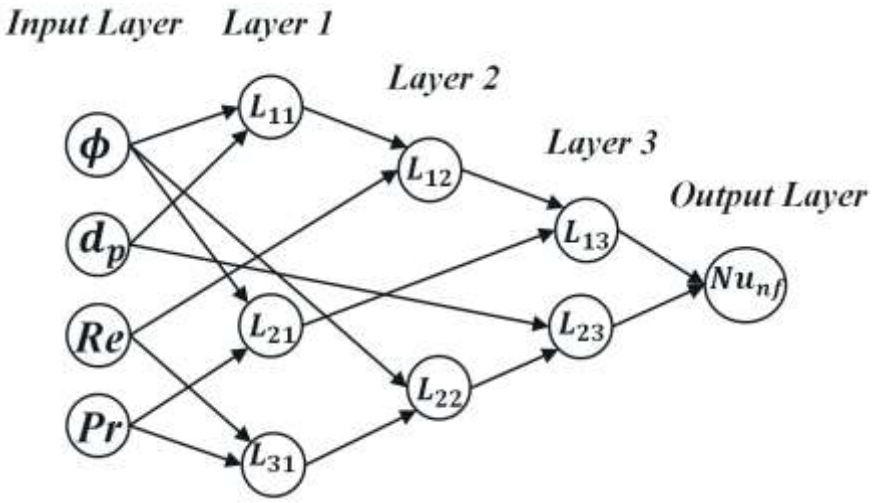

Figure 5.1: Structure of the GA-PNN hybrid system for the Nusselt number of TiO_2-water nanofluids modelling

The corresponding polynomial representation of the model for the Nusselt number of TiO_2-water nanofluid is shown below:

$$L_{11} = a_{1,0} + a_{1,1}.\phi + a_{1,2}.d_p + a_{1,3}.\phi.d_p + a_{1,4}.\phi^2 + a_{1,5}.{d_p}^2$$
$$L_{21} = a_{2,0} + a_{2,1}.\phi + a_{2,2}.Pr + a_{2,3}.\phi.Pr + a_{2,4}.\phi^2 + a_{2,5}.Pr^2$$
$$L_{31} = a_{3,0} + a_{3,1}.Re + a_{3,2}.Pr + a_{3,3}.Re.Pr + a_{3,4}.Re^2 + a_{3,5}.Pr^2$$
$$L_{12} = a_{4,0} + a_{4,1}.Re + a_{4,2}.L_{11} + a_{4,3}.Re.L_{11} + a_{4,4}.Re^2 + a_{4,5}.{L_{11}}^2$$
$$L_{22} = a_{5,0} + a_{5,1}.\phi + a_{5,2}.L_{31} + a_{5,3}.\phi.L_{31} + a_{5,4}.\phi^2 + a_{5,5}.{L_{31}}^2$$
$$L_{13} = a_{6,0} + a_{6,1}.L_{12} + a_{6,2}.L_{21} + a_{6,3}.L_{12}.L_{21} + a_{6,4}.{L_{12}}^2 + a_{6,5}.{L_{21}}^2$$
$$L_{23} = a_{7,0} + a_{7,1}.L_{22} + a_{7,2}.d_p + a_{7,3}.L_{22}.d_p + a_{7,4}.{L_{22}}^2 + a_{7,5}.{d_p}^2$$
$$Nu_{nf} = a_{8,0} + a_{8,1}.L_{13} + a_{8,2}.L_{23} + a_{8,3}.L_{13}.L_{23} + a_{8,4}.{L_{13}}^2 + a_{8,5}.{L_{23}}^2$$

$$[\mathbf{a}_{ij}] = \begin{bmatrix} 67.39861967 & 155.3890385 & -0.54661578 & -67.4937622 & 0.006683105 & 1.25041801 \\ -625.276506 & 5.001759885 & 467.1605151 & 54.2212255 & -58.2092747 & -42.824571 \\ 2.197 \times 10^{-7} & 0.002868903 & 2.308 \times 10^{-7} & -2.92 \times 10^{-8} & -7.15 \times 10^{-7} & 0.00177207 \\ 4.509 \times 10^{-7} & 0.005725457 & 3.199 \times 10^{-5} & -1.44 \times 10^{-8} & 0.000360089 & 1.292 \times 10^{-5} \\ 12.62326281 & -28.6139037 & 0.792949239 & 12.08935958 & -0.00018628 & 0.194649498 \\ 50.15011252 & 0.442351847 & -0.56421161 & -0.00034801 & 0.001662117 & 0.003198651 \\ -9.63382038 & 1.031554882 & 0.624331389 & 0.000229741 & -0.00289168 & -0.00401269 \\ -2.18155351 & 0.533902305 & 0.507308577 & -0.00521318 & -0.00314481 & 0.008270173 \end{bmatrix}$$

5.5.2. Pressure Drop Prediction

The structure of the GA-PNN model for predicting the pressure drop of TiO_2-water nanofluid is shown in Figure 5.2, corresponding to the genome representation of

1211221333122323, in which ***1, 2*** and ***3*** stand for volume concentration ϕ (%), average particle diameter d_p (nm) and the Reynolds number *Re*, respectively.

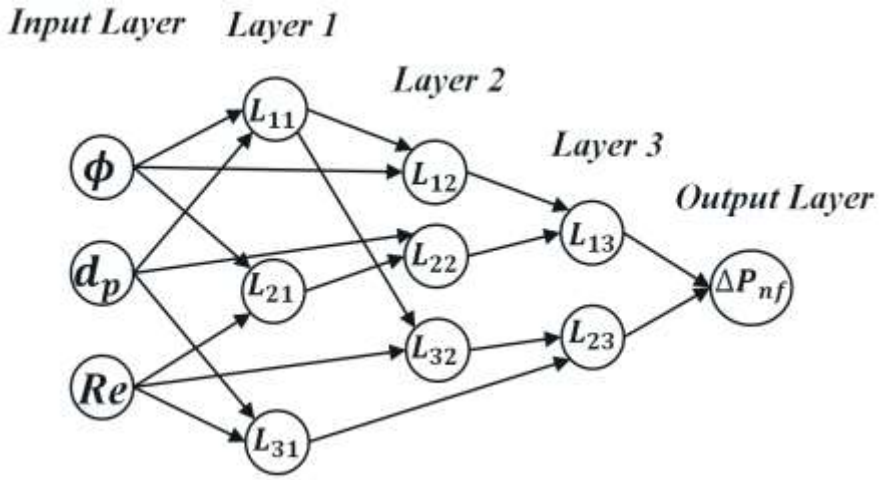

Figure 5.2: Structure of the GA-PNN hybrid system for pressure drop of TiO_2-water nanofluid modelling

The corresponding polynomial representation of the model for the pressure drop of TiO_2-water nanofluid is shown below:

$$L_{11} = a_{1,0} + a_{1,1}.\phi + a_{1,2}.d_p + a_{1,3}.\phi.d_p + a_{1,4}.\phi^2 + a_{1,5}.{d_p}^2$$
$$L_{21} = a_{2,0} + a_{2,1}.\phi + a_{2,2}.Re + a_{2,3}.\phi.Re + a_{2,4}.\phi^2 + a_{2,5}.Re^2$$
$$L_{31} = a_{3,0} + a_{3,1}.d_p + a_{3,2}.Re + a_{3,3}.d_p.Re + a_{3,4}.{d_p}^2 + a_{3,5}.Re^2$$
$$L_{12} = a_{4,0} + a_{4,1}.L_{11} + a_{4,2}.\phi + a_{4,3}.L_{11}.\phi + a_{4,4}.{L_{11}}^2 + a_{4,5}.\phi^2$$
$$L_{22} = a_{5,0} + a_{5,1}.d_p + a_{5,2}.L_{21} + a_{5,3}.d_p.L_{21} + a_{5,4}.{d_p}^2 + a_{5,5}.{L_{21}}^2$$
$$L_{32} = a_{6,0} + a_{6,1}.L_{11} + a_{6,2}.Re + a_{6,3}.L_{11}.Re + a_{6,4}.{L_{11}}^2 + a_{6,5}.Re^2$$
$$L_{13} = a_{7,0} + a_{7,1}.L_{12} + a_{7,2}.L_{22} + a_{7,3}.L_{12}.L_{22} + a_{7,4}.{L_{12}}^2 + a_{7,5}.{L_{22}}^2$$
$$L_{23} = a_{8,0} + a_{8,1}.L_{32} + a_{8,2}.L_{31} + a_{8,3}.L_{32}.L_{31} + a_{8,4}.{L_{32}}^2 + a_{8,5}.{L_{31}}^2$$
$$\Delta P_{nf} = a_{9,0} + a_{9,1}.L_{13} + a_{9,2}.L_{23} + a_{9,3}.L_{13}.L_{23} + a_{9,4}.{L_{13}}^2 + a_{9,5}.{L_{23}}^2$$

$$[\mathbf{a}_{ij}] = \begin{bmatrix} -4.901\times10^{-7} & -2.521\times10^{-5} & 0.00040705 & -0.0013582 & 1.415\times10^{-9} & 1.994\times10^{-6} \\ 4.346\times10^{-8} & 2.525\times10^{-8} & 0.00045035 & 2.638\times10^{-8} & 3.889\times10^{-9} & -8.86\times10^{-5} \\ 7.78933893 & 2.341589898 & -0.2035313 & 2.66252775 & 0.109419333 & -0.31805789 \\ 5.39159929 & -11.5340018 & 0.86942588 & 4.75545983 & 0.013934046 & -0.09116812 \\ -31.694717 & 16.11679573 & 6.16097472 & -1.9169856 & -0.19310173 & -1.30663773 \\ -6.4420171 & 1.178165895 & 0.43875907 & -0.0061312 & -0.00702419 & -0.00039369 \\ 0.31629638 & 0.318197046 & 0.65454924 & -0.0766096 & -0.15295112 & 0.231249939 \\ 1.53695886 & -0.00558705 & 0.37241296 & -0.0113919 & 0.008688029 & 0.047656331 \\ -0.1436674 & 0.770220048 & 0.27359825 & -0.0298951 & -0.04116522 & 0.069972926 \end{bmatrix}$$

UNIVERSITEIT VAN PRETORIA
UNIVERSITY OF PRETORIA
YUNIBESITHI YA PRETORIA

5.6. MULTI-OBJECTIVE OPTIMISATION BY USING NSGA-II

In most real-engineering problems, a unique solution based on the single-objective optimisation techniques is unable to present an acceptable result for the other objective functions, especially when there is more than one objective function that may be in conflict with one another. Multi-objective optimisation is defined as a technique that gives a reasonable set of solutions for all objective functions by finding the vector of decision variables when the constraints are satisfied. This set of solutions satisfies the objective functions at an acceptable level without being dominated by other sets. This set of non-dominated solutions is called the Pareto optimal set. The corresponding objective function value for a given Pareto optimal set is referred to as the Pareto front.

Various multi-objective algorithms have been applied for solving engineering problems in the last two decades [164, 165, 169–175], among them the modified non-dominated sorting genetic algorithm II (NSGA-II), which was chosen for this investigation.

There are different operators for the NSGA-II algorithm including initialisation, evaluation, fast non-dominated sorting, crowding distance assignment, selection, crossover and mutation. The procedure and flow diagram of this algorithm are shown below:

NSGA II Algorithm
Step 1: generate a parent population P_0 of size N, randomly
Step 2: set $t = 0$
Step 3: create offspring population Q_0 of size N, by application of crossover and mutation to P_0
Step 4: if the stop criterion is satisfied, stop and return P_t
Step 5: set $R_t = P_t \cup Q_t$
Step 6: set $F = (F_1, F_2, \dots, F_K) =$ fast-non-dominated-sort (R_t)
Step 7: for $i = 1: k$ do the following sub-steps:
    7.1: calculate the crowding-distance-assignment (F_i)
    7.2: set P_{t+1} as follows:
        if $|P_{t+1}| + |F_i| \leq N$;

UNIVERSITEIT VAN PRETORIA
UNIVERSITY OF PRETORIA
YUNIBESITHI YA PRETORIA

$P_{t+1} = P_{t+1} \cup F_i$
then ($|P_{t+1}| + |F_i| > N$);
$P_{t+1} = P_{t+1} \cup F_i[1:(N - |P_{t+1}|)]$

Step 8: this step consists of the following two sub-steps:

8.1: select parent from P_{t+1} by using binary tournament selection on the crowding distance

8.2: create offspring population Q_{t+1} of size *N*, by application of crossover & mutation to P_{t+1}

Step 9: set $t = t + 1$ and go to the fourth step

The NSGA-II uses a fast non-dominated sorting operator for fitness assignments. In the process of a fitness assignment, the solution set not dominated by any other solutions in the population is assigned as the first front and given the highest fitness value; the solution set dominated by solutions in the first front is assigned as the second front and given the second-highest fitness value. This procedure will iterate until all the solution sets are given a fitness value. The crowding distance is the normalised distance between a solution vector and its closest neighbouring solution vector in each of the fronts.

The selection is achieved in binary tournament of two solution vectors. The solution vector with the lowest front number is selected if the two solution vectors are from different fronts. If both the solution vectors are on the same front, the solution with the highest crowding distance is selected.

In the NSGA-II algorithm, simulated binary crossover (SBX) and highly disruptive polynomial mutation approaches are used for crossover and mutation operators. The SBX applies to two parent solutions and creates two offsprings. The difference between an offspring and parent depends on the crossover index, which is a non-negative real number. A large value of the crossover index gives a higher probability for creating 'near-parent' solutions and a small value of it allows distant solutions to be selected as an offspring. The application of highly disruptive polynomial mutation gives the system the possibility of doing larger jumps in the search space and avoiding

the local optimal points [176]. The detailed information about the NSGA-II Algorithm, fast non-dominated sorting operator, crowding-distance-assignment operator, selection method and simulated binary crossover (SBX) operator are fully described in Refs [166 and 176]. The conflicting objectives in this study are the Nusselt number and pressure drop that are optimised with respect to the volume concentration ϕ, average particle diameter d_p, the Reynolds number *Re* and the Prandtl number *Pr*, which are called design variables. In this two-objective optimisation problem, the goal is finding the best design variable value in order to maximise the Nusselt number and minimise the pressure drop simultaneously.

5.7 RESULT AND DISCUSSION

Figure 5.3, shows the experimental results of Sajadi and Kazemi [159] compared with the GA-PNN model for the Nusselt number of TiO_2-water nanofluid and also correlations with a particle size of 30 nm and volume concentration of 0.1% at various Reynolds numbers ranging from 6 000 to 30 000. The model for Nusselt number is in very good agreement with the experimental data (*MAE* = 3.7, *MRE* = 3.5% and *RMSE* = 4.4). The proposed GA-PNN model is well matched with the experimental data and predicts the Nusselt number better than all correlations [158, 163, 167 and 168].

Figure 5.4, shows the experimental results of Duangthongsuk and Wongwises [158] compared with the GA-PNN model. Also, the correlations from literature for a particle size of 21 nm and volume concentration of 1% for a TiO_2-water nanofluid over a Reynolds number range from 4 500 to 14 500. The GA-PNN model is in good agreement with the experimental data (*MAE* = 3.4, *MRE* = 3.7% and *RMSE* = 3.6), and the GA-PNN proposed model and Sajadi and Kazemi [168] correlation predict the Nusselt number better than other correlations [163, 167 and 168].

UNIVERSITEIT VAN PRETORIA
UNIVERSITY OF PRETORIA
YUNIBESITHI YA PRETORIA

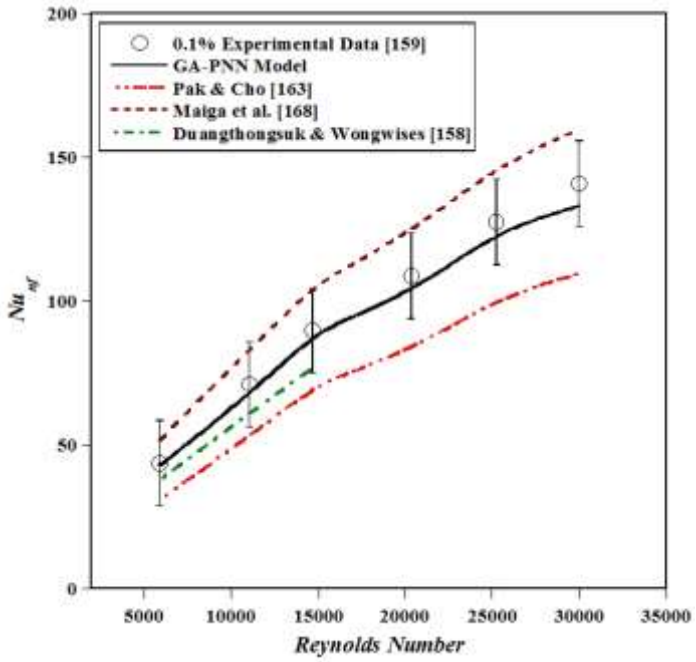

Figure 5.3: Comparison of the experimental data of Sajadi and Kazemi [159] with the GA-PNN proposed model for the Nusselt number and existing correlations (TiO_2-water nanofluid, with an average particle size of 30 nm at a volume concentration of 0.1%)

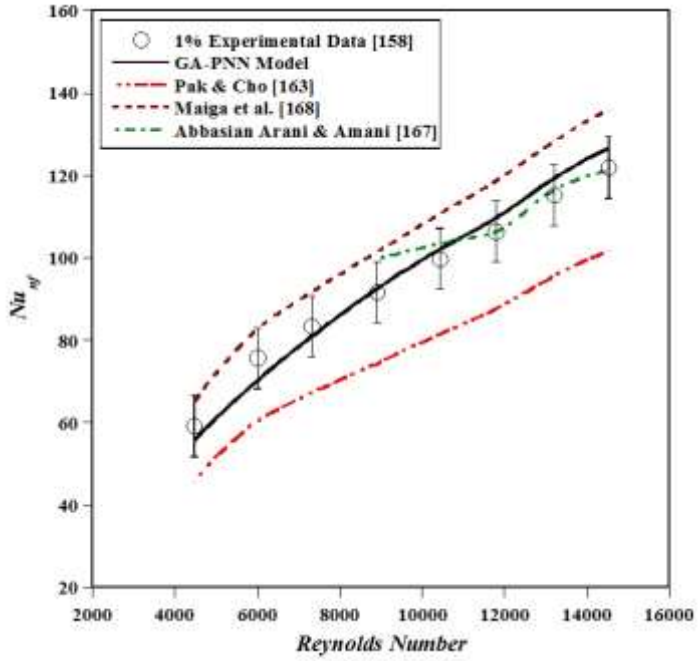

Figure 5.4: Comparison of the experimental data of Duangthongsuk and Wongwises [158] with the GA-PNN proposed model for the Nusselt number and existing correlations (TiO_2 water nanofluid, with an average particle size of 21 nm at a volume concentration of 1%)

UNIVERSITEIT VAN PRETORIA
UNIVERSITY OF PRETORIA
YUNIBESITHI YA PRETORIA

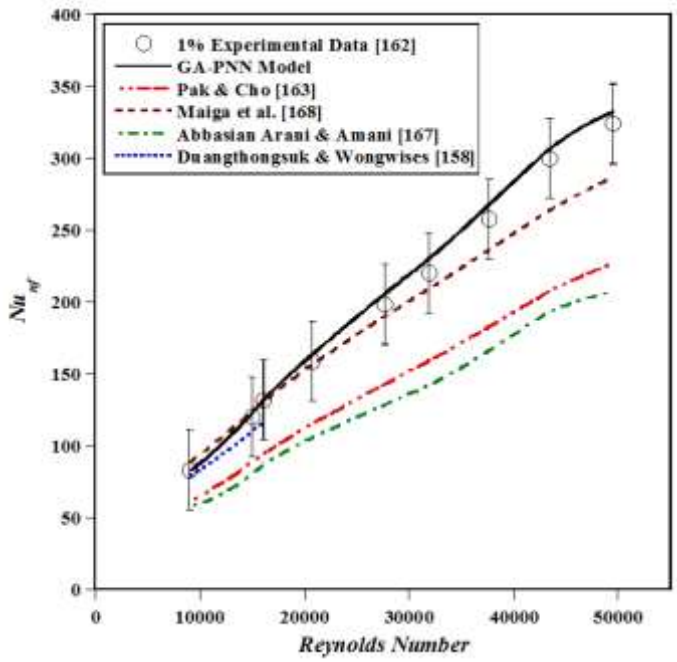

Figure 5.5: Comparison of the experimental data of Abbasian Arani and Amani [162] with the GA-PNN proposed model for the Nusselt number and existing correlations (TiO_2-water nanofluid, with an average particle size of 50 nm at a volume concentration of 1%)

Figure 5.5, shows the experimental results of Abbasian Arani and Amani [162] compared with the GA-PNN model. Also, the correlations from literature for a particle size of 50 nm and volume concentration of 1% for a TiO_2-water nanofluid. The GA-PNN model is in great agreement with the experimental data (MAE = 5.9, MRE = 2.7% and RMSE = 6.9), and the GA-PNN proposed model and Maiga *et al* [168] correlation predict the Nusselt number better than other correlations.

In Figure 5.6 and Figure 5.7, the experimental results of Abbasian Arani and Amani [162] are compared with those of the GA-PNN model and the correlations for the Nusselt number of TiO_2-water nanofluid with particle sizes of 10 nm and 20 nm, and volume concentration of 1.5% and 2%, respectively.

Based on the result of Figure 5.6 the GA-PNN model is well-matched with the experimental data in comparison with the correlations (*MAE* = 5.6, *MRE* = 4.8% and

RMSE = 8.1), especially in the high Reynolds number range from 20 000 to 44 000. Figure 5.7, shows that the GA-PNN model is in a good agreement with the experimental data (*MAE* = 20.3, *MRE* = 8.1% and *RMSE* = 21.3) and predicts the Nusselt number the best while the existing correlations significantly under-predicted the experimental data.

Considering Figure 5.6 and Figure 5.7, it can be concluded that for TiO_2-water nanofluids with an increase in Reynolds number as well as volume concentration the existing correlations are unable to predict the Nusselt number properly and the GA-PNN model predicts the Nusselt number better than those of the correlations in literature in all cases.

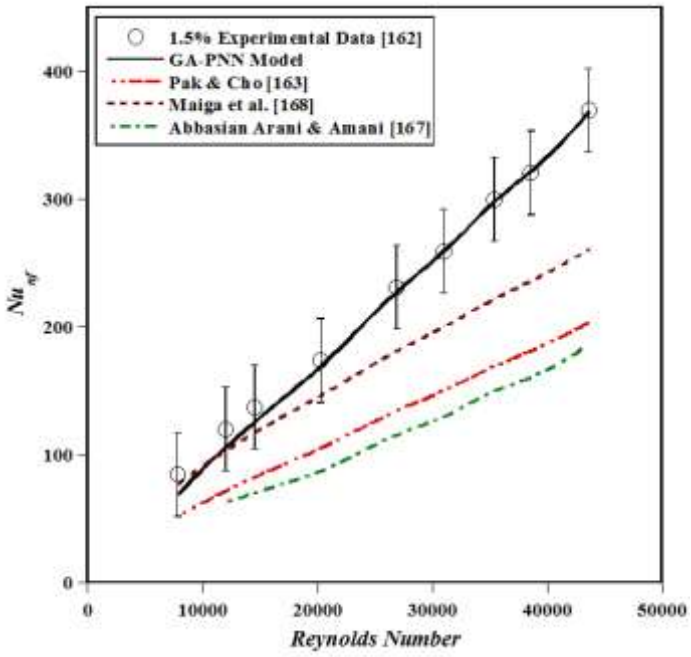

Figure 5.6: Comparison of the experimental data of Abbasian Arani and Amani [162] with the GA-PNN proposed model for the Nusselt number and existing correlations (TiO_2-water nanofluid, with an average particle size of 10 nm at a volume concentration of 1.5%)

UNIVERSITEIT VAN PRETORIA
UNIVERSITY OF PRETORIA
YUNIBESITHI YA PRETORIA

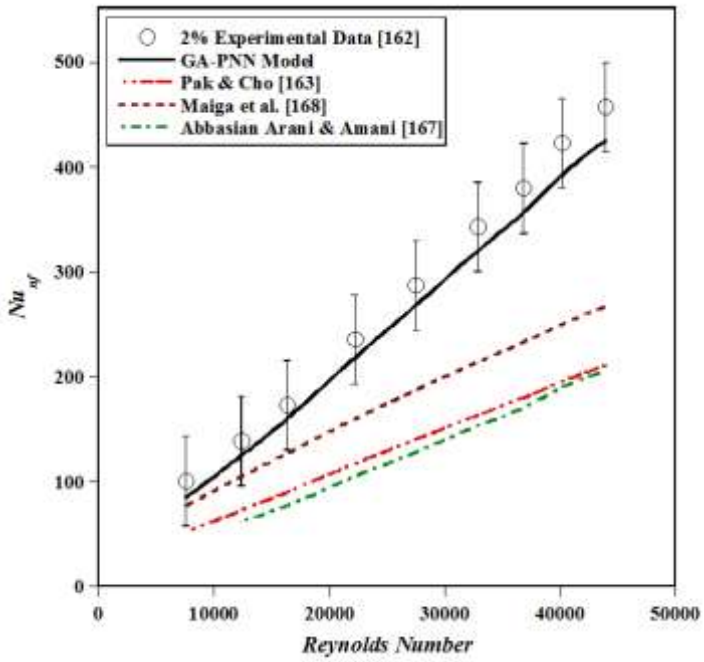

Figure 5.7: Comparison of the experimental data of Abbasian Arani and Amani [162] with the GA-PNN proposed model for the Nusselt number and existing correlations (TiO_2-water nanofluid, with an average particle size of 20 nm at a volume concentration of 2%)

Figure5.8a shows a comparison between the experimental results of Sajadi and Kazemi [159] and the GA-PNN model for the pressure drop of a TiO_2-water nanofluid with a particle size of 30 nm, volume concentration of 0.15% and Reynolds number ranging from 6 000 to 30 000. The GA-PNN model (*MAE* = 0.47, *MRE* = 5.0% and *RMSE* = 0.53) corresponds very well with the experimental data.

In Figure5.8b, the experimental results of Duangthongsuk and Wongwises [158] are compared with those of the GA-PNN model and the correlations for the pressure drop of TiO_2-water nanofluid with a particle size of 21 nm, and a volume concentration of 1.5% and Reynolds number ranging from 4 500 to 14 500. The GA-PNN model predicts the pressure drop the best when compared with the measurements (*MAE* = 0.12, *MRE* = 2.0% and *RMSE* = 0.21).

UNIVERSITEIT VAN PRETORIA
UNIVERSITY OF PRETORIA
YUNIBESITHI YA PRETORIA

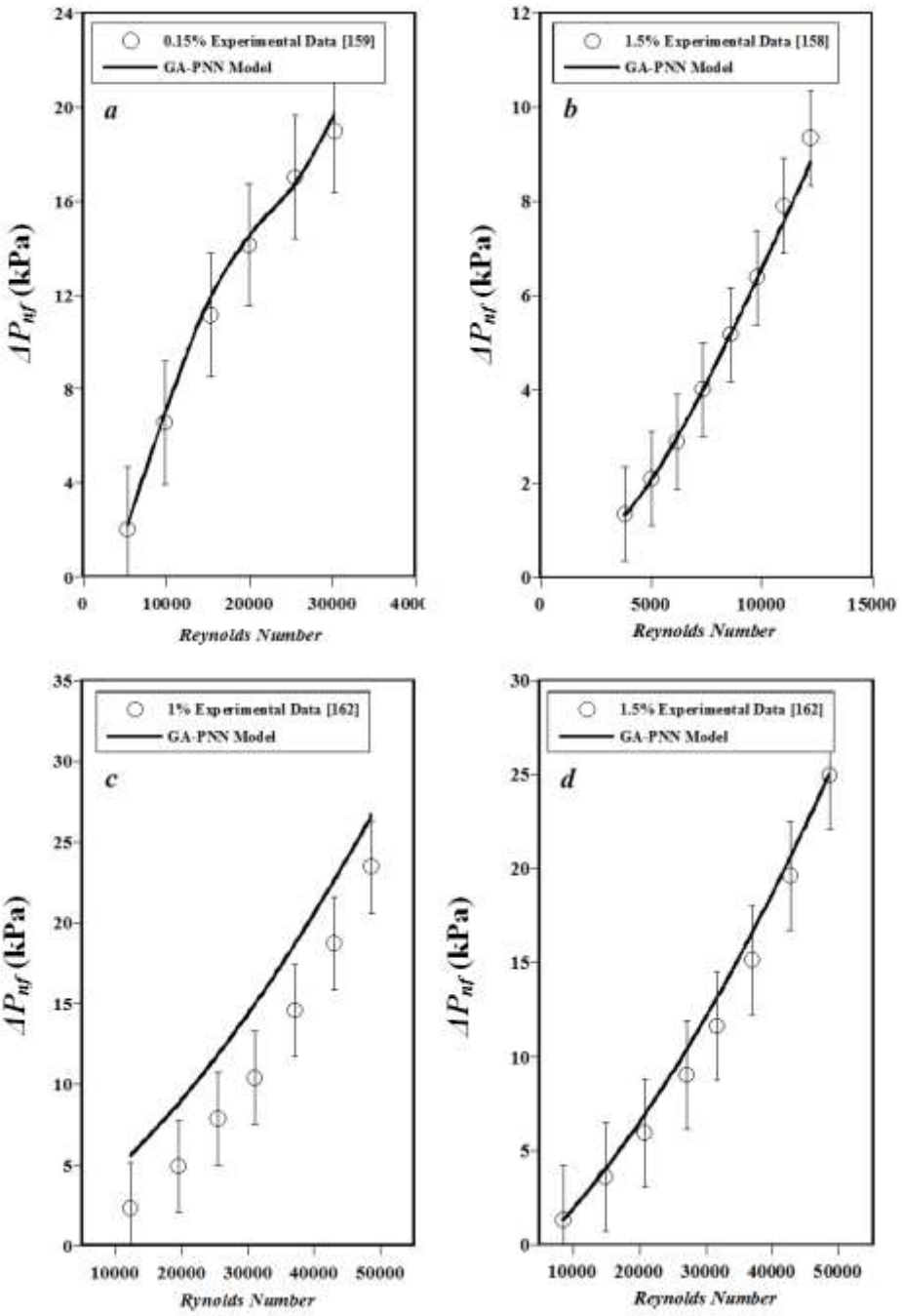

Figure 5.8: Comparison of the experimental data [158, 159 and 162] with the GA-PNN proposed model for pressure drop (a-TiO_2-water nanofluid, with an average particle size of 30 nm at a volume concentration of 0.15% [159] b-TiO_2-water nanofluid, with an average particle size of 21 nm at a volume concentration of 1.5% [158] c-TiO_2-water nanofluid, with an average particle size of 30 nm at a volume concentration of 1% [160] d-TiO_2-water nanofluid, with an average particle size of 50 nm at a volume concentration of 1.5% [162])

Figure5.8c shows the experimental results of Abbasian Arani and Amani [162] compared with the GA-PNN model for a particle size of 30 nm and volume concentration of 1%. The GA-PNN model is not in such a good agreement with the experimental data and the (*MAE* = 3.9, *MRE* = 54.4% and *RMSE* = 3.9).

Although the proposed model is not well-matched with the experimental data, the model trend is the same as experimental data and because the proposed model over-predicted the experimental data, it might give us more conservative result points in the optimisation part.

In Figure5.8d, the experimental result of Abbasian Arani and Amani [162] is compared with those of the GA-PNN model for a particle size of 50 nm and volume concentration of 1.5%. The GA-PNN model matches the data very well (*MAE* = 0.835, *MRE* = 8.9% and *RMSE* = 1.01).

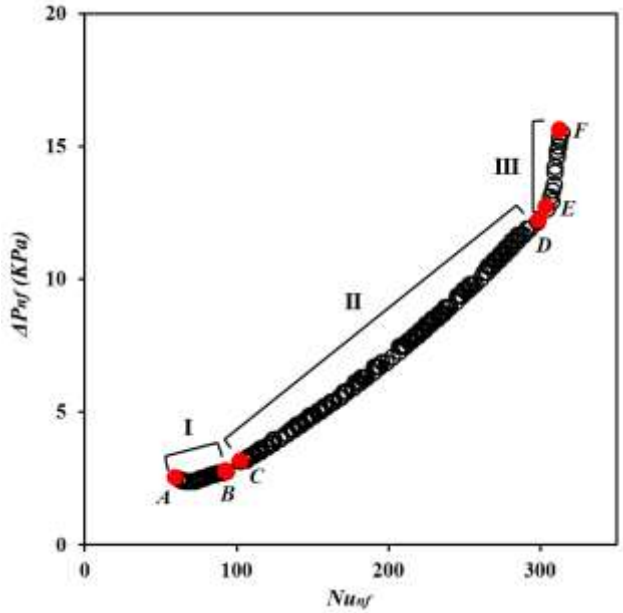

Figure 5.9: Multi-objective Pareto front of the Nusselt number and pressure drop

UNIVERSITEIT VAN PRETORIA
UNIVERSITY OF PRETORIA
YUNIBESITHI YA PRETORIA

Figure 5.9, shows the Pareto front of the Nusselt number and pressure drop. By choosing the appropriate value for one objective function may cause a poor value for the second objective function. In this Pareto front, all the points (Pareto sets) are optimum points based on the multi-objective optimisation concepts and the final design point should be chosen by the designer based on the importance of each objective function in the design procedure. In this Pareto front, the optimal design points are divided into three sections and the corresponding design variables (input variables) as well as objective functions for the six optimal points, which are shown in Table 5-1, (they are related to start and end points).

In Section I, which is started at point A and ends at B, the Nusselt number increases by 45% (from 64.23 to 91.11) when the pressure drop increases by 14% (from 2.42 to 2.75). In Section II which starts at point C and ends at D, there is a direct relationship between the increase in the pressure drop and increase in Nusselt number. In this section, the pressure drop increases by 271% when the Nusselt number increases by 179%. It is obvious that the design points in Section III should not be chosen as the best design points, because of the 19% increase in the pressure drop; while there is no significant increase in the Nusselt number from Point E to Point F. So, choosing the final design points from Section II is a better choice in comparison with the other sections.

Table 5-1: The value of design variables (input variables) and objective functions of the start and end section points

Points	ϕ (%)	d_p (nm)	*Re*	*Pr*	*Nu*	ΔP (kPa)
A	1.93	50	6010	3.19	64.234	2.422
B	1.68	40	8768	4.12	93.106	2.754
C	1.52	35	10143	4.31	106.666	3.284
D	1.31	20	30857	3.5	297.864	12.199
E	1.28	20	32238	3.47	307.299	12.99
F	1.15	20	35120	3.72	313.878	15.521

However, it is important to notice that all the points in this Pareto front are optimal points and the designer could choose any of these optimal points for the best design point. It is related to the importance of objective functions in the design procedure.

5.8 CONCLUSION AND RECOMMENDATIONS

In this chapter, the GA-PNN hybrid system was used for modelling the convective heat transfer characteristics and pressure drop of TiO_2-water nanofluid in fully developed turbulent flow based on an input-output experimental data set as function of the Reynolds number, the Prandtl number, nanoparticle volume concentration and average nanoparticle diameter. In the GA-PNN hybrid system, consisting of a neural network and genetic algorithm part, the genetic algorithm was used to find the best network weights for minimising the training error and finding the optimal structure for a GMDH-type polynomial neural network. In the neural network part of this hybrid system, the group method of data handling (GMDH) learning approach was used to learn a second-rate polynomial neural network. The structure of the proposed models based on the genome representation for the Nusselt number as well as pressure drop with respect to effective (input) parameters has been developed. The results of the models were compared with the experimental data points and with existing correlations from literature. The statistical error analysis shows that the proposed models are in good agreement compared with experimental data and shows better accuracy with experimental data in comparison with the existing correlations.

The proposed models for the Nusselt number and pressure drop were used in a multi-objective optimisation problem based on the NSGA-II algorithm. The Pareto front of these two conflicting objective functions was shown and discussed.

Application of the constructal theory and modified NSGA-II multi-objective optimisation method together can be a challenging subject for future work to find a model for prediction of the most optimised nanofluids composition. For this future

research work, the advantages of two different optimisation technique (modified NSGA-II multi-objective optimisation method and constructal theory) may be used to predict the most optimised nanofluids composition for energy efficiency propose.

6

CHAPTER 6: CONCLUSIONS AND RECOMMENDATIONS

6.1. SUMMARY

Due to the advantages of application of nanofluids in comparison with conventional heat transfer fluids, nanofluids as a new generation of heat transfer fluids has received significant attention over the last two decades.

However, there is still a problem for modelling and predicting the thermophysical properties of nanofluids. Since there are too many factors affecting the thermophysical properties of nanofluids including nanoparticle type, shape, size, temperature, volume concentration, and the nanofluids preparation method which most of the times are in conflict with each other for thermal improvement. So, the necessity of a research on thermophysical properties of nanofluids to find accurate models is essential. The aim of this dissertation is to try to overcome this problem by proposing accurate models for thermophysical properties of nanofluids by using GA-PNN, FCM-ANFIS techniques and input-output experimental data. To do so, two methods of artificial intelligence methods (GA-PNN and FCM-ANFIS) have been implemented to model effective thermal conductivity and viscosity of nanofluids. The results of the proposed model were compared with the experimental data as well as well-cited correlations and in almost all case studies the proposed models have shown a good agreement with experimental data.

Furthermore, the convective heat transfer characteristics and pressure drop of the nanofluids in a turbulent flow regime have been modelled by the GA-PNN hybrid system and consequently the resulting models have been used to optimise the Nusselt number versus pressure drop by NSGA-II which is a multi-objective optimisation technique. The optimisation result was shown in a Pareto front to show all the optimum design points.

UNIVERSITEIT VAN PRETORIA
UNIVERSITY OF PRETORIA
YUNIBESITHI YA PRETORIA

6.2. CONCLUSIONS

Chapter 2 has provided a review on possible mechanisms which could potentially influence the thermal conductivity enhancement of nanofluids. Brownian motion of nanoparticles, nanoparticle size, concentration, distribution and formation of aggregates, nanolayering of the liquid at the liquid/particle interface, electric charge on the surface of nanoparticle, thermophoretic effect, preparation and surfactants are different factors which have been introduced and explained. Furthermore, theoretical models which have been proposed by different researchers for thermal conductivity of nanofluids are reviewed based on the influence of Brownian motion, nanolayering as well as clustering and some hybrid models that are taken into account two parameters are presented in this chapter.

Chapter 3 of this dissertation showed the high capability of artificial intelligent methods for modelling engineering problems containing nanofluids based on input-output experimental data. The FCM-ANFIS and the GA-PNN approaches were developed for modelling the effective thermal conductivity of nanofluids as function of particle size, temperature and volume concentration. After a literature review of experimental works on the thermal conductivity of Al_2O_3-water nanofluids; particle size, temperature and volume concentration have been chosen as the most effective parameters on effective thermal conductivity. 232 input-output experimental data points obtained from literature have been used to model the effective thermal conductivity by using the FCM-ANFIS and GA-PNN approaches. The result shows that the proposed models are in good agreement compared with experimental data and the FCM-ANFIS approach shows better agreement with experimental data in comparison with the GA-PNN method.

In chapter 4, the FCM-ANFIS approach was used for modelling the viscosity of nanofluids as a function of particle size, volume concentration and temperature. 536 experimental data points for Al_2O_3, CuO, TiO_2 and SiO_2 nanoparticles with water as base fluid were obtained from literature to model the viscosity of nanofluids by using the input-output data points by using the FCM-ANFIS method. The results of the

FCM-ANFIS method were compared with the experimental data points and with several well-cited correlations from literature and in almost all cases, the proposed FCM-ANFIS models were in very good agreement with the experimental data.

Finally, in chapter 5, the GA-PNN hybrid system was used for modelling the convective heat transfer characteristics and pressure drop of TiO_2-water nanofluid in a fully developed turbulent flow based on an input-output experimental data set as function of the Reynolds number, the Prandtl number, nanoparticle volume concentration and average nanoparticle diameter. The results of the models were compared with the experimental data points and with existing correlations from literature. The statistical error analysis shows that the proposed models are in good agreement compared with experimental data and shows better accuracy with experimental data in comparison with the existing correlations. The proposed models for the Nusselt number and pressure drop were used in a multi-objective optimisation problem based on the NSGA-II algorithm. The Pareto front of these two conflicting objective functions was shown and discussed in section 5.7.

6.3. RECOMMENDATIONS

Since the proposed models based on GA-PNN and especially FCM-ANFIS approaches showed a fair agreement with experimental data for the thermal conductivity and viscosity of nanofluids, the FCM-ANFIS method is a very good candidate to model other thermophysical properties of nanofluids like thermal diffusivity or electrical conductivity based on the input-output data sets. Since there is still a challenge to find the optimised sonication power and time to prepare the nanofluids in the two-step procedure, it can therefore be recommended to apply artificial intelligence models to minimise required sonication power and time.

The joint application of the constructal theory and modified NSGA-II multi-objective optimisation method to optimise the thermo-physical property of nanofluids can be a

challenging subject for future works as well. Therefore, these two methods may recover the weakness of one another and increase the efficiency of optimisation.

REFERENCES

[1] Das, S. K., Choi, S.U.S., Yu, W., Pradeep T. (2007) *Nanofluid science and technology*, John Wiley & Sons Inc., Hoboken, New Jersey.

[2] Wang, X.Q., Mujumdar, A.S., Heat transfer characteristics of nanofluids: review. *International Journal of Thermal Science, 46* (2007) 1–19.

[3] Pang, C., Jung, J.-Y., Kang, Y.T., Aggregation based model for heat conduction mechanism in nanofluids. *International Journal of Heat and Mass Transfer, 72* (2014) 392-399.

[4] Keblinski, P., Phillpot, S.R., Choi, S.U.S., Eastman, J.A., Mechanisms of heat flow in suspensions of nano-sized particles (nanofluids). *International Journal of Heat and Mass Transfer, 45* (2002) 855–863.

[5] Wang, J.J., Zheng, R.T., Gao, J.W., Chen, G., Heat conduction mechanisms in Nanofluids and Suspensions. *Nano Today, 7* (2012) 124–136.

[6] Nelson, E., (1967). *Dynamical Theories of Brownian Motion*. Princeton, N.J.: Princeton University Press.

[7] Einstein, A., On the movement of small particles suspended in a stationary liquid demanded by the molecular kinetic theory of heat. *Annalen der Physik, 17* (1905) 549.

[8] Chen, G., (2005) *Nanoscale Energy Transport and conversion, a parallel treatment of Electrons, Molecules, Phonons and Photons*. Oxford University Press.

[9] Chon, C. H., Kihm, K. D., Lee, S. P., Choi, S.U.S., Empirical correlation finding the role of temperature and particle size for nanofluid (Al_2O_3) thermal conductivity enhancement. *Applied Physics Letter, 87(15)* (2005) 153107-1–153107-3.

[10] Li, C.H., Peterson, G.P., The effect of particle size on the effective thermal conductivity of Al_2O_3-water nanofluids. *Journal of Applied Physics, 101,* (2007), 044312.

[11] Patel, H.E., Sundararajan, T., Das, S.K., An experimental investigation into the thermal conductivity enhancement in oxide and metallic nanofluids. *Journal of Nanoparticle Research, 12* (2010) 1015–1031.

[12] Murshed, S.M.S., Leong, K.C., Yang, C., Enhanced thermal conductivity of TiO_2-water based nanofluids. *International Journal of Thermal Sciences, 44(4)* (2005), 367–373.

[13] Das, S. K., Putra, N., Thiesen, P., Roetzel, W., Temperature Dependence of Thermal Conductivity Enhancement for Nanofluids. *Journal of Heat Transfer, Transactions of the ASME, 125(4)* (2003) 567–574.

[14] Putra, N., Roetzel, W., Das, S.K., Natural convection of nano-fluids. *Heat and Mass Transfer, 39* (2003) 775–784.

[15] Lee, S., Choi, S.U.S., Li, S., Eastman, J.A., Measuring thermal conductivity of fluids containing oxide nanoparticles. *Journal of Heat Transfer, 121(2)* (1999) 280–289.

[16] Wang, X., Xu, X., Choi, S.U.S., Thermal conductivity of nanoparticle-fluid mixture. *Journal of Thermophysics and Heat Transfer, 13(4)* (1999) 474–480.

[17] Li, C.H., Peterson, G.P., Experimental investigation of temperature and volume fraction variations on the effective thermal conductivity of nanoparticle suspensions (nanofluids). *Journal of Applied Physics, 99* (2006), 084314.

[18] Kim, S.H., Choi, S.R., Kim, D., Thermal conductivity of metal-oxide nanofluids: particle size dependence and effect of laser irradiation. *Journal of Heat Transfer, 129* (2007) 298-307.

[19] Timofeeva, E.V., Routbort, J.L., Singh, D., Particle shape effects on thermophysical properties of alumina nanofluids. *Journal of Applied Physics, 106,* (2009) 014304.

[20] Hong, K. S., Hong, T. K., Yang, H. S., Thermal conductivity of Fe nanofluids depending on the cluster size of nanoparticles. *Applied Physics Letters, 88(3)* (2006) 031901.

[21] Yu, C.-J., Richter, A. G., Datta, A., Durbin, M.K., Dutta, P., Observation of molecular layering in thin liquid films using X-Ray reflectivity. *Physical Review Letters, 82,* (1999) 2326.

[22] Choi, S. U. S., Zhang, Z. G., Yu, W., Lockwood, F. E., Grulke, E. A., Anomalous thermal conductivity enhancement in nanotube suspensions. *Applied Physics Letters, 79(14)* (2001) 2252–2254.

[23] Xue, L., Keblinski, P., Phillpot, S.R., Choi, S.U.S., Eastman, J.A., Effect of liquid layering at the liquid-solid interface on thermal transport. *International Journal of Heat and Mass Transfer, 47* (2004) 4277–4284.

[24] Tillman, P., Hill, J.M., Determination of nanolayer thickness for a nanofluid. *International Communications in Heat and Mass Transfer, 34* (2007) 399–407.

[25] Wamkam, C.T., Opoku, M.K., Hong, H., Smith, P., Effects of pH on heat transfer nanofluids containing ZrO_2 and TiO_2 nanoparticles. *Journal of Applied Physics, 109* (2011) 024305.

[26] Lee, D., Kim, J.W., Kim, B.G., A new parameter to control heat transport in nanofluids: surface charge state of the particle in suspension. *The Journal of Physical Chemistry, B 110* (2006) 4323–4328.

[27] Sohn, Y.M., Baek, S.W., Kim, D.Y., Thermophoresis of particles in gas-particle two-phase flow with radiation effect. *Numerical Heat Transfer; Part A, 41(2) (2002),* 165-181.

[28] McNab, G.S., Meisen, A., Thermophoresis in liquids. *Journal of Colloid and Interface Science, 44(2),* (1973) 339.

[29] Buongiorno, J., Convective transport in nanofluids. *Journal of Heat Transfer, 128(3)* (2006) 240–250.

[30] Koo, J., Kleinstreuer, C., Impact Analysis of Nanoparticle Motion Mechanisms on the Thermal Conductivity of Nanofluids. *International Communications in Heat and Mass Transfer, 32* (2005) 1111–1118.

[31] Nasiri, A., Shariaty-Niasar, M., Rashidi, A., Amrollahi, A., Khodafarin, R., Effect of dispersion method on thermal conductivity and stability of nanofluid. *Experimental Thermal and Fluid Science, 35* (2011) 717–723.

[32] Hwang, Y., Lee, J.K., Lee, C.H., Jung, Y.M., Cheong, S.I., Lee, C.G., Ku, B.C., Jang, S.P., Stability and thermal conductivity characteristics of nanofluids. *Thermochimica Acta, 455(1–2)* (2007) 70–74.

[33] Ghadimi, A., Saidur, R., Metselaar, H.S.C., A review of nanofluid stability properties and characterization in stationary conditions. *International Journal of Heat and Mass Transfer, 54 (17–18)* (2011) 4051–4068.

[34] Xuan, Y., Li, Q., Hu, W., Aggregation structure and thermal conductivity of nanofluids. *Journal of American Institute of Chemical Engineers (AIChE), 49(4)* (2003) 1038–1043.

[35] Koo, J., Kleinstreuer, C., A new thermal conductivity model for nanofluids. *Journal of Nanoparticle Research, 6(6)* (2004) 577–588.

[36] Wasp, F.J., Solid-liquid flow slurry pipeline transportation. *Trans. Tech. Pub.*, Berlin, (1977).

[37] Prasher, R., Bhattacharya, P., Phelan, P.E., Thermal conductivity of nanoscale colloidal solutions (nanofluids). *Physical Review Letters, 94(2),* (2005) 025901-1–025901-4.

[38] Bhattacharya, P., Phelan, P.E., Prasher, R., Brownian-motion-based convective-conductive model for the effective thermal conductivity of nanofluids. *Journal of Heat Transfer, 128* (2006) 588–595.

[39] Xu, J., Yu, B., Zou, M. and Xu, P., A new model for heat conduction of nanofluids based on fractal distributions of nanoparticles. *Journal of Physics D: Applied Physics, 39(20)* (2006) 4486–4490.

[40] Vladkov, M., Barrat, J.L., Modeling transient absorption and thermal conductivity in a simple nanofluid. *Nano Letters, vol. 6, no. 6*, pp. 1224–1228, 2006.

[41] Li, C.H., Peterson, G.P., Mixing effect on the enhancement of the effective thermal conductivity of nanoparticle suspensions (nanofluids). *International Journal of Heat and Mass Transfer, 50* (23–24) (2007) 4668–4677.

[42] Sarkar, S., Selvam, R.P., Molecular dynamics simulation of effective thermal conductivity and study of enhanced thermal transport mechanism in nanofluids. *Journal of Applied Physics, 102(7),* (2007) 074302-1–074302-7.

[43] Yu-Hua, L., Wei, Q., Jian-Chao, F., Temperature dependence of thermal conductivity of nanofluids. *Chinese Physics Letters* 25(9) (2008) 3319.

[44] Shukla, R.K., Dhir, V.K., Effect of Brownian motion on thermal conductivity of nanofluids. *Journal of Heat Transfer, 130(4),* (2008) 042406-1–042406-13.

[45] Yang, B., Thermal conductivity equations based on Brownian motion in suspensions of nanoparticles (nanofluids). *Journal of Heat Transfer, 130(4),* (2008) 042408-1-042408-5.

[46] Nie, C., Marlow, W.H., Hassan, Y.A., Discussion of proposed mechanisms of thermal conductivity enhancement in nanofluids. *International Journal of Heat and Mass Transfer, 51* (2008) 1342–1348.

[47] Vasu, V., Krishna, K.R., Kumar, A.C.S., Analytical prediction of thermophysical properties of fluids embedded with nanostructured materials. *International Journal of Nanoparticles, 1(1)* (2008) 32–49.

[48] Jain, S., Patel, H.E., Das, S.K., Brownian dynamics simulation for the prediction of effective thermal conductivity of nanofluid. *Journal of Nanoparticle Research, 11(4)* (2009) 767–773.

[49] Jung, J.Y., Yoo, J.Y., Thermal conductivity enhancement of nanofluids in conjunction with electrical double layer (EDL). *International Journal of Heat and Mass Transfer, 52* (2009) 525–528.

[50] Murshed, S.M.S., Leong, K.C., Yang, C., A combined model for the effective thermal conductivity of nanofluids. *Applied Thermal Engineering, 29* (2009) 2477–2483.

[51] Emami-Meibodi, M., Vafaie-Sefti, M., Rashidi, A.M., Amrollahi, A., Tabasi, M., Sid-Kalal, H., A model for thermal conductivity of nanofluids. *Materials Chemistry and Physics, 123* (2010) 639–643.

[52] Emami-Meibodi, M., Vafaie-Sefti, M., Rashidi, A.M., Amrollahi, A., Tabasi, M., Sid-Kalal, H., Simple model for thermal conductivity of nanofluids using resistance model approach. *International Communications in Heat and Mass Transfer, 37* (2010) 555–559.

[53] Teng, T., Hung, Y., Teng, T., Mo, H., Hsu, H., The effect of alumina/water nanofluid particle size on thermal conductivity. *Applied Thermal Engineering, 30* (2010) 2213–2218.

[54] Mehta, S., Chauhan, K.P., Kanagaraj, S., Modeling of thermal conductivity of nanofluids by modifying Maxwell's equation using cell model approach. *Journal of Nanoparticle Research, 13* (2011) 2791–2798.

[55] Xiao, B., Yang, Y., Chen, L., Developing a novel form of thermal conductivity of nanofluids with Brownian motion effect by means of fractal geometry. *Powder Technology, 239* (2013) 409–414.

[56] Babaei, H., Keblinski, P., Khodadadi, J. M., A proof for insignificant effect of Brownian motion-induced micro convection on thermal conductivity of nanofluids by utilizing molecular dynamics simulations, *Journal of Applied Physics, 113* (2013) 084302.

[57] Henderson, J.R., Swol, F.V., On the interface between a fluid and a planar wall: Theory and simulations of a hard sphere fluid at a hard wall. *Molecular Physics, 51* (1984) 991–1010.

[58] Yu, C.J., Richter, A.G., Datta, A., Durbin, M.K. and Dutta, P., Molecular layering in a liquid on a solid substrate: An X-ray reflectivity study. *Physica, B 283* (2000) 27–31.

[59] Yu, W., Choi, S.U.S., The role of interfacial layers in the enhanced thermal conductivity of nanofluids: A renovated Maxwell model. *Journal of Nanoparticle Research, 5* (2003) 167–171.

[60] Feng, Y., Yu, B., Zou, M., The effective thermal conductivity of nanofluids based on the nanolayer and the aggregation of nanoparticles. *Journal of Physics D: Applied Physics, 40* (2007) 3164-3171.

[61] Yu, W. and Choi, S.U.S., The role of interfacial layers in the enhanced thermal conductivity of nanofluids: A renovated Hamilton-Crosser model. *Journal of Nanoparticle Research, 6* (2004) 355-361.

[62] Xue, L., Keblinski, P., Phillpot, S.R., Choi, S.U.S., Eastman, J.A., Two regimes of thermal resistance at a liquid-solid interface. *Journal of Chemical Physics, 118(1)* (2003) 337–339.

[63] Xue, Q.Z., Model for effective thermal conductivity of nanofluids. *Physics Letters, A 307* (2003) 313–317.

[64] Xie, H., Fujii, M., Zhang X., Effect of interfacial nanolayer on the effective thermal conductivity of nanoparticle-fluid mixture. *International Journal of Heat and Mass Transfer, 48* (2005) 2926–2932.

[65] Leong, K.C., Yang, C., Murshed S.M.S., A model for the thermal conductivity of nanofluids – the effect of interfacial layer, Journal of Nanoparticle Research, *8* (2006) 245–254.

[66] Li, L., Zhang, Y., Ma, H., Yang, M., An investigation of molecular layering at the liquid-solid interface in nanofluids by molecular dynamics simulation. *Physics Letters, A 372* (2008) 4541–4544.

[67] Zhou, X.F., Gao, L., Thermal conductivity of nanofluids: Effects of graded nanolayers and mutual interaction. *Journal of Applied Physics, 103*, (2008) 083503.

[68] Lin, Y.S., Hsiao, P.Y., Chieng, C.C., Roles of nanolayer and particle size on thermophysical characteristics of ethylene glycol-based copper nanofluids. *Applied Physics Letters, 98* (2011) 153105.

[69] Hwang, Y., Lee, J.K., Jeong, Y.M., Cheong, S.I., Ahn, Y.C., Kim, S.H., Production and dispersion stability of nanoparticles in nanofluids. *Journal of Powder Technology, 186* (2008) 145–153.

[70] Karthikeyan, N.R., Philip, J., Raj, B., Effect of clustering on the thermal conductivity of nanofluids. *Materials Chemistry and Physics, 109* (2008) 50–55.

[71] Wang, B.X., Zhou, L.P., Peng, X.F., A fractal model for predicting the effective thermal conductivity of liquid with suspension of nanoparticles. *International Journal of Heat and Mass Transfer, 46* (2003) 2665–2672.

[72] Murshed, S.M.S., Leong, K.C., Yang, C., Thermophysical and electro-kinetic properties of nanofluids – A critical review. *Applied Thermal Engineering, 28* (2008) 2109–2125.

[73] Prasher, R., Phelan, P.E. and Bhattacharya, P., Effect of aggregation kinetics on the thermal conductivity of nanoscale colloidal solution (nanofluids). *Nano Letters, 6* (2006) 1529–1534.

[74] Okeke, G., Witharana, S., Antony, S.J., Ding, Y., Computational analysis of factors influencing thermal conductivity of nanofluids. *Journal of Nanoparticle Research, 13* (2011) 6365–6375.

[75] Witharana, S., Hodges, C., Xu, D., Lai, X., Ding, Y., Aggregation and settling in aqueous polydisperse alumina nanoparticle suspensions. *Journal of Nanoparticle Research, 14(15),* (2012) 0851.

[76] Viota, J.L., González-Caballero, F., Durán, J.D.G., Delgado, A.V., Study of the colloidal stability of concentrated bimodal magnetic fluids. *Journal of Colloid and Interface Science, 309* (2007) 135–139.

[77] Yeganeh, M., Shahtahmasebi, N., Kompany, A., Goharshadi, E.K., Youssefi, A. and Šiller L., Volume fraction and temperature variations of the effective thermal conductivity of nano-diamond fluids in deionized water. *International Journal of Heat and Mass Transfer, 53* (2010) 3186–3192.

[78] Strandberg, R., Das, D.K., Influence of temperature and properties variation on nanofluids in building heating. *Energy Conversion and Management, 51* (2010) 1381–1390.

[79] Duangthongsuk, W., Wongwises, S., Measurement of temperature-dependent thermal conductivity and viscosity of TiO_2-water nanofluids. *Experimental Thermal and Fluid Science, 33* (2009) 706–714.

[80] Nguyen C.T., Desgranges F., Roy G., Galanis N., Mare´ T., Boucher S., Angue Mintsa, H., Temperature and particle-size dependent viscosity data for water-based nanofluids –

Hysteresis phenomenon. *International Journal of Heat and Fluid Flow, 28* (2007) 1492–1506.

[81] Wanga, X., Zhu, D., and Yang, S., Investigation of pH and SDBS on enhancement of thermal conductivity in nanofluids. *Chemical Physics Letters, 470* (2009) 107–111.

[82] Li, X.F., Zhu, D.S., Wang, X.J., Wang, N., Gao, J.W., Li, H., Thermal conductivity enhancement dependent pH and chemical surfactant for Cu-H_2O nanofluids. Thermochimica Acta, *469(1–2)* (2008) 98–103.

[83] Xie, H., Yu, W., Li, Y., Chen, L., Discussion on the thermal conductivity enhancement of nanofluids. *Nanoscale Research Letters, 6(1)* (2011) X1–12.

[84] Zhu, D., Li, X., Wang, N., Wang, X., Gao, J. and Li, H., Dispersion behavior and thermal conductivity characteristics of nanofluids. *Current Applied Physics, 9* (2009) 131–139.

[85] Anoop, K.B., Sundararajan, T., Das, S.K., Effect of particle size on the convective heat transfer in nanofluid in the developing region. *International Journal of Heat and Mass Transfer, 52* (2009) 2189–2195.

[86] Pastoriza-Gallego, M.J., Casanova, C., Legido, J.L., Pineiro, M.M., CuO in water nanofluid: Influence of particle size and polydispersity on volumetric behaviour and viscosity, *Fluid Phase Equilibria 300* (2011) 188–196.

[87] Ji, Y., Ma, H., Su, F., Wang, G., Particle size effect on heat transfer performance in an oscillating heat pipe. *Experimental Thermal and Fluid Science, 35(4)* (2011) 724–727.

[88] Avsec, J., The combined analysis of phonon and electron heat transfer mechanism on thermal conductivity for nanofluids. *International Journal of Heat and Mass Transfer, 51* (2008) 4589–4598.

[89] Prasher, R., Generalized equation for phonon radiative transport. *Applied Physics Letters, 83(1)* (2003) 48–50.

[90] Li, Y.H., Qu, W., Feng, J.C., Temperature dependence of thermal conductivity of nanofluids. *Chinese Physics Letters, 25(9),* (2008) 3319.

[91] Nabi, S., Shirani, E., Simultaneous effects of Brownian motion and clustering of nanoparticles on thermal conductivity of nanofluids. *Iranian Journal of Science and Technology: Transactions of Mechanical Engineering, 36* (2012) 53–68.

[92] Li, F.C., Yang, J.C., Zhou, W.W., He, Y.R., Huang, Y.M., Jiang, B.C., Experimental study on the characteristics of thermal conductivity and shear viscosity of viscoelastic-fluid-based nanofluids containing multiwalled carbon nanotubes. *Thermochimica Acta, 556* (2013) 47–53.

[93] Maxwell, J.C., (1891). *A treatise on electricity and magnetism,* Oxford: Clarendon.

[94] Hamilton, R.L., Crosser, O.K., Thermal conductivity of heterogeneous two-component systems. *I & EC Fundamentals, 1* (1962) 182–191.

[95] Jang, S.P., Choi, S.U.S., Role of Brownian motion in the enhanced thermal conductivity of nanofluids. *Applied Physics Letters, 84* (2004) 4316–4318.

[96] Bruggeman, D.A.G., Berechnung verschiedener physikalischer Konstanten von heterogenen Substanzen. I. Dielektrizitätskonstanten und Leitfähigkeiten der Mischkörper aus isotropen Substanzen. *Annalen der Physik, 416(7)* (1935) 636–679.

[97] Lu, S.Y., Lin, H.C., Effective conductivity of composites containing aligned spheroidal inclusions of finite conductivity. *Journal of Applied Physics, 79(9)* (1996) 6761–6769.

[98] Jeffrey D.J., Conduction through a random suspension of spheres. *Proceedings of Royal Society, 335* (1973) 355–367.

[99] Davis, R.H., The effective thermal conductivity of a composite material with spherical inclusions. *International Journal of Thermophysics, 7* (1986) 609–620.

[100] Sastry, N.N.V., Bhunia, A., Sundararajan, T., Das, S.K., Predicting the effective thermal conductivity of carbon nanotube based nanofluids. *Nanotechnology, 19* (2008) 055704.

[101] Syam Sundar, L., Singh, M.K., Sousa, A.C.M., Investigation of thermal conductivity and viscosity of Fe_3O_4 nanofluid for heat transfer applications. *International Communications in Heat and Mass Transfer, 44,* (2013) 7–14.

[102] Kumar, D.H., Patel, H.E., Kumar, V.R.R., Sundararajan, T., Pradeep, T., Das, S.K., Model for heat conduction in nanofluids. *Physical Review Letters, 93(4),* (2004) 144301-1–144301-4.

[103] Murshed, S.M.S., Leong, K.C., Yang, C., Investigations of thermal conductivity and viscosity of nanofluids. *International Journal of Thermal Sciences, 47* (2008) 560–568.

[104] Shima, P.D., Philip, J., Baldev R., Role of microconvection induced by Brownian motion of nanoparticles in the enhanced thermal conductivity of stable nanofluids. *Applied Physics Letters, 94* (2009) 223101.

[105] Masuda, H., Ebata, A., Teramae, K., Hishinuma, N., Alteration of thermal conductivity and viscosity of liquid by dispersing ultra-fine particles (dispersion of c-Al_2O_3, SiO_2 and TiO_2 ultra-fine particles). *Netsu Bussei 4* (1993) 227–233.

[106] Timofeeva, E.V., Gavrilov, A.N., McCloskey, J.M., Tolmachev, Y.V., Thermal conductivity and particle agglomeration in alumina nanofluids: experiment and theory. *Physical Review, E 76* (2007) 061203.

[107] Zhang, X., Gu, H., Fujii, M., Effective thermal conductivity and thermal diffusivity of nanofluids containing spherical and cylindrical nanoparticles. *Experimental Thermal and Fluid Science, 31* (2007) 593–599.

[108] Ju, Y.S., Kim, J., Hung, M.T., Experimental Study of Heat Conduction in Aqueous Suspensions of Aluminium Oxide Nanoparticles. *Journal of Heat Transfer, 130* (2008) 092403-1.

[109] Varol, Y., Avci, E., Koca, A., Oztop, H.F., Prediction of flow fields and temperature distributions due to natural convection in a triangular enclosure using Adaptive-Network-Based Fuzzy Inference System (ANFIS) and Artificial Neural Network (ANN). *International Communications in Heat and Mass Transfer, 34* (2007) 887–896.

[110] Hasiloglu, A., Yilmaz, M., Comakli, O., Ekmekci, I., Adaptive neuro-fuzzy modeling of transient heat transfer in circular duct air flow. *International Journal of Thermal Sciences, 43* (2004) 1075–1090.

[111] Sun, T., Yan, S.J., Cao, G.Y., Zhu, X.J., Modelling and control PEMFC using fuzzy neural networks. *Journal of Zhejiang University SCIENCE, 6A-10* (2005) 1084–1089.

[112] Jang, J.S.R., Adaptive Network, Based fuzzy inference. *CiteSeer^x Publication, No.47* (1993).

[113] Lippmann, R.P., An introduction to computing with neural networks. *IEEE magazine, 3(4)* (1987) 4–22.

[114] Jang, J.S.R., ANFIS; Adaptive network-based fuzzy inference systems. *IEEE transactions on systems, man and cybernetics, 23(3)* (1993) 665–685.

[115] Hanboy, D., Baylar, A., Ozpolat, E., Predicting flow conditions over stepped chutes based on ANFIS. *Soft computing, 13* (2009) 701–707.

[116] Guijas, D., Cordero, J.T., Alarcon, J., An adaptive neuro-fuzzy approach to control a distillation column. *Neural computing and applications, 9* (2000) 211–217.

[117] Jalalifar, H., Mojedifar, S., Sahebi, A.A., Nezamabadi-pour, H., Application of the adaptive neuro-fuzzy inference system for prediction of a rock engineering classification system. *Computers and Geotechnics, 38* (2011) 783–790.

[118] Bezdek, J.C., (1973). *Fuzzy Mathematics in Pattern Classification*. PhD dissertation, Cornell University, Ithaca, New York.

[119] Kim, S.S., Lee, D.J., Kwak, K.C., Park, J.H., Ryu, J.W., Speech recognition using integra-normalizer and neuro-fuzzy method. *Conference Record of the Asilomar Conference on Signals, Systems and Computers, 2* (2000) 1498–1501.

[120] Othman, M.F., Moh, T., Neuro fuzzy classification and detection technique for bioinformatics problems. *Proceedings of the First Asia International Conference on Modelling & Simulation* (AMS'07) 0-7695-2845-7/07 375–380.

[121] Ibrahim, S., Khalid, N.E.A., Manaf, M., Seed-Based Region Growing (SBRG) vs. Adaptive Network-Based Inference System (ANFIS) vs. Fuzzy C-Means (FCM): Brain abnormalities segmentation. *Proceedings of World Academy of Science, Engineering and Technology, 68* (2010) 425-435.

[122] Pesteei, S.M., Mehrabi, M., Modeling of convection heat transfer of supercritical carbon dioxide in a vertical tube at low Reynolds numbers using neural network. *International Communications in Heat and Mass Transfer, 37(7)* (2010) 901–906.

[123] Ivakhnenko, A.G., The Group Method of Data Handling – A rival of the method of stochastic approximation. *Soviet Automatic Control, 13* (3) (1966) 43–55.

[124] Fujimoto, K., Nakabayashi, S., Applying GMDH algorithm to extract rules from examples. *Systems Analysis Modelling Simulation, 43 (10)* (2003) 1311–1319.

[125] Lemke, F., Müller, J.A., Self-organizing data mining. *Systems Analysis Modelling Simulation, 43(2),* (2003) 231–240.

[126] Saemi, M., Ahmadi, M., Yazdian-Varjani, A., Design of neural networks using genetic algorithm for the permeability estimation of the reservoir. *Journal of Petroleum Science and Engineering, 59* (2007) 97–105.

[127] Nikolaev, N.Y., Iba, H., learning polynomial feed-forward neural networks by genetic programming and back-propagation. *IEEE transactions on Neural Networks, 14(2)* (2003) 337–350.

[128] Serebryakova, M.A., Dimov, S.V., Bardakhanov, S.P., Novopashin, S.A, Thermal conductivity, viscosity and rheology of a suspension based on Al_2O_3 nanoparticles and mixture of 90% ethylene glycol and 10% water. *International Journal of Heat and Mass Transfer 83* (2015) 187-191.

[129] Bakhshan, Y., Saljooghi, M., A new correlation for viscosity of nanofluids with considering the temperature dependence, *Journal of Computational and Theoretical Nanoscience* 11(3) (2014) 583-588.

[130] Alawi, O.A., Sidik, N.A.C., Influence of particle concentration and temperature on the thermophysical properties of CuO/R134a nanorefrigerant. *International Communications in Heat and Mass Transfer* 58(1) (2014) 79-84.

[131] Namburu, P.K., Kulkarni, D.P., Dandekar, A., Das, D.K., Experimental investigation of viscosity and specific heat of silicon dioxide nanofluids. *Micro & Nano Letters, 2(3)* (2007) 67–71.

[132] Lu, W.Q., Fan, Q.M., Study for the particle's scale effect on some thermophysical properties of nanofluids by a simplified molecular dynamics method. *Engineering Analysis with Boundary Elements, 32* (2008) 282–289.

[133] Schmidt, A.J., Chiesa, M., Torchinsky, D.H., Johnson, J.A., Boustani, A., et al., Experimental investigation of nanofluid shear and longitudinal viscosities. *Applied Physics Letters, 92* (2008) 244107.

[134] Chandrasekar, M., Suresh, S., Chandra Bose, A., Experimental investigations and theoretical determination of thermal conductivity and viscosity of Al_2O_3/water nanofluid. *Experimental Thermal and Fluid Science, 34* (2010) 210–216.

[135] Chevalier, J., Tillement, O., Ayela, F., Rheological properties of nanofluids flowing through microchannels. *Applied Physics Letters, 91* (2008) 233103.

[136] Chen, L., Xie, H., Yu, W., Li, Y., Rheological behaviors of nanofluids containing multi-walled carbon nanotube. *Journal of Dispersion Science and Technology, 32* (2011) 550–554.

[137] Lee, S.W., Park, S.D., Kang, S., Bang, I.C., Kim, J.H., Investigation of viscosity and thermal conductivity of SiC nanofluids for heat transfer applications. International Journal of Heat and Mass Transfer, 54 (2011) 433–438.

[138] Prasher, R., Song, D., Wang, J., Phelan, P., Measurements of nanofluid viscosity and its implications for thermal applications. *Applied Physics Letters, 89* (13) (2006) 133108.

[139] Chen, H., Ding, Y., Tan, C., Rheological behaviour of nanofluids. *New Journal of Physics, 9 (10)* (2007) 267.

[140] Chen, H., Ding, Y., He, Y., Tan, C., Rheological behaviour of ethylene glycol-based titania nanofluids. *Chemical Physics Letters, 444 (4–6)* (2007) 333–337.

[141] Tavman, I., Turgut, A., Chirtoc, M., Schuchmann, H.P., Tavman, S., Experimental investigation of viscosity and thermal conductivity of suspensions containing nanosized ceramic particles. *Archives of Materials Science and Engineering, 34(2)* (2008) 99-104.

[142] Lee, J.H., Hwang, K.S., Jang, S.P., Lee, B.H., Kim, J.H., Choi, S.U.S., Choi, C.J., Effective viscosities and thermal conductivities of aqueous nanofluids containing low volume concentrations of Al_2O_3 nanoparticles. *International Journal of Heat and Mass Transfer, 51* (2008) 2651–2656.

[143] Turgut, A., Tavman, I., Chirtoc, M., Schuchmann, H.P., Sauter, C., Tavman, S., Thermal conductivity and viscosity measurements of water-based TiO_2 nanofluids. *International Journal of Thermophysics, 30* (2009) 1213–1226.

[144] Anoop, K.B., Kabelac, S., Sundararajan, T., Das, S.K., Rheological and flow characteristics of nanofluids: Influence of electroviscous effects and particle agglomeration. *Journal of Applied Physics, 106* (2009) 034909.

[145] Pastoriza-Gallego, M.J., Casanova, C., Páramo, R., Barbés, B., Legido, J.L., A study on stability and thermophysical properties (density and viscosity) of Al_2O_3 in water nanofluid. *Journal of Applied Physics, 106,* (2009) 064301.

[146] Kwek, D., Crivoi, A., Duan, F., Effects of Temperature and Particle Size on the Thermal Property Measurements of Al_2O_3-Water Nanofluids. *Journal of Chemical & Engineering Data, 55* (2010) 5690–5695.

[147] Fedele, L., Colla, L., Bobbo, S., Viscosity and thermal conductivity measurements of water-based nanofluids containing titanium oxide nanoparticles. *International Journal of Refrigeration, 35* (2012) 1359–1366.

[148] Einstein, A., Eine neue Bestimmung der Moleküldimensionen. *Annalen der Physik, 324(2)* (1906) 289–306.

[149] Brinkman, H.C., The viscosity of concentrated suspensions and solution. *Journal of Chemical Physics, 20(4)* (1952) 571.

[150] Batchelor, G.K., Effect of Brownian motion on the bulk stress in a suspension of spherical particles. *Journal of Fluid Mechanics, 83 (1)* (1977) 97–117.

[151] Abu-Nada, E., Masoud, Z., Oztop, H.F., Campo, A., Effect of nanofluid variable properties on natural convection in enclosures. *International Journal of Thermal Sciences, 49* (2010) 479–491.

[152] Abedian, B., Kachanov, M., On the effective viscosity of suspensions. *International Journal of Engineering Science, 48* (2010) 962–965.

[153] Masoud-Hosseini, S., Moghadassi, A.R., Henneke, D.E., A new dimensionless group model for determining the viscosity of nanofluids. *Journal of Thermal Analysis and Calorimetry, 100(3)* (2010) 873–877.

[154] Graf, W.H., (1971). *Hydraulics of Sediment Transport*. McGraw-Hill, New York.

[155] Avsec, J., Oblak, M., The calculation of thermal conductivity, viscosity and thermodynamic properties for nanofluids on the basis of statistical nanomechanics. *International Journal of Heat and Mass Transfer, 50* (2007) 4331–4341.

[156] Mehrabi, M., Rezazadeh, S., Sharifpur, M., Meyer, J.P., Modeling of proton exchange membrane fuel cell (PEMFC) performance by using genetic algorithm-polynomial neural network (GA-PNN) hybrid system. Proceedings of the ASME 2012 10th Fuel Cell Science. Engineering and Technology Conference (FuelCell2012), San Diego, USA, 2012, paper number FuelCell2012-91391.

[157] Mehrabi, M., Sharifpur, M., Meyer, J.P., Application of the FCM-based neuro-fuzzy inference system and genetic algorithm-polynomial neural network approaches to modelling

the thermal conductivity of alumina–water nanofluids. *International Communications in Heat and Mass Transfer, 39* (2012) 971–977.

[158] Duangthongsuk, W., Wongwises, S., An experimental study on the heat transfer performance and pressure drop of TiO_2-water nanofluids flowing under a turbulent flow regime. *International Journal of Heat and Mass Transfer, 53* (2010) 334–344.

[159] Sajadi, A.R., Kazemi, M.H., Investigation of turbulent convective heat transfer and pressure drop of TiO_2/water nanofluid in circular tube. *International Communications in Heat and Mass Transfer, 38* (2011) 1474–1478.

[160] Godson, L., Raja, B., Mohan Lal, D., Wongwises, S., Convective heat transfer characteristics of silver-water nanofluid under laminar and turbulent flow conditions. *Journal of Thermal Science and Engineering Applications, 4(3)* (2012) 031001.

[161] Keshavarz Moraveji, M., Hejazian, M., Modeling of turbulent forced convective heat transfer and friction factor in a tube for Fe_3O_4 magnetic nanofluid with computational fluid dynamics. *International Communications in Heat and Mass Transfer, 39* (2012) 1293–1296.

[162] Abbasian Arani, A.A., Amani, J., Experimental investigation of diameter effect on heat transfer performance and pressure drop of TiO_2-water nanofluid. *Experimental Thermal and Fluid Science, 44* (2013) 520–533.

[163] Pak, B.C., Cho, Y.I., Hydrodynamic and heat transfer study of dispersed fluids with submicron metallic oxide particles. *Experimental Heat Transfer, 11 (2)* (1998) 151–170.

[164] Pareto, V., (1896). Cours d'economic politique. Rouge, Lausanne, Switzerland.

[165] Marler, R.T., Arora, J.S., Survey of multi-objective optimization methods for engineering. *Structural and Multidisciplinary Optimization, 26* (2004) 369–395.

[166] Deb, K., Pratap, A., Agarwal, S., Meyarivan, T., A fast and elitist multi-objective genetic algorithm: NSGA-II. *IEEE Transactions on Evolutionary Computation, 6(2)* (2002) 182–197.

[167] Abbasian Arani, A.A., Amani, J., Experimental study on the effect of TiO_2–water nanofluid on heat transfer and pressure drop. *Exp. Therm. Fluid Sci., 42* (2012) 107–115.

[168] Maiga, S.E.B., Nguyen, C.T., Galanis, N., Roy, G., Mare, T., Coqueux, M., Heat transfer enhancement in turbulent tube flow using Al_2O_3 nanoparticles suspension. *International Journal of Numerical Methods for Heat and Fluid Flow, 16* (3) (2006) 275–292.

[169] Hajela, P., Lin, C.Y., Genetic search strategies in multicriterion optimal design. *Structural Optimization, 4(2)* (1992) 99–107.

[170] Srinivas, N., Deb, K., Multiobjective optimization using nondominated sorting in genetic algorithms. *Evolutionary Computation, 2(3)* (1994) 221-248.

[171] Zitzler, E., Thiele, L., Multiobjective evolutionary algorithms: a comparative case study and the strength Pareto approach. *IEEE Transactions on Evolutionary Computation, 3(4)* (1999) 257–271.

[172] Knowles, J.D., Corne, D.W., Approximating the nondominated front using the Pareto archived evolution strategy. *Evolutionary Computation, 8(2)* (2000) 149–172.

[173] Sarker, R., Liang, K.H., Newton, C., A new multiobjective evolutionary algorithm. *European Journal of Operational Research, 140(1)* (2002) 12–23.

[174] Yen, G.G., Lu, H., Dynamic multiobjective evolutionary algorithm: adaptive cell-based rank and density estimation. *IEEE Transactions on Evolutionary Computation, 7(3)* (2003) 253–274.

[175] Yen, G.G., Lu, H., Rank-density-based multiobjective genetic algorithm and benchmark test function study. *IEEE Transactions on Evolutionary Computation, 7(4)* (2003) 325–343.

[176] Hamdan, M., A dynamic polynomial mutation for evolutionary multi-objective optimization algorithms. *International Journal on Artificial Intelligence Tools, 20(1)* (2011) 209–219.